UNIVERSITE D'AIX-MARSEILLE

ED 463 – SCIENCES DU MOUVEMENT HUMAIN

UMR 7287 - INSTITUT DES SCIENCES DU MOUVEMENT

Thèse présentée pour obtenir le grade universitaire de docteur

Discipline : Sciences du Mouvement Humain

Timothée Roberts

Conception et intégration de dispositifs innovants à base de matériaux organiques pour application à la prothèse myoélectrique.

À soutenir le 12/09/2018 devant le jury :

PAYSANT Jean	PU-PH, CHRU de Nancy	Rapporteur
CAVALLARI Paolo	Professeur, State University of Milan	Rapporteur
BENAR Christian-G	DR INSERN; Aix-Marseille Université	Examinateur
HERVE Thierry	Directeur, MicroVitae Technologies	Examinateur
DE GRAAF Jozina	MCF, Aix-Marseille Université	Directrice de thèse
BOUQUET Valery	Ingénieur, MicroVitae Technologies	Invité

Numéro national de thèse/suffixe local : 2015AIXM0082/001ED62

Remerciements

Je tiens tout d'abord à remercier Jozina De Graaf et Thierry Hervé pour m'avoir permis de réaliser ces travaux de thèse.

Je veux remercier les rapporteurs, Jean Paysant et Paolo Cavallari, pour le temps qu'ils ont accordé à la lecture de cette thèse et à l'élaboration de leurs rapports.

Je remercie ensuite Eloïse Bihar pour la collaboration amicale et productive que nous avons eue.

Je remercie aussi tous les techniciens, ingénieurs de recherche et chercheurs de l'école des Mines qui m'ont formé et aidé à utiliser les différents équipements dont j'ai eu besoin.

Je réserve ensuite un remerciement particulier à Valéry Bouquet, mon collègue de bureau, pour toutes les discussions philosophiques que nous avons eues durant ces 3 dernières années.

Enfin, je réserve un grand merci à ma famille et mes amies pour leur patience et leur support.

Sommaire

I. Introduction

1) Contexte

Ma recherche de thèse s'incorpore dans le projet de recherche PhantoMovControl mené par Dr. Jozina De Graaf, qui a pour but (1) de mieux comprendre la réorganisation neurophysiologique après amputation d'un membre supérieur, et (2) de trouver une alternative aux contrôles de prothèses myoélectriques aujourd'hui sur le marché.

Selon l'INSEE (2004) [1], il y aurait en France 40 000 amputés dont 5% de membres supérieurs. On compte 1 million d'amputations annuelles dans le monde selon l'Advanced Amputee Solutions en 2010[2]. L'équipe a montré récemment que 77% des patients amputés de membre supérieur ont un *membre fantôme mobile*, c'est-à-dire qu'ils peuvent le bouger volontairement [3]. Contrairement à ce que l'on pense souvent, ces mouvements ne sont pas imaginés mais bien [4] dans le sens que des commandes motrices spécifiques sont envoyées du cortex moteur vers les muscles. Ces commandes atterrissent sur la musculature résiduelle, donnant lieu à une activité musculaire dont le patron est spécifique au mouvement [5].

Le but du projet PhantoMovControl est d'explorer la réorganisation neuromusculaire au niveau du membre résiduel et de l'utiliser pour améliorer le contrôle des prothèses. Concernant ce dernier point, il est en effet nécessaire d'envisager un nouveau type de contrôle pour les prothèses myoélectriques qui ont aujourd'hui encore un contrôle très archaïque. Pour un amputé de bras ayant conservé (au moins partiellement) son biceps et son triceps, les contractions de ces deux muscles sont généralement utilisées de façon binaire pour contrôler la prothèse. Par exemple, une contraction du biceps seul servira à fermer la main et une contraction du triceps seul permettra de l'ouvrir ; une co-contraction des deux muscles fera tourner la main de la prothèse au niveau du poignet, le sens en fonction d'un seuil choisi. De façon générale, deux muscles antagonistes sont choisis pour réaliser ces actions. Cette méthode n'est pas naturelle pour les patients car ils doivent apprendre à produire une activité musculaire basée sur des seuils d'activité, chose que nous n'avons pas l'habitude de faire (on contrôle la posture ou le mouvement mais pas l'activité musculaire sous-jacente). L'apprentissage est alors long, et puisque le contrôle de la prothèse reste cognitivement difficile, il y a un taux important de rejet de 35% [6]. De plus, peu de mouvements peuvent être réalisés avec ce mode de contrôle, ce qui n'est pas

favorable à l'utilisation des nouvelles prothèses polydigitales avec leur grand nombre de degrés de liberté et qui sont depuis 2016 remboursées par la Sécurité sociale. L'utilisation des patrons d'activité des muscles résiduels lors de l'exécution de mouvements fantômes pourrait rendre le contrôle plus naturel (sans apprentissage) pour un nombre de degrés de liberté potentiellement plus important. En effet, le patient exécute son mouvement fantôme et la prothèse l'imite en utilisant les activités musculaires produites pendant le mouvement fantôme.

La première validation de ce concept est déjà faite [7,8]. La figure 1 représente un patient équipé pour un test de contrôle de prothèse basé sur l'exécution de mouvements fantômes. La prothèse est pour l'instant positionnée à côté du patient. Remarquez que le membre résiduel est tapissé d'électrodes classiques (Ambu) qui sont épaisses et contiennent un gel conducteur. Les prothèses myoélectriques actuelles ont deux paires d'électrodes sèches intégrées dans le manchon mais ne permettent pas d'y rajouter d'autres paires, or pour un bon contrôle basé fantôme, il faudrait un minimum de 6 paires d'électrodes[7]. Les électrodes classiques ne sont pas intégrables dans le manchon de la prothèse du patient à cause de leur épaisseur (voir l'agrandissement d'une électrode dans la figure 1). Afin de valider ce mode de contrôle dans des conditions réelles, il a fallu développer des électrodes fines et sèches qui seront intégrables dans le manchon de prothèses. Ceci était le premier objectif du travail de ma thèse.

Afin d'obtenir plus d'informations sur la distribution spatiale optimale des électrodes sur le membre résiduel, le deuxième objectif de ma thèse était d'explorer la réorganisation neuromusculaire avec les matrices d'électrodes développées. Après avoir détaillé la base de l'électromyographie dans la section suivante, les deux buts du projet de thèse seront détaillés.

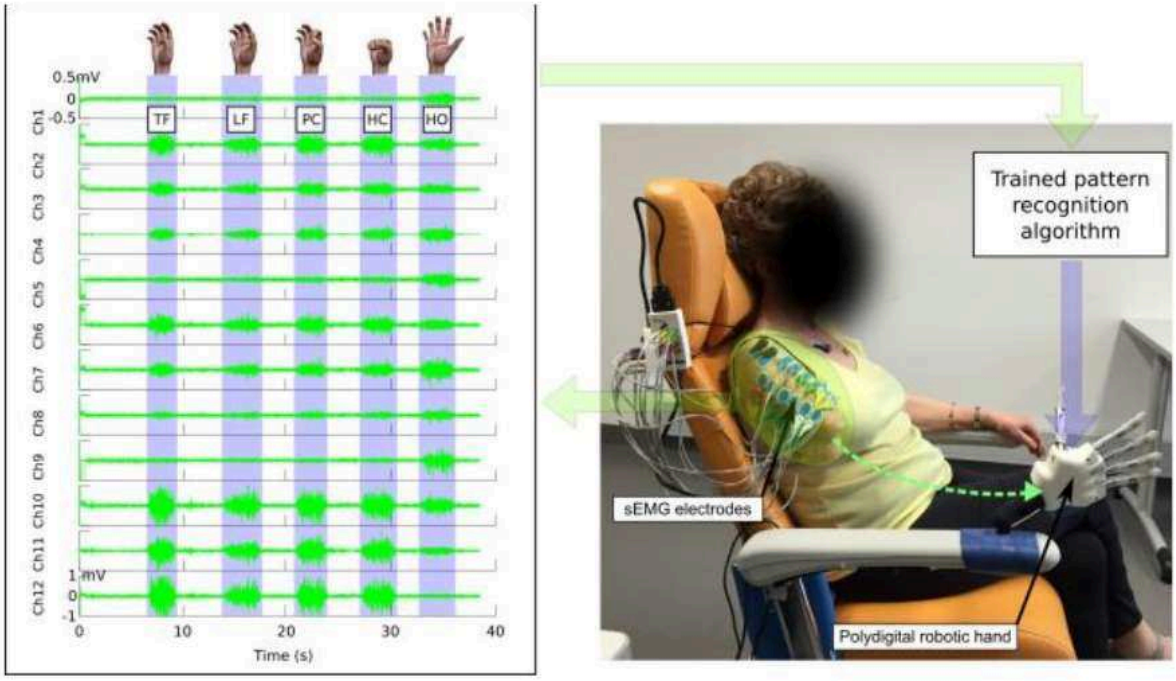

Figure 1. Participant amputé contrôlant une prothèse via les contractions associées par les mouvements de son membre [8].

2) Activité musculaire

L'électrophysiologie est le vaste domaine de la mesure de grandeurs électriques provenant de cellules ou de tissus biologiques. Trois cibles sont très connues, parmi beaucoup d'autres, pour faire partie de ce domaine : le cœur avec l'électrocardiographie (ECG), le cerveau avec l'électroencéphalographie (EEG) et les muscles avec l'électromyographie (EMG). Ces différents sous-domaines de l'électrophysiologie font référence à des techniques de mesures aujourd'hui très normalisées. Par exemple, un montage monopolaire utilise trois électrodes : une électrode de mesure qui sera placée sur le site d'intérêt, une électrode de référence qui sera placée sur un point en fonction de ce que l'on veut mesurer, et enfin une électrode de terre/masse qui permet de tirer le potentiel global du média dans lequel on mesure vers le potentiel de référence. Le rôle de l'électrode de terre/masse est d'éviter qu'une surtension ne se crée entre le média et l'électronique ce qui saturerait l'entrée des amplificateurs d'instrumentation. Cette technique permet d'avoir le niveau de tension par rapport à la référence d'un ou de plusieurs sites si plusieurs électrodes de mesure sont utilisées. Une variante de cette technique est le montage bipolaire. Ici, 3 électrodes sont utilisées : 2 électrodes de mesure qui seront soustraites l'une à l'autre, et une électrode de terre/masse. Cette technique peut soit permettre d'observer le passage d'une onde de polarisation comme dans le cadre de

l'électromyographie de surface (sEMG), soit de permettre de voir une différence de polarisation comme dans le cadre de l'ECG. Contrairement au montage monopolaire, deux mesures ne sont pas directement comparables car elles sont le résultat d'une différence locale. D'autres techniques existent, comme celle utilisant des tétrodes, mais celle-ci est beaucoup plus spécifique à l'application. Dans notre cas, nous cherchons à mesurer des activités musculaires dans le cadre du contrôle d'une prothèse. Nous allons donc, ici, nous intéresser à la sEMG.

Lors d'une contraction musculaire, le cortex moteur envoie des commandes motrices qui projettent, plus ou moins directement, sur une population de motoneurones au niveau de la corne ventrale de la moelle. Ceux-ci vont innerver des fibres musculaires en y évoquant des potentiels d'action qui se propagent dans les deux sens le long des fibres musculaires à partir des zones d'innervation (voir figure 2 à gauche). Ces images sont prises du livre The ABC of EMG[9].

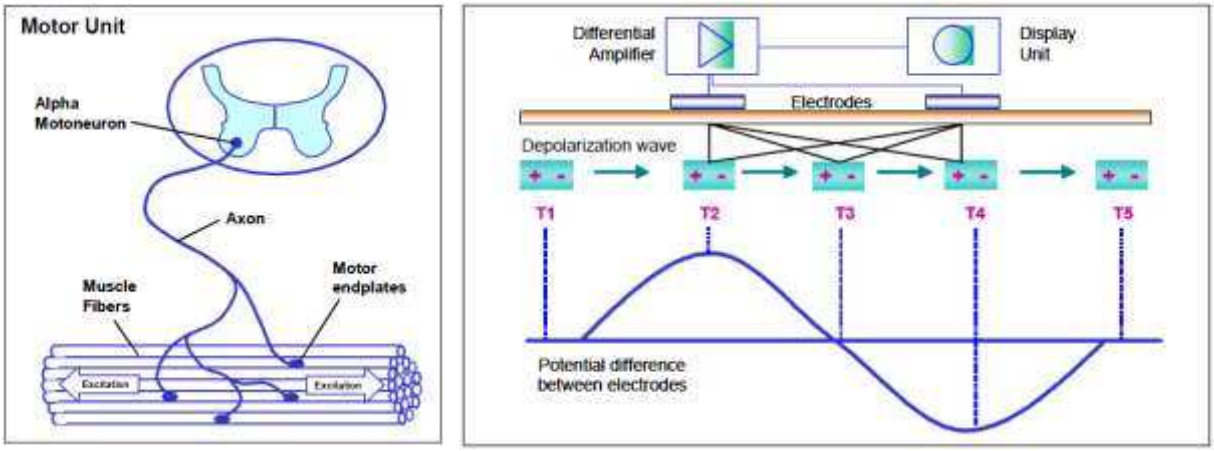

Figure 2. A gauche, innervation des fibres musculaires par les axones provenant d'un motoneurone. A droite, influence de la position des électrodes par rapport à la vague de dépolarisation sur une mesure bipolaire en surface de la peau (image prise du livre ABC of EMG).

Classiquement, dans le but de mesurer l'activité des fibres musculaires en surface de la peau, une configuration bipolaire est utilisée. Comme vu précédemment, cela permet de faire une différence locale et de retirer toutes les activités électriques autres que le déplacement des potentiels d'actions le long des fibres musculaires. L'information reçue est alors la somme du passage de potentiels d'action sur toutes les fibres musculaires se trouvant dans le volume de détection des électrodes. Étant donné que le potentiel se propage dans les deux sens par rapport à la zone d'innervation, le signal induit sera nul pour une paire d'electrodes bipolaires positionnées autour du point d'innervation ayant généré les potentiels d'action.

La distance entre les deux électrodes est aussi très importante. Plus cette distance sera grande plus des signaux parasites venant de muscles environnants seront enregistrés. Ce « bruit » dû à l'enregistrement de signaux électrophysiologiques non souhaités est appelé *cross-talk*. De l'autre côté, le volume de détection des électrodes diminue avec la réduction de distance entre ces électrodes. Cela veut dire que les signaux provenant de fibres musculaires plus profondes dans le muscle seront perdus si l'on rapproche trop les électrodes. Lynn et al. (1978) [10] proposent une règle qui dit que la distance entre les électrodes correspond à la distance à laquelle les fibres musculaires contribuent significativement au signal enregistré. C'est pourquoi suivant ces deux règles, il est classiquement conseillé d'avoir une distance inter-électrodes entre 1 et 2 cm. Il est primordial, suivant ce que l'on veut mesurer, de bien choisir la distance entre les électrodes. Tout dépend donc de ce que nous cherchons à mesurer.

Comme cité précédemment, il a été démontré que les membres fantômes ne sont pas imaginés. En effet, l'implication du réseau sensorimoteur cortical est similaire pour l'exécution d'un mouvement réel (i.e., d'un membre intact) que pour l'exécution d'un mouvement fantôme [4]. Ceci est confirmé par le fait qu'un mouvement fantôme est toujours associé à des contractions de la musculature [5]. En effet, sans contraction musculaire pendant une tentative de mouvement fantôme, le patient déclare de ne pas avoir de mobilité [5]. Dans la littérature, le membre fantôme est le plus souvent associé à une réorganisation corticale suite à l'amputation [11–13]. En gros, cette réorganisation consisterait à un « envahissement de l'aire corticale qui s'occupait avant l'amputation du membre perdu par les aires corticales adjacentes », résultat observé chez le singe [11,14–16] et plus récemment chez l'homme [17,18]. Ces dernières études ont montré chez des amputés du membre supérieur qu'une stimulation magnétique transcrânienne (TMS) de l'aire de la main évoque des contractions musculaires au niveau du membre résiduel. Ils en concluent que les neurones de l'ancienne aire de la main s'occupent désormais du membre résiduel. Cependant, dans les mêmes études, les patients déclarent ressentir un mouvement de leur main évoqué par la TMS. Si nous y rajoutons que 77% des patients peuvent volontairement contrôler leur membre fantôme, on doit en conclure que les représentations *motrice* et *somatosensorielle* du membre amputé sont toujours présentes au niveau cortical. L'hypothèse de la réorganisation corticale ne peut donc entièrement expliquer le phénomène de mobilité fantôme.

Une hypothèse alternative, plus prometteuse, porte sur une réorganisation neuromusculaire, donc périphérique. Des études faites chez les singes montrent qu'après

une amputation, les motoneurones spinaux qui innervaient le membre désormais disparu, survivent. Ceci suggère fortement qu'après l'axotomie, les axones repoussent et se projettent sur des fibres musculaires environnantes, donc du membre résiduel [19,20]. Si ceci est vrai, les résultats mentionnés ci-dessus de Gagné et collègues (2011) [17] doivent être interprétés de façon différente. En effet, si l'aire corticale s'occupant auparavant du membre manquant ne disparaît pas, elle envoie toujours des commandes au membre disparu. Or, puisque la cible des axones a été modifiée, cet envoi de commandes motrices résulte en une contraction de fibres de la musculature résiduelle. La musculature résiduelle à son tour, renvoie des afférences pour signaler qu'il y a eu mouvement. Cette hypothèse expliquerait donc les activités de la musculature résiduelle évoquées par la TMS ainsi que le ressenti de mouvements évoqués du membre fantôme. On peut en conclure que la mobilité par exemple de la main fantôme, est le résultat d'un envoi de commandes motrices à partir de l'aire de la main de M1 ciblant les muscles impliqués dans les mouvements de la main comme avant l'amputation. Et ces commandes motrices arrivant sur la musculature résiduelle évoquent des contractions de la musculature plus proximale. En supposant une ré-innervation périphérique, de nouvelles zones d'innervation devraient apparaître sur les muscles résiduels. Ceci impliquerait que plusieurs motoneurones spinaux activent une même fibre musculaire. Une poly-innervation des fibres musculaires a déjà été trouvée dans le cas d'absence de réponse musculaire à un envoi de commandes après injection de toxine botulique [21]. De façon intéressante, dans le cas d'amputation, l'axotomie est également suivie d'une absence de réponse musculaire.

Pour tester cette dernière hypothèse, il nous faudra distinguer les zones d'innervations initiales de celles découlant d'une réinnervation. Il a été montré précédemment que l'utilisation d'un grand nombre de canaux sEMG pouvait permettre la localisation des zones [22]. Pour cela, le maillage de la matrice d'électrodes doit être le plus fin possible pour augmenter la précision de la localisation ce qui est contraire à ce que l'on a vu précédemment concernant la profondeur de détection. Il nous faut donc bien définir la distance entre les électrodes qui vont nous permettre de valider cette discrimination des zones d'innervations « natives » et « postopératoires ».

3) Fabrication d'électrodes de mesure électro-physiologiques

Classiquement en sEMG, des électrodes Ag/AgCl combinées avec du gel sont utilisées. Il est très facile d'en trouver dans le commerce, comme par exemple les électrodes Ambu Blue

Sensor (comme N-00-S/25, Fig. x). Cependant, dans notre cas, leur utilisation pose problème. D'abord, on ne peut réduire la distance inter-électrodes en dessous de 2 cm. Ensuite, il est très fastidieux de poser suffisamment d'électrodes pour rechercher des zones d'innervations. La position relative des électrodes est approximative. Finalement, on ne peut envisager d'utiliser de telles électrodes dans une prothèse myoélectrique étant donné leur volume ainsi que la rapidité avec laquelle le gel conducteur sèche [23]. Malheureusement, ce gel permet justement d'assurer un contact stable et de faible impédance durant l'acquisition des signaux physiologiques. Dans la littérature, des tentatives de contourner ce problème ont été d'améliorer le contact entre l'électrode sèche (i.e., sans gel) et la peau en cherchant à utiliser un support d'électrode très fin (inférieur à 200 µm), flexible pour se conformer au mieux au membre à mesurer, si possible ayant une certaine adhérence à la peau pour stabiliser le contact, et avec de l'élasticité pour pouvoir supporter les déformations de la peau lors de mouvements ou de tensions mécaniques[24–30]. Aujourd'hui, aucune solution idéale n'a été proposée pour des électrodes sèches, qui sont pourtant nécessaires pour notre application clinique. C'est alors sur cet aspect que je me suis penché durant une partie importante de mes travaux.

D'abord, j'ai cherché une méthode de fabrication adéquate. Dans la littérature, de nombreux matériaux et substrats sont utilisés. Aussi, de nombreuses techniques de fabrication sont utilisées pour déposer de fines couches de matériaux sur des substrats minces. Comme présenté par Koutsouras et al. (2017) [31], on peut fréquemment retrouver l'impression par gravure, la flexographie, la sérigraphie, mais aussi des technologies sans contact telles que le dépôt de matériaux par aérosol ou par jet d'encre. On peut aussi trouver des techniques plus exotiques, souvent utilisées pour des substrats spécifiques, comme par exemple une technique inspirée de la teinture de Kimono [32]. On peut aussi utiliser des techniques d'évaporation dans les processus de photolithographie[33] qui permettent d'avoir une finesse de design (proximité de deux dépôts de matériaux sans qu'ils ne se touchent) autour, voire en dessous, du micromètre, alors que les autres techniques ont classiquement une précision de dépôt comprise entre 10 et 100 micromètres. Cependant, d'autres paramètres sont à prendre en compte. La taille maximale de substrat que l'on peut utiliser qui est, par exemple, basée sur la taille des wafers[1] pour les insoleuses de photolithographie est un de ces paramètres (outil qui permet de changer les propriétés physiques d'une résine par application d'une lumière ultraviolet). Les matériaux et les

[1] Disque de silicium, souvent 4 pouces, utilisé en microélectronique pour la fabrication de transistors.

substrats que l'on peut utiliser diffèrent selon les méthodes de fabrication choisies. Par exemple, la photolithographie utilise des procédés différents suivant les matériaux à déposer (l'évaporation pour les métaux ou le *spincoating*, dépôt par effet centrifuge pour des polymères). De même, pour l'impression par jet d'encre, on est limité par les encres qui ont été développées et qui doivent, selon les différentes techniques d'impression, respecter une certaine viscosité pour pouvoir être éjectées par la tête d'impression (entre 5 et 20 centipoises pour la Dimatix DMP-2800). Enfin, un dernier paramètre important est la complexité du procédé de fabrication. Les procédés de photolithographie permettent une très bonne résolution mais au prix de nombreuses étapes de fabrication et de l'utilisation de masques d'un coût très élevé, ce qui rendent compliqués les changements de motif. C'est pour ces raisons que l'impression par jet d'encre a regagné en popularité ces dernières années dans le cadre de la recherche, et plus spécifiquement l'impression jet d'encre goutte à goutte utilisant une technologie piézoélectrique, comme le fait par exemple l'imprimante Dimatix DMP-2800. Celle-ci permet, grâce à un programme dédié, de contrôler l'endroit où doit tomber chaque goutte d'encre sur le matériel. Elle a une précision d'approximativement 20 µm (suivant l'encre utilisée et l'optimisation des paramètres d'éjections) et permet de travailler sur des surfaces assez importantes (format A4 ou plus sur des technologies industrielles). De plus, le fait d'imprimer sans contact permet d'envisager de déposer les matériaux sur des substrats [34]. Effectivement, il est très difficile de travailler avec des masques (« pochoir ») sur des substrats élastiques. C'est pourquoi avec l'arrivée des encres [35] et polymères conducteurs [36], la technologie « jet d'encre » a été beaucoup étudiée dans le cadre de fabrication de transistor organique [37], de diode polymère [38], de microsystèmes électromécaniques [39], de cellule solaire polymère [40] et maintenant de capteurs [41]. De plus, le poly (3,4-éthylènedioxythiophène) polystyrène sulfonate (PEDOT : PSS), un polymère pouvant être imprimé, est particulièrement intéressant pour notre application. Premièrement, il est disponible dans le commerce, par exemple chez Heraeus, sous forme d'encre compatible avec les technologies d'impressions. De plus, c'est un polymère chimiquement stable qui a une bonne stabilité thermique et une bonne conductivité. Cette conductivité peut être modifiée grâce à l'utilisation de certains solvants et de traitement de surface [42]. Suivant les traitements, la conductivité du PEDOT: PSS peut alors varier de 1 à 4380 $S.cm^{-1}$ [43]. Dans le commerce, l'encre Clevios PH1000, solution à base de PEDOT: PSS, a une conductivité supposée de 850 $S.cm^{-1}$. Enfin, il a été prouvé que ce polymère était biocompatible [44,45]. Parmi tous les choix de procédés de fabrication et de matériaux conducteurs possibles, j'ai choisi de travailler avec l'imprimante jet d'encre Dimatix DMP 2800, et l'encre PEDOT : PSS.

Ensuite, j'ai travaillé sur des substrats différents. Tout d'abord le **Kapton** qui est un film de polyimide créé par DuPont (Kapton 100HN). Il est thermiquement stable entre -269°C et 400°C, souple et résistant. Il est beaucoup utilisé pour la création de circuits électroniques souples ou en tant qu'isolant thermique dans l'aéronautique et l'automobile. Le Kapton n'est pas élastique mais est très résistant, souple et déjà intégré dans des processus de fabrication industrielle. En parallèle, j'ai travaillé sur d'autres substrats comme du **textile** qui est souple et assez agréable au contact de la peau. Cette solution permettrait d'incorporer des électrodes directement dans un vêtement ou un manchon de prothèses. Beaucoup de recherches se sont intéressées au textile mais à ma connaissance aucune application commerciale n'en a été faite. Ensuite, j'ai testé le support en **papier** qui est flexible mais pas étirable. Ce dernier nous a intéressés car il pourrait permettre la création d'électrodes jetables pour un faible coût. Enfin, nous nous sommes intéressés au papier **tattoo temporaire**. En effet, celui-ci peut fournir la meilleure conformation à la peau que l'on pourrait souhaiter, et il est fin et léger. Le problème avec ce dernier est sa connexion avec le système d'acquisition. Zucca et Bareket[46,47] ont utilisé un simple fil de cuivre placé entre les différentes couches de l'électrode tattoo pour le connecter. Cependant, une simple tension sur le fil de cuivre arrache le tattoo. Nous avons donc voulu tenter une autre approche en combinant l'électrode tattoo avec du textile. En effet, un des problèmes des électrodes textiles dans un manchon est que si une tension mécanique est appliquée au manchon, il se déforme. Ceci peut entraîner un déplacement de l'électrode par rapport au site que l'on veut mesurer. De plus, ces électrodes textiles ont bien souvent un mauvais contact avec la peau. Nous avons donc exploré l'utilisation des électrodes tattoo pour cibler la zone de mesure et en même temps améliorer le contact des électrodes textiles. On sait donc maintenant comment fabriquer une électrode et choisir le substrat. Cependant, dans le cadre de la création de matrice, d'autres questions entrent en jeu.

Comme on l'a vu dans la Section 2, la distance entre les électrodes et la position de celles-ci par rapport aux fibres musculaires et les jonctions neuromusculaires sont très importantes. Dans le cadre de matrices sEMG, la littérature s'est plutôt dirigée vers des distances inter-électrodes entre 5 mm et 1 cm [48–50]. En effet, cela semble offrir un bon compromis entre le volume de détection des couples d'électrodes et la résolution nécessaire à l'analyse des données dans le cadre de la détection des zones d'innervation. Dans notre cas, un problème se pose sur la forme et la taille de la matrice. En effet, il y a une importante disparité morphologique entre individus après une amputation du membre supérieur. La hauteur de l'amputation étant très variable entre les patients, il existe une différence de

taille de la musculature résiduelle. De plus, les muscles sont laissés libres au niveau distal et s'accrochent aux tissus environnants, donc ils se réarrangent de façons variables. Par conséquence, il est difficile de définir une matrice standard idéale pour tous les patients. Nous avons donc choisi plus ou moins arbitrairement une surface de 5x5 cm avec une distance inter électrode de 7mm. 4x7 électrodes sont présentes sur cette matrice. Si la taille des muscles résiduels l'exige, nous pourrons combiner plusieurs matrices.

4) Travail de la thèse

Durant ma thèse, j'ai développé et testé des électrodes. J'ai ensuite cherché à utiliser certaines de ces électrodes pour localiser les zones d'innervation de muscles du bras chez un sujet sain. Dans le Chapitre 2, nous développerons la fabrication et la caractérisation d'une matrice d'électrodes sur un support **Kapton**. Ce chapitre abordera aussi les premiers essais de localisation de zones d'innervation grâce à ces matrices. Dans les chapitres suivants, j'aborderai la fabrication et la caractérisation d'électrodes sur, respectivement, supports **textiles** (Chapitre 3), **papier** (Chapitre 4) et papier **tattoo temporaire** (Chapitre 5). Enfin, avant de discuter les résultats (Chapitre 7), nous nous attarderons sur les méthodes d'analyse permettant de détecter les zones d'innervation à partir de signaux sEMG et les essais préliminaires que nous avons menés (Chapitre 6).

II. Matrice d'électrodes flexibles imprimées pour la cartographie neuromusculaire

Ce chapitre présente la fabrication et la caractérisation d'une matrice d'électrodes à base de PEDOT:PSS sur un support souple Kapton par impression de jet d'encre. Comme précisé dans l'introduction (Chapitre 1), cette technologie d'impression a plusieurs avantages, comme l'absence de processus abrasif, la possibilité de rapidement changer une erreur de design, le temps de fabrication court. De plus, en tant que processus additif et sans contact, celui-ci peut facilement s'incorporer dans un processus de fabrication sur des substrats divers et pour un coût peu élevé. La mesure d'impédance électrochimique in vivo a permis de montrer la stabilité temporelle d'une matrice d'électrodes ainsi fabriquée. Grâce à ces impédances, nous avons pu proposer un circuit équivalent reflétant les caractéristiques électrochimiques de l'électrode en contact avec la peau. Nous avons ainsi mis en valeur que la résistance de transfert de charge reste stable durant les deux mois suivant la fabrication. La mesure de signaux sEMG et ECG a permis de valider que les matrices mesurent des signaux électrophysiologiques en surface de la peau de façon comparable à ceux obtenus avec des électrodes Ag/AgCl commerciales utilisant du gel conducteur. Finalement, les signaux sEMG obtenus grâce à ces matrices ont été utilisés pour localiser les zones d'innervation du muscle biceps bracchi. Cela suggère que les technologies sans contacts comme l'impression jet d'encre sont des technologies intéressantes dans le cadre de la fabrication de capteurs ultrafins multifonctionnels pour l'acquisition de grandeurs physiologiques.

Flexible Inkjet-Printed Multielectrode Arrays for Neuromuscular Cartography

*Timothée Roberts, Jozina B. De Graaf, Caroline Nicol, Thierry Hervé, Michel Fiocchi, and Sébastien Sanaur**

Flexible Poly(3,4-ethylenedioxythiophene)-poly(styrenesulfonate) (PEDOT:PSS) conductive-polymer multielectrode arrays (MEAs) are fabricated without etching or aggressive lift-off processes, only by additive solution processes. Inkjet printing technology has several advantages, such as a customized design and a rapid realization time, adaptability to different patients and to different applications. In particular, inkjet printing technology, as additive and "contactless" technology, can be easily inserted into various technological fabrication steps on different substrates at low cost. In vivo electrochemical impedance spectroscopy measurements show the time stability of such MEAs. An equivalent circuit model is established for such flexible cutaneous MEAs. It is shown that the charge transfer resistance remains the same, even two months after fabrication. Surface electromyography and electrocardiography measurements show that the PEDOT:PSS MEAs record electrophysiological activity signals that are comparable to those obtained with unitary Ag/AgCl commercial electrodes. Additionally, such MEAs offer parallel and simultaneous recordings on multiple locations at high surface density. It also proves its suitability to reconstruct an innervation zone map and opens new perspectives for a better control of amputee's myoelectric prostheses. The employment of additive technologies such as inkjet printing suggests that the integration of multifunctional sensors can improve the performances of ultraflexible brain-computer interfaces.

1. Introduction

1.1. Surface Electromyography (sEMG)

Surface electromyography (sEMG) signal is the electrical manifestation of the neuromuscular activation associated with a contracting muscle, which is commonly used to infer motor control strategies, and to assess neuromuscular alterations with fatigue and/or pathology.[1–4] It is a complex signal affected by many factors, among which the anatomical and physiological properties of the muscle-tendon unit as well as the characteristics of the instrumentation used to detect it.[5] In studies focusing on muscle coordination, sEMG recordings are generally used rather than invasive intramuscular recordings (via needle or wire) to provide more global and representative information about the activity of the whole muscle of interest.[6,7] Yet, muscle activity is not uniform over the muscle because of the heterogeneity in both muscle fiber distribution and orientation as well as of cross-talk and relative electrode shift with respect to the muscle.[8] Therefore, muscle cartography using multielectrodes arrays can provide more accurate information on muscle activity.[9]

In arm muscles, it has been suggested that multiple innervation zones may correspond to different groups of motor units that can become involved at different contraction force levels.[10,11] In arm amputees, recently performed sEMG recordings suggest focal and cyclic activation of specific volumes in residual arm muscles during cyclic phantom finger and wrist movements.[12] The association between focal sEMG activity and the executed phantom movement opens new perspectives of improvement in the control of the corresponding movement of myoelectric arm prostheses via multielectrode arrays. It has already been shown that increasing the electrode density gives more information about the sent motor commands and thus potentially gives

T. Roberts, Dr. J. B. De Graaf, Dr. C. Nicol
Institut des Sciences du Mouvement, CNRS
Aix Marseille Université
ISM UMR 7287
163, Avenue de Luminy, CP, 910
13288 Marseille Cedex 9, France
T. Roberts, Dr. T. Hervé
Microvitae Technologies
Hôtel Technologique
Europarc Sainte Victoire
Bâtiment 6 Route de Valbrillant, 13590 Meyreuil, France
M. Fiocchi, Dr. S. Sanaur
Department of Bioelectronics
Ecole Nationale Supérieure des Mines
CMP-EMSE, 880, route de Mimet
13541 Gardanne, France
E-mail: sebastien.sanaur@mines-stetienne.fr

DOI: 10.1002/adhm.201600108

more accurate myoelectric prosthesis control with a higher number of degrees of freedom.[13]

1.2. Electrodes and Materials for Neuromuscular Recordings

Such an application in prosthesis control could be possible if the multielectrode arrays are flexible, easily customable for patients and integrated into the socket of prostheses. Today, standard commercial electrodes used for surface electromyography are unitary packaged Ag/AgCl electrodes. These are metallic, rigid and usually require the application of a conductive gel in order to improve surface contact with the skin and decrease the electrode impedance in order to record long-time viable signals. An elegant solution for circumventing high impedance magnitudes is provided by enhancing the contact of the electrodes with the human body by using ultrathin, flexible, and, ideally, sticky and stretchable substrates on which electrodes are patterned.[16–20] Taking advantages of mechanical properties of flexible substrates, some emerging works currently use the mechanical deformation as a sensing parameter.[21,22] Yet, beyond substrate mechanical properties, the nature of the material forming the electrodes plays a key role in the impedance magnitude and the signal-to-noise ratio. Poly(3,4-ethylenedioxythiophene)-poly(styrenesulfonate) (PEDOT: PSS) conducting polymer as electrode material is potentially a good candidate for recording. Indeed, it is 'soft' and looks like thin film, dried material exhibiting high conductivity (around 1000 S cm^{-1}). It has already been used as unitary flexible electrodes (i) in electroencephalography[23] and (ii) in stable cutaneous impedance recording.[24]

For an application in prosthesis control with high-density recording, a high number of unitary Ag/AgCl skin-surface commercial electrodes would be required, leading to an important increase in the number of wires connecting the electrodes to the recording device interface. Moreover, given the thickness of current commercial surface electrodes, it is impossible to integrate the electrodes and the wires inside the socket of the prosthesis. To date, the socket is firmly attached to the residual limb by close skin contact in order not to lose it when forces are applied.

The technological challenges to overcome in myoelectric prostheses control directly call for sensors and electrodes integration.[15] In the particular case of prostheses for upper-limb amputees, the important variability in the level of amputation, and thus in the spatial localization of neural reorganization after surgery, requires individual probe-fabrication for each patient. This is not only true for the electrodes but also for the socket and the way of controlling the prostheses.[15] Thus, innovations in fabrication technology are required and should ideally increase the adaptability of the prosthesis to each individual patient without increasing the cost of it.

In the present paper, we report on the fabrication of flexible PEDOT: PSS multielectrode arrays (MEAs). We use inkjet printing technology as additive technology which gives (i) a rapid customized prototyping (from the electrodes design up to the fabrication of the multielectrode arrays), and (ii) the benefit of directly patterning electrodes on thin flexible foils at any desired location. Moreover, we validate the lifetime of such MEAs by electrochemical impedance spectroscopy (EIS) characterization on the skin of a healthy volunteer and by establishing its equivalent circuit model. In this study, we record and show electrocardiography (ECG) signals to standardize and prove the reliability of such MEAs. All measurements have been compared to those obtained with Ag/AgCl coated/gelled-electrodes (0.95 cm diameter), supplied from the AMBU (Ambu Blue Sensor N, N-00-S/25) company referenced later in this paper as commercial wet Ag/AgCl electrodes. Finally, this study aims to evaluate the capacity of these MEAs to localize main innervation zones on upper-limb muscles. The results obtained here provide new opportunities to use such PEDOT: PSS MEAs as a candidate for obtaining high resolution EMG recording from amputees' residual limbs.

2. PEDOT: PSS Multielectrode Arrays: Design and Realization

The MEA is composed by a 4 × 7 electrodes matrix onto polyimide foil for a total size of 100 × 50 mm^2. A 50 × 50 mm^2 active electrode surface is patterned onto polyimide plastic foil. In general, the size of the electrodes should be large enough to record a reasonable zone of motor units, but small enough to avoid crosstalk from others muscles. Then, on one end of the MEA, we integrated 28 connection pads, each 2.8 mm wide. In the center of the MEA, PEDOT: PSS active electrodes are patterned up to a 4 × 4 mm^2 area, separated by 2.8 mm distance within a column and by 9.5 mm distance within a row. In this design, the distance between interconnection lines is 700 µm; the width of the interconnection tracks is 300 µm. The polyimide substrate is 50 µm thick and exhibit elongation lower than 10% after a thermal treatment at 400 °C during 1 h.[25] In our fabrication process, such flexible foils are not undergoing annealing temperatures higher than 150 °C, so they do not suffer from any mechanical fragility. Our fabrication process mainly involves inkjet printing technology. Inkjet printing is a solution-process which provides fast and low cost design modification and fabrication. While losing in terms of surface density in comparison to other fabrication processes, the processing time is rapid and the waste of material very low. Moreover, inkjet printing technology resolution is good enough for such envisaged applications here.[26] Silver nanoparticle ink is patterned on top of the polyimide substrate as first low-resistivity layer providing: (i) the connection electrodes which are connected to the sEMG recording system, (ii) the interconnection tracks until electrodes location, and (iii) the basement for active electrodes sites. Directly after deposition, silver features are baked for 1 h at 150 °C and converted in low-resistivity thin films. Such silver features show good adhesion on polyimide foil since adhesive scotch-tape tests do not peel any silver layer. **Figure 1**a shows the full design of such a multielectrode array, incorporating the disposable connection pads, 300 µm wide tracks, and an array of 4 × 7 electrodes. Consecutively, commercial graphics ink is used (i) as electrical insulator and inkjet printed on top of the silver tracks in order to avoid crosstalk, short circuits and (ii) as an encapsulation layer in order to avoid oxidation of the bottom silver layer. Such photo sensitive ink is polymerized, cured, and dried by UV light exposure. At this step, inkjet printing gives the clear benefits of noncontact,

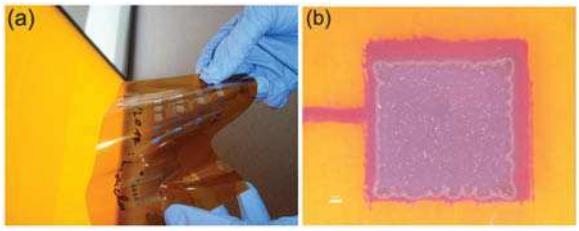

Figure 1. a) Inkjet-printed silver layer on 50 µm-thick polyimide foil. b) The inkjet-printed electrical insulator is covering the inkjet-printed silver bottom-layer. The white scale bar (left-bottom corner, similar size as the figure panel label) represents 400 µm.

mask-less and additive technique since the noncovering of the metallic parts is easily and directly generated in a single-pass fabrication, without any etching. Thus, the entire surface is covered by such an electrical insulator except at the electrode locations (Figure 1b) and where the MEAs are connected to the sEMG recording system. As is the case for the bottom silver layer, the encapsulation of the electrical insulator is robust and cannot be peeled-off by the scotch-tape test. Finally, the PEDOT: PSS solution is drop-casted on the top of the silver electrodes. PEDOT: PSS is then dried by placing the MEAs on a hot plate for 1 h at 100 °C. In such MEAs, the PEDOT: PSS layer is directly interfacing the skin. The Figure S1 (Supporting Information) shows the cross-section of the Kapton/ silver/ PEDOT: PSS layers, which are imaged by scanning electron microscopy (SEM). Tables S1–S3 (Supporting Information) indicate the atoms composition within the cross-section and allow us to distinguish every layer, as marked in the Figure S1 in the Supporting Information. The interfaces between each layer are smooth and explain the good adhesion properties. For the EIS measurements and the electrophysiological recordings (ECG and EMG), the MEAs was cut at the center of the 300 µm wide tracks and connected by using a laboratory homemade ZIF connector (Figure S2, Supporting Information).

3. Results and Discussion

3.1. Resistance Measurements

2-point probe measurements of resistance per length-unit are done along the silver tracks of the MEA from the electrodes sites to the disposable connection pads (Figure 1a). For each electrode, values of $1 \pm 0.1\ \Omega\ mm^{-1}$ have been found. A low resistance fluctuation for all the electrodes indicated a good reproducibility of the inkjet printing technique. After PEDOT: PSS deposition, no particular drop of resistance per length-unit is observed. Such stable resistance measurements are important to setup further sEMG recordings with a minimum fluctuation of resistivity.

3.2. In Vivo Electrochemical Impedance Spectroscopy

Electrochemical Impedance Spectroscopy (EIS) is directly performed on the surface of the skin of a healthy volunteer in

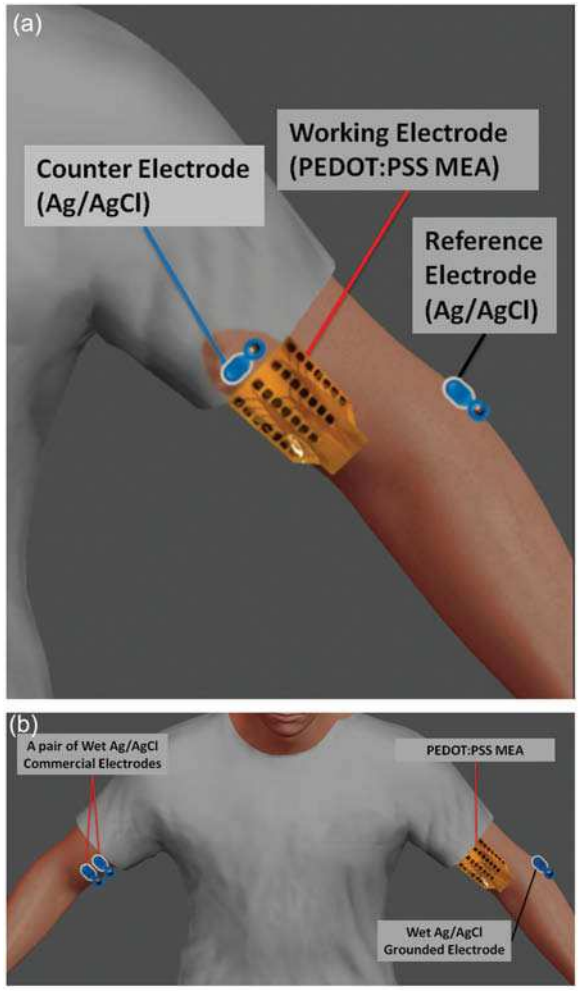

Figure 2. Schematic representation of the setups in in vivo conditions. a) Electrochemical impedance spectroscopy (EIS): One electrode of the PEDOT: PSS multielectrode array served as working electrode and is located in the center of the biceps; The counter and reference electrodes are located on the upper part of the biceps and in the proximal forearm, respectively. b) Surface electromyography (sEMG) recording: A pair of commercial wet Ag/AgCl electrodes located on the right biceps served as control measurements. Two pairs of PEDOT: PSS bipolar electrodes within the MEAs are recorded. The grounded electrode (commercial wet Ag/AgCl) is located on the proximal forearm.

order to gain more insight into the evolution of the impedance in *in vivo* conditions. The PEDOT: PSS multielectrode arrays are placed on the arm of the volunteer as shown in **Figure 2**a. One of its electrodes is used as the working (test) electrode. The setup of EIS measurements involves a three-electrode configuration where the reference and counter electrodes are single unitary Ag/AgCl commercial gelled-electrodes (0.95 cm diameter), supplied from the AMBU (Ambu Blue Sensor N, N-00-S/25) company. An equivalent electrical circuit is established. Numerous papers describe the equivalent electrical circuit both for Ag/AgCl as working electrode [27–29] and for PEDOT: PSS in presence of liquid electrolyte.[30–35] To our knowledge, an equivalent circuit was never described for the PEDOT: PSS in case of a direct and a "dry" contact with the skin.

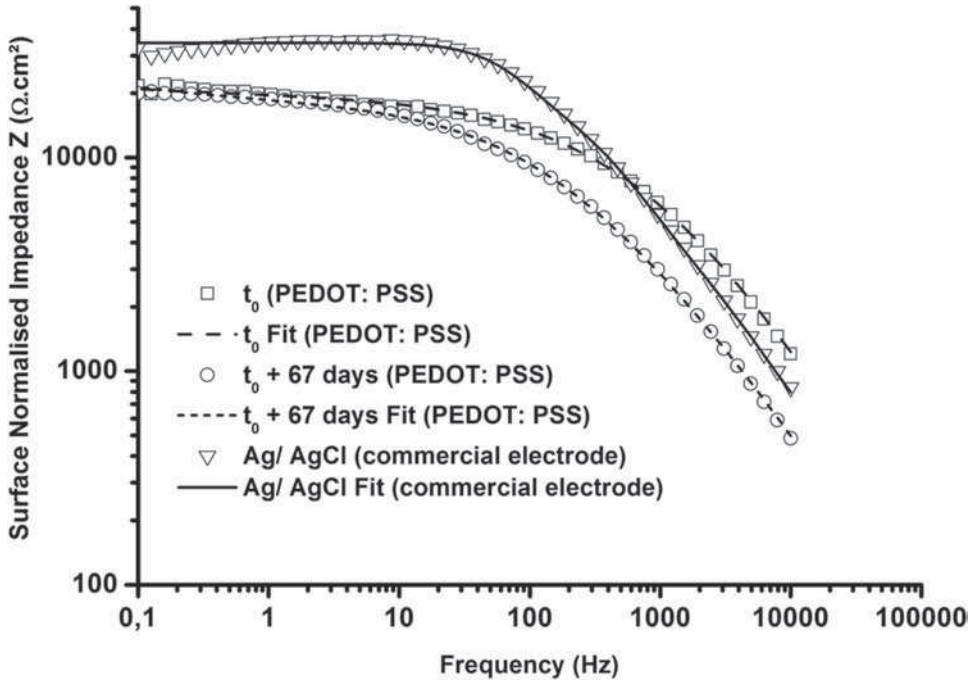

Figure 3. Bode plot: electrochemical impedance as a function of frequency. Comparison between a PEDOT: PSS electrode (at different lifetimes) and a wet Ag/AgCl commercial electrode.

Figure 3 displays a Bode plot representing the absolute value of the total impedance Z normalized to the surface area (in cm^2) of each electrode as a function of the frequency (from 0.1 Hz to 10 kHz). Figure 3 shows the surface-normalized Z impedance of i) PEDOT: PSS electrodes at different time intervals, and ii) commercial wet Ag/AgCl electrodes. Ag/AgCl electrodes display higher impedances. The PEDOT: PSS multielectrode arrays show impedance stability along the time. Indeed, no drastic evolution is observed 67 days after fabrication. Interestingly, at frequencies higher than 10 Hz, the impedance of the aged PEDOT: PSS electrodes (after 67 days) are lower than "fresh" PEDOT: PSS ones. We assume here that the PEDOT: PSS is filled by water coming from the surrounding atmospheric environment and is thus swelled-up. We assume that this PEDOT: PSS swelling phenomenon has the consequence to increase the thickness of the PEDOT: PSS layer[36] and thus to expand or facilitate the exchange between ions and the conducting polymer backbone (PEDOT), explaining the decrease in impedance. As additional information, a similar multielectrode array made of silver active electrodes without PEDOT: PSS has been tested by EIS. But, the inkjet-printed silver sites oxidized during EIS measurements and no recordings were possible to obtain. Such configuration without PEDOT: PSS can thus be excluded for further sEMG recording. The frequency interval of interest for EMG recording is comprised between 10 Hz and 450 Hz. In that interval, "fresh" and aged PEDOT: PSS MEAs record lower impedance than Ag/AgCl wet commercial electrodes. Previous reports have dealt with such cutaneous electrodes for electrophysiological recordings.[37,38] These ones were driven with different healthy volunteers, different temperature conditions, and with or without use of a conductive gel. At a frequency of 1 kHz, Leleux et al. and[37] Isik et al.[38] reported an impedance of 6.4×10^3 and 3×10^3 Ω cm ^{2} with ionic liquid gel, respectively. Here, we report 3×10^3 Ω cm ^{2} without the use of a gel. Interestingly, such normalized impedances are all in the same order of magnitude in spite of different working conditions.

The Bode phase plot gives a general view of the electrodes behavior (Figure S3, Supporting Information). Indeed, electrodes show a conductive behavior for $0° < \Theta_{phase} < 45°$ and a capacitive behavior for $45° < \Theta_{phase} < 90°$.[39] When freshly fabricated, PEDOT: PSS electrode switches its behavior around a frequency of 1 kHz. Below 1 kHz, such electrodes are working in a conductive mode. But 67 days after fabrication, the transitory frequency is shifted-down to 300 Hz. As a comparison, the commercial wet Ag/AgCl electrodes have a transitory behavior at 100 Hz (Figure S3, Supporting Information). So, 67 days after fabrication, the PEDOT: PSS electrodes remain in a conductive mode, especially in comparison to the commercial wet Ag/AgCl electrodes.

Numerous previous studies reported equivalent circuit models to describe impedance behavior of conducting polymers bioelectrodes.[30–35] All these cases involve an electrolyte at the interface with conducting polymers. Here, such cutaneous electrodes do not involve electrolyte. The model presented in this work is consistent with the experimental data and is comprising of i) a conducting polymer coating capacitance (C_C), ii) a double layer interface capacitance (Z_{CPE}), iii) a charge transfer resistance (Rct), and iv) a finite diffusion impedance (Z_W) (Figure S5, Supporting Information). **Table 1** synthesizes the extracted parameters. A direct comparison of EIS measurements done right after fabrication or after 67 days shows that the charge transfer resistance (R_{ct}) is not evolving; this indicates a good stability in time for delivering electronic current. Constant phase

Table 1. Equivalent circuit model of the PEDOT: PSS electrode–skin interface. The working electrode is PEDOT: PSS.

Measurement time	Drop-casted PEDOT: PSS				
	C_C [nF]	Z_{CPE}	Z_W [$\mu\Omega^{-1}$]	R_{ct} [kΩ]	χ^2
t_0 (PEDOT: PSS)	1.4	$Y_0 = 176$ nΩ^{-1}, $N = 0.508$	$Y_0 = 126$	125	0.04
t_0 + 67d (PEDOT: PSS)	3.39	$Y_0 = 246$ nΩ^{-1}, $N = 0.563$	$Y_0 = 50$	117	0.037

C_C: Coating capacitance. Z_{CPE}: Constant phase element $\left(Z_{CPE} = \frac{1}{Y_0(j\omega)^N}\right)$ where Y_0 is the admittance (Ω^{-1}), N is the value of the exponent of the constant phase element and $\omega = 2\pi f$ is the angular frequency with f the frequency. Z_W: Warburg impedance $\left(Z_W = \frac{1}{Y_0\sqrt{j\omega}}\right)$. R_{ct}: Charge transfer resistance. χ^2: Nonlinear least-squares fitting coefficient.

element impedance (Z_{CPE}) relates the interface capacitance as a combination of the double layer capacitance (Helmoltz capacitance) and the diffuse layer capacitance (Gouy–Chapman capacitance). Right after fabrication or 67 days after fabrication, PEDOT: PSS MEAs show quite balanced diffusion (resistive) and capacitive behavior ($N = 0.508$ and $N = 0.563$, respectively, in Table 1). Interestingly, the same model tested without Z_{CPE} impedance results in a highest fitting coefficient (χ^2). In the case of these cutaneous electrodes, a double layer interface is created by insertion of water or humidity between the skin and the electrode, which thus follows such Guy–Chapman–Stern theoretical prediction. The Warburg impedance (Z_W) gives additional diffusional impedance to the model. Warburg impedance has a typical fingerprint which is shown in Figure S4 in the Supporting Information by a linear track in the Nyquist plot. Admittance (Y_0) from Warburg impedance is lowering after 67 days but remains in the same order of magnitude (Table 1).

3.3. Electrocardiography Recording

In electrophysiological applications, an ECG signal is a vital parameter which is recorded to show the relevant working of the electrodes. Here, such PEDOT: PSS MEAs recorded ECG signals (**Figure 4**) in a healthy volunteer. In the experiment setup, one PEDOT: PSS MEAs is placed on the left wrist as the positive input of the bipolar measurement while two Ag/AgCl commercial gelled-electrodes (0.95 cm diameter), supplied from the AMBU (Ambu Blue Sensor N, N-00-S/25) company are placed i) on the right wrist as the negative input of the bipolar measurement, and ii) on the right foot as a grounded common reference electrode, respectively. In a second time, as a control experiment, an additional recording is done by replacing the PEDOT: PSS MEAs with a commercial Ag/AgCl electrode. Figure 4 shows a 5 s time-interval of such ECG recordings from the same volunteer. The ECG signals are similar and clearly show the PQRST complexes that the physicians and cardiologists practically exploit in their diagnosis. Being a good marker for signal amplitude, a root-mean-square (RMS) analysis has been done on the entire recording. These analyses show the same results with 121 µV for the PEDOT: PSS electrode recording against 87 µV for the wet commercial Ag/AgCl electrodes. Both RMS values are close to 100 µV, showing that both signals are pretty similar in terms of sensed amplitude. This result is linked to the results of the electrochemical impedance measurement (Figure 3) where it shows that both impedances for frequencies below 500 Hz are close to each other. These results prove thus that these PEDOT: PSS MEAs are suitable for others *in vivo* electrophysiological applications.

3.4. Neuromuscular Recording

sEMG recordings were done by using the same PEDOT: PSS MEAs on a healthy volunteer. Figure 2b represents the measurement setup. Two PEDOT: PSS electrode sites on the left upper arm were used in comparison with two Ag/AgCl commercial gelled-electrodes (0.95 cm diameter), supplied from the AMBU (Ambu Blue Sensor N, N-00-S/25) company, located on the right upper arm for the control condition. As explained before, the silver-based multielectrode array was oxidized during the EIS measurement and thus not used in this in-vivo sEMG recording. Two sEMG recordings are shown in Figure S7 in the Supporting Information, one at the center of the PEDOT: PSS MEAs (Figure S7a, Supporting Information) and one from the wet Ag/AgCl electrode (Figure S7b, Supporting Information). While the surface is smaller, the sEMG signal amplitude recorded from the PEDOT: PSS MEAs electrode is similar, even a bit higher, than the one recorded from the wet commercial electrodes. The recorded frequency contents are also comparable, as confirmed by a fast Fourier tansform (Figure S8, Supporting Information).

The calculated signal-to-noise ratio (SNR) validates the recordings quality. The SNRs show comparable recordings. Indeed, the SNRs obtained for the PEDOT: PSS electrode is 24.8 dB against 26.7 dB for the wet Ag/AgCl commercial electrode. Here, the SNRs are calculated for each recording using the formula described in the Experimental Section. Two intervals of each recording were selected with and without muscular activity in order to compare the "signal" recording from the "noise" recording.

One year after such unitary recordings, the neuromuscular cartography of the biceps from a healthy volunteer has been performed. Such recordings are done (i) to validate such MEAs as potential electrodes capable of commanding the movements of arm-prostheses and (ii) to map the innervation zones which are reconstructed after surgery on upper-limb amputees. Thus, 16 simultaneous bipolar acquisitions are recorded by using a PEDOT: PSS MEAs on the left arm biceps. The **Figure 5**a indicates the location on the biceps of such PEDOT: PSS MEAs which stick to the skin simply by humidifying it. A grounded common reference electrode is located on the elbow using a commercial wet Ag/AgCl electrode. After 5 s of rest, eight quick contractions are realized and followed by one long contraction. The Figure S9 (Supporting Information) shows the resulting

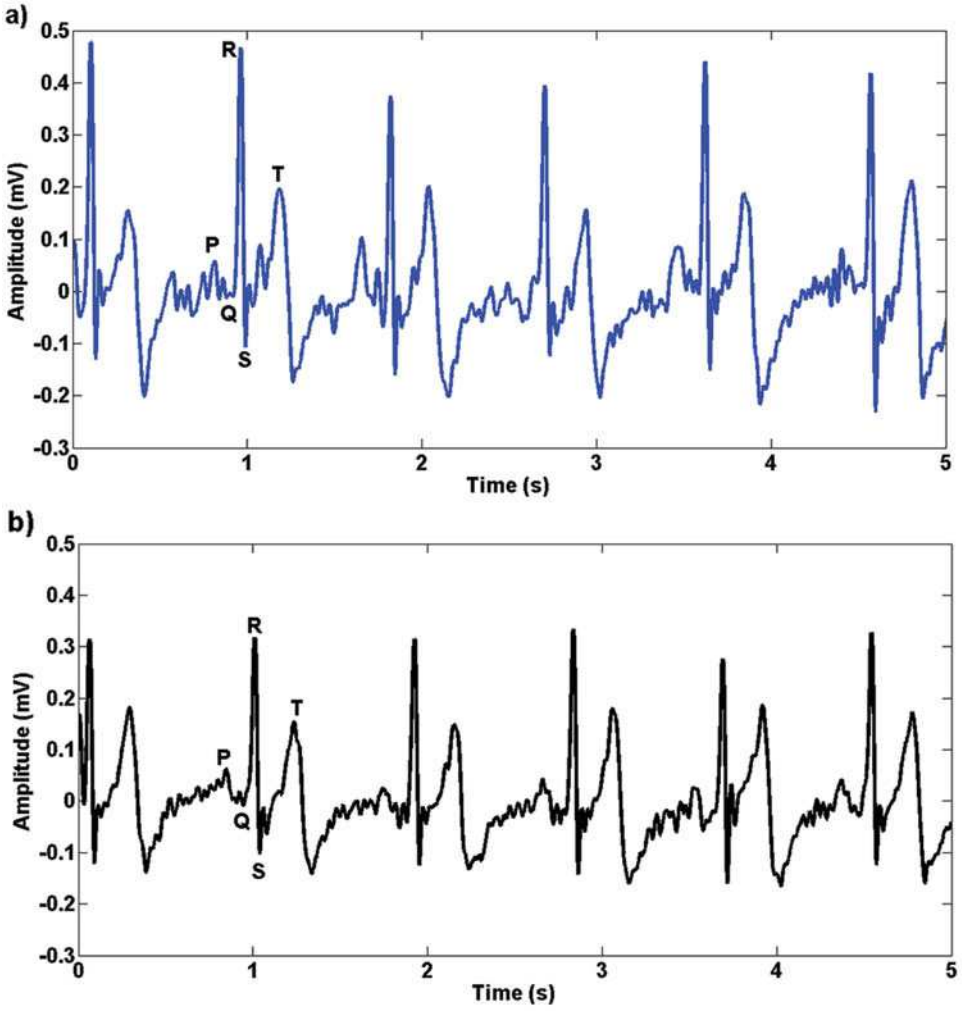

Figure 4. ECG signals recorded by a) PEDOT: PSS electrodes and b) by a pair of commercial wet Ag/AgCl electrodes, respectively.

sEMG recordings. The Figure 5b shows how the sEMG bipolar measurements are spatially linked to the location of each electrode on the MEAs. The square between two electrodes represents a node in the MEAs and particularly displays the RMS calculated value at this node (Figure 5b). By calculating the RMS values from these sEMG recordings, the position of the innervations zones can be located (Figure 5b). Indeed, the innervations zones are supposed to present the lowest RMS value along a group of muscle fibers. Such RMS calculation is reported in detail in the Experimental Section. The mapping

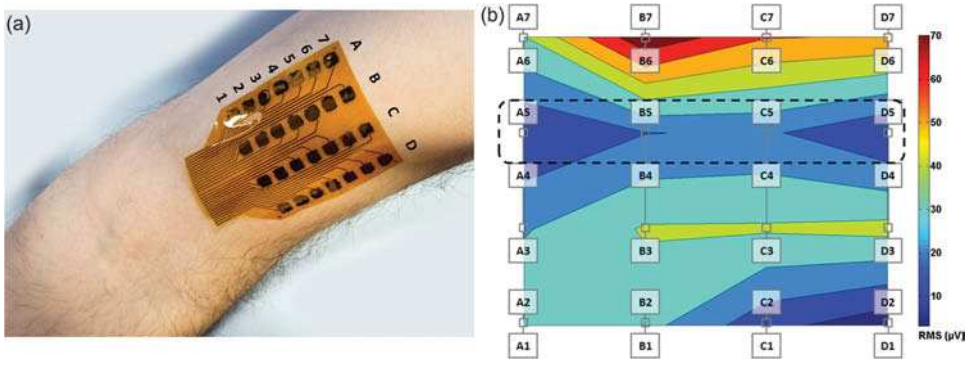

Figure 5. Recording of biceps muscle activity using a PEDOT: PSS multielectrode array (MEA) consisting of 28 electrodes. a) Photo showing the position of the flexible MEA sticking to the upper arm. b) Cartography of the RMS values. Note the symmetry of the EMG amplitude around the main innervations zone at the expected line 5 (as marked by a black dotted rectangle).

(Figure 5b) shows that the amplitudes are smaller in the columns A and D (on the edge of the MEA) than in the columns B and C (in the center of the MEA). This can be explained by the highest proportion of muscle fibers which are located in the center of the MEAs. A spatial distortion can be observed around line 4 which is due to the fact that these electrodes were used in two different bipolar EMG recordings, contrary to the other electrodes. The RMS value being equally spaced on the Figure 5b, the electrodes position looks thus distorted on the mapping. But more interestingly, by analyzing the results column by column and by comparing the values of each line, the approximate innervations zones location can be estimated around the 5th line. According to the location of the MEAs on the muscle,[40] this result is in accordance with the approximate position of innervations zones which are functioning on a normal healthy patient.

4. Conclusion

We fabricated flexible conducting polymer PEDOT: PSS multielectrode arrays without etching or aggressive lift-off processes, only by additive solution processes. Inkjet printing technology is the additive technology that we use here and has several advantages, such as a customized design and a rapid realization time, adaptability to different patients and for different applications. In particular, inkjet printing technology, as additive and 'contactless' technology, can be easily inserted into various technological fabrication steps on different substrates at low cost. In vivo EIS measurements show the time stability of such MEAs. An equivalent circuit model is established for such flexible cutaneous PEDOT: PSS MEAs. By this model, we show that the charge transfer resistance remains the same, even two months after fabrication. Surface electromyography and electrocardiography measurements show that the PEDOT: PSS MEAs record electrophysiological activities with signals comparable to those obtained with unitary wet Ag/AgCl commercial electrodes. Additionally, such PEDOT: PSS MEAs offer parallel and simultaneous recordings on multiple locations at high surface density for such applications. It also proves its suitability to reconstruct a mapping of the innervations zones and opens new perspectives for a better control of amputee's myoelectric prostheses. The employment of additive technologies such as inkjet printing suggests that the integration of multifunctional sensors could improve the performances of ultraflexible brain-computer-interfaces.

5. Experimental Section

sEMG MEA Fabrication: Multielectrode arrays were fabricated on 50 µm-thick polyimide foils, provided by DuPont (100HN Kapton). Such 50 µm-thick foils are thin enough to be flexible. Before the whole fabrication process, the foils were cleaned by O_2 plasma at low power for 2 min. The silver conductive tracks and the insulating/encapsulation layer were inkjet-printed using a DMP-2800 Dimatix printer. Relevant parameters for high inkjet-printing quality are, among others, the pulse voltage, the drop spacing, the waveform settings, the cartridge temperature, anthe d substrate temperature during printing. First, by using the drop watcher, the waveform settings were optimized. Waveform settings are composed of four segments. The first one is used to fill the chamber. A subsequent voltage pulse decreases the volume of the ink chamber and increases the pressure in the ink chamber, thereby ejecting a droplet from the ink chamber. A third segment is used as a recovery step before falling to the resting potential of the forth segment; it avoids the air to go inside the nozzle and to clog the latter. Conductive ink is composed of DGP HR-A silver nanoparticle dispersions, obtained from Advanced NAnoPROducts (ANAPRO). After silver printing, the samples were baked at 150 °C for 15 min. The U9054 insulating/encapsulation ink was supplied by the Sun Chemical company and was used to prevent short-circuits between silver interconnection lines. The insulating ink was dried and polymerized by UV light for 5 min at 920 W. A layer of PEDOT: PSS conducting polymer was used as interface between the silver layer and the skin. A volume of 8 µL of PEDOT: PSS conducting polymer was drop-casted. PEDOT: PSS was then baked at 110 °C for 1 h. The PEDOT: PSS conducting polymer dispersion is composed of 20 mL of PEDOT: PSS (Clevios PH1000-Heraeus), 1 mL of ethylene glycol (10% v/v) (Sigma–Aldrich), 2 droplets of dodecylbenzenesulfonic acid, and 0.2 mL of (3-Glycidyloxypropyl) trimethoxysilane.

Sample Preparation for the SEM Cross Section: The Figure S1 (Supporting Information) was imaged by an Ultra 55 microscope from Carl Zeiss company. Such SEM tool includes an energy dispersive X-ray (EDX) detector from Oxford company. The EDX cartography allowed the element microanalysis (Tables S1, S2, and S3, Supporting Information). The PEDOT: PSS MEAs were bonded on a metallic part which is copper double-sided. The whole part thus constituted was coated by a rigid transparent resin. Finally, such sample was cut by a diamond saw blade and polished manually by a felt and a finishing product (0.3 and 0.05 µm size particles).

In Vivo Electrochemical Impedance Spectroscopy Measurements: The setup used for EIS measurement is presented in the Figure 2a and involves a 3-electrode configuration with two types of electrodes. The working electrodes were fabricated as previously presented in the sEMG MEA fabrication experimental section. The counter-electrode and the reference electrode used in this experiment are Ag/AgCl commercial gelled-electrodes (0.95 cm diameter), supplied from the AMBU (Ambu Blue Sensor N, N-00-S/25) company. The measurements were done by using a potentiostat (Autolab with a FRA module, Metrohm B. V.) and the associated software NOVA (v 1.8.17). The NOVA software was then used to develop the equivalent circuit model. EIS was done according to the following parameters: no constant differential voltage was applied; a sinusoidal signal was applied with 10 mV rms amplitude and a frequency sweep from 0.1 Hz to 10 kHz.

Signal to Noise Ratio (SNR): Synchronized contractions of the left and right biceps brachii muscles were recorded by the help of a pair of Ag/AgCl commercial gelled-electrodes (0.95 cm diameter), supplied from the AMBU (Ambu Blue Sensor N, N-00-S/25) company on one side and the inkjet-printed MEAs on the other side. An Eego mylab amplifier from ANT Neuro was used to record the signals. Two commercial electrodes, located 2 cm apart center (according to the standard recommendations), were positioned over the biceps muscle of the right arm in order to record a control signal. A PEDOT: PSS multielectrode array was placed on the left arm at the same location on the biceps muscle. A signal was recorded on one pair of the PEDOT: PSS electrode at the center of the matrix, each placed 0.7 cm apart, center to center. Finally, a third commercial wet Ag/AgCl electrode was placed on the left elbow and grounded to a known potential for common mode rejection. A Matlab script was used for the signal processing (filtering), displaying the signal, and calculating the SNR. The signal processing is composed of a 4th order type I Chebyshev band-pass filter with a low cut-off frequency of 10 Hz and a high cut-off frequency of 300 Hz, and a 4th order notch filter at 50 Hz. The SNR value of the signal was extracted with help of the snr() function of Matlab. This function calculates the RMS value of the signal of interest signal divided by the RMS value of noise

$$SNR(signal, noise) = 20\log\sqrt{\left(\frac{mean(signal^2)}{mean(noise^2)}\right)}$$

The SNRs were calculated using this formula in order to compare the EMG signal from the PEDOT: PSS electrodes to the EMG signal from

the commercial wet Ag/AgCl electrodes. Two intervals of each recording were selected: one with muscular activity which is the "signal" in the formula and another one with no muscular activity as the "noise".

Biopotential (ECG and EMG) Recordings: ECG and EMG signals were recorded in order to evaluate the PEDOT: PSS array. An ECG signal was measured by placing the array on the left wrist as the positive input of a bipolar measurement. Two Ag/AgCl commercial gelled-electrodes (0.95 cm diameter), supplied from the AMBU (Ambu Blue Sensor N, N-00-S/25) company were used, one on the right wrist as the negative input for all bipolar measurement and one on the right foot as the grounded reference electrode common for all recordings. In a second time, the MEA was replaced by a commercial wet Ag/AgCl electrode for comparison. A fourth order Chebyshev band-pass filter going from 0.01 to 40 Hz is used to filter the signals. For comparison purposes, a RMS value was calculated

$$RMS(signal) = \sqrt{mean(signal^2)}$$

We determined the RMS over an interval of 10s. Then, an EMG measurement was done placing the PEDOT: PSS array on the left arm in the middle of the muscle bundle as shown in Figure 2b. EMG signals are often measured using standard bipolar sEMG. The position of such electrodes is determined by following the general guidelines which were developed in the 'Surface ElectroMyoGraphy for the Non-Invasive Assessment of Muscles' (SENIAM) project.[40] The electrodes are positioned (i) with respect to the longitudinal location, halfway of the most distal motor endplate zone and the distal tendon, and (ii) with respect to the transversal location, away from the edge. A grounded common reference electrode was placed on the left elbow using a commercial wet Ag/AgCl electrode.

Cartography of Neuromuscular Activity by sEMG: The signal processing was similar to the one done in the previous unitary sEMG measurements (Figure S7, Supporting Information). Here, 16 bipolar measurements were recorded simultaneously. Four bipolar inputs were allocated for each column of seven electrodes. The 4th electrode of each column is used by two bipolar measurements. A RMS value was calculated for each bipolar measurement in order to have an estimation of the position of the innervations zone location. In this case, the RMS value was calculated from a portion of the signal containing muscle activity.

Supporting Information

Supporting Information is available from the Wiley Online Library or from the author.

Acknowledgments

This work was supported by a DefiSens CNRS 2013 Grant No. 75114, through the ReorgAmp project. The authors would also like to acknowledge Franck Eirmbter (from Sun Chemical company) who gave us free samples of U9054 UV ink that is used in the present paper. The authors would like to thank Paolo Musardo for preparation of cross section sample and for imaging by SEM.

Received: January 30, 2016
Revised: March 14, 2016
Published online: April 29, 2016

[1] C. J. De Luca, *Crit. Rev. Biomed. Eng.* **1984**, *11*, 251.
[2] R. Merletti, M. Knafilitz, C. J. De Luca, *J. Appl. Physiol.* **1990**, *69*, 1810.
[3] R. Merletti, D. Farina, M. Gazzoni, M. P. Schieroni, *Muscle Nerve* **2002**, *25*, 65.
[4] D. Farina, M. Gazzoni, R. Merletti, *J. Electromyogr Kinesiol.* **2003**, *13*, 319.
[5] J. V. Basmajian, C. J. De Luca, *Muscles Alive: Their Functions Revealed by Electromyography*, 5th ed., Williams & Wilkins, Baltimore, USA **1985**.
[6] C. Frigo, R. Shiavi, *Applications in Movement and Gait Analysis, Electromyography: Physiology, Engineering and Noninvasive Applications*, Wiley, Hoboken, USA **2004**.
[7] A. Holtermann, K. Roeleveld, J. S. Karlsson, *J. Electromyogr. Kinesiol.* **2005**, *15*, 131.
[8] F. Hug, *J. Electromyogr. Kinesiol.* **2011**, *21*, 1.
[9] S. Man, C. Cescon, T. Vieira, S. Herle, G. Lazea, R. Merletti, *E-Health and Bioengineering Conference (EHB)*, IEEE, USA, 24–26 Nov. **2011**.
[10] T. Masuda, H. Miyano, T. Sadoyama, *IEEE Trans. Biomed. Eng.* **1985**, *32*, 36.
[11] T. Rantalainen, A. Kłodowski, H. Piitulainen, *J. Electromyogr. Kinesiol.* **2012**, *22*, 80.
[12] J. B. De Graaf, N. Jarrassé, C. Nicol, A. Touillet, J. Paysant, presented at *ESPRMSOFMER (CO11-002 Presentation)*, Marseille, France, 26–31 May **2014**.
[13] M. Rojas-Martínez, M. A. Mañanas, J. F. Alonso, R. Merletti, *J. Electromyogr. Kinesiol.* **2013**, *23*, 33.
[14] P. Zhou, M. M. Lowery, K. B. Englehart, H. Huang, G. Li, L. Hargrove, J. P. A. Dewald, T. A. Kuiken, *J. Neurophysiol.* **2007**, *98*, 2974.
[15] C. Castellini, P. Artemiadis, M. Wininger, A. Ajoudani, M. Alimusaj, A. Bicchi, B. Caputo, W. Craelius, S. Dosen, K. Englehart, D. Farina, A. Gijsberts, S. B. Godfrey, L. Hargrove, M. Ison, T. Kuiken, M. Markovi, P. M. Pilarski, R. Rupp, E. Scheme, *Front. Neurorobot.* **2014**, *8*, 22.
[16] D. Khodagholy, T. Doublet, M. Gurfinkel, P. Quilichini, E. Ismailova, P. Leleux, T. Herve, S. Sanaur, C. Bernard, G. G. Malliaras, *Adv. Mater.* **2011**, *23*, H268.
[17] A. Campana, T. Cramer, D. T. Simon, M. Berggren, F. Biscarini, *Adv. Mater.* **2014**, *26*, 3874.
[18] G. A. Salvatore, N. Munzenrieder, T. Kinkeldei, L. Petti, C. Zysset, I. Strebel, L. Buthe, G. Tröster, *Nat. Commun.* **2014**, *5*, 2982.
[19] J. Viventi, D. H. Kim, L. Vigeland, E. S. Frechette, J. A. Blanco, Y. S. Kim, A. E. Avrin, V. R. Tiruvadi, S. W. Hwang, A. C. Vanleer, D. F. Wulsin, K. Davis, C. E. Gelber, L. Palmer, J. Van der Spiegel, J. Wu, J. L. Xiao, Y. G. Huang, D. Contreras, J. A. Rogers, B. Litt, *Nat. Neurosci.* **2011**, *14*, 1599.
[20] X. Huang, Y. Liu, H. Cheng, W. Shin, J. A. Fan, Z. Liu, C-J. Lu, G-W. Kong, K. Chen, D. Patnaik, S-H. Lee, S. Hage-Ali, Y. Huang, J. A. Rogers, *Adv. Funct. Mater.* **2014**, *24*, 3846.
[21] M. Segev-Bar, H. Haick, *ACS Nano* **2013**, *7*, 8366.
[22] M. Segev-Bar, G. Konvalina, H. Haick, *Adv. Mater.* **2015**, *27*, 1779.
[23] P. Leleux, J. M. Badier, J. Rivnay, C. Bénar, T. Herve, P. Chauvel, G. G. Malliaras, *Adv. Healthcare Mater.* **2013**, *3*, 490.
[24] P. Leleux, C. Johnson, X. Strakosas, J. Rivnay, T. Herve, R. M. Owens, G. G. Malliaras, *Adv. Healthcare Mater.* **2014**, *3*, 1377.
[25] Dupont™ Kapton® polyimide film: General descriptions, http://www.dupont.com/content/dam/assets/products-and-services/membranes-films/assets/DEC-Kapton-general-specs.pdf.
[26] R. G. Scalisi, M. Paleari, A. Favetto, M. Stoppa, P. Ariano, P. Pandolfi, A. Chiolerio, *Org. Electron.* **2015**, *18*, 89.
[27] Y. M. Chi, T-P. Jung, G. Cauwenberghs, *IEEE Rev. Biomed. Eng.* **2010**, *3*, 106.
[28] L-F. Wang, J.-Q. Liu, B. Yang, C.-S. Yang, *IEEE Sens. J.* **2012**, *12*, 2898.
[29] N. Meziane, J. G. Webster, M. Attari, A. J. Nimunkar, *Physiol. Meas.* **2013**, *34*, R47.

[30] J. Bobacka, A. Lewenstam, A. Ivaska, *J. Electroanal. Chem.* **2000**, *489*, 17.
[31] X. Y. Cui, D. C. Martin, *Sens. Actuators, B* **2003**, *89*, 92.
[32] J. Y. Yang, D. C. Martin, *Sens. Actuators, A* **2004**, *113*, 204.
[33] P. Danielsson, J. Bobacka, A. Ivaska, *J. Solid State Electrochem.* **2004**, *8*, 809.
[34] L. Koene, W. J. Hamer, J. H. W. De Wit, *J. Appl. Electrochem.* **2006**, *36*, 545.
[35] M. Abidian, D. Martin, *Biomaterials* **2008**, *29*, 1273.
[36] E. Stavrinidou, P. Leleux, H. Rajaona, D. Khodagholy, J. Rivnay, M. Lindau, S. Sanaur, G. G. Malliaras, *Adv. Mater.* **2013**, *25*, 4488.
[37] P. Leleux, C. Johnson, X. Strakosas, J. Rivnay, T. Herve, R. M. Owens, G. G. Malliaras, *Adv. Healthcare Mater.* **2014**, *3*, 1377.
[38] M. Isik, T. Lonjaret, H. Sardon, R. Marcilla, T. Herve, G. G. Malliaras, E. Ismailova, D. Mecerreyes, *J. Mater. Chem. C* **2015**, *3*, 8942.
[39] S. Cotrone, M. Ambrico, H. Toss, M. D. Angione, M. Magliulo, A. Mallardi, M. Berggren, G. Palazzo, G. Horowitz, T. Ligonzo, L. Torsi, *Org. Electron.* **2012**, *13*, 638.
[40] H. J. Hermens, B. Freriks, C. Disselhorst-Klug, G. Rau, *J. Electromyogr. Kinesiol.* **2000**, *10*, 361.

ADVANCED HEALTHCARE MATERIALS

Supporting Information

for *Adv. Healthcare Mater.,* DOI: 10.1002/adhm.201600108

Flexible Inkjet-Printed Multielectrode Arrays for Neuromuscular Cartography

*Timothée Roberts, Jozina B. De Graaf, Caroline Nicol, Thierry Hervé, Michel Fiocchi, and Sébastien Sanaur**

Supporting Information

Flexible inkjet-printed multi-electrode arrays for neuromuscular cartography

Timothée Roberts, Jozina B. De Graaf, Caroline Nicol, Thierry Herve, Michel Fiocchi, Sébastien Sanaur*

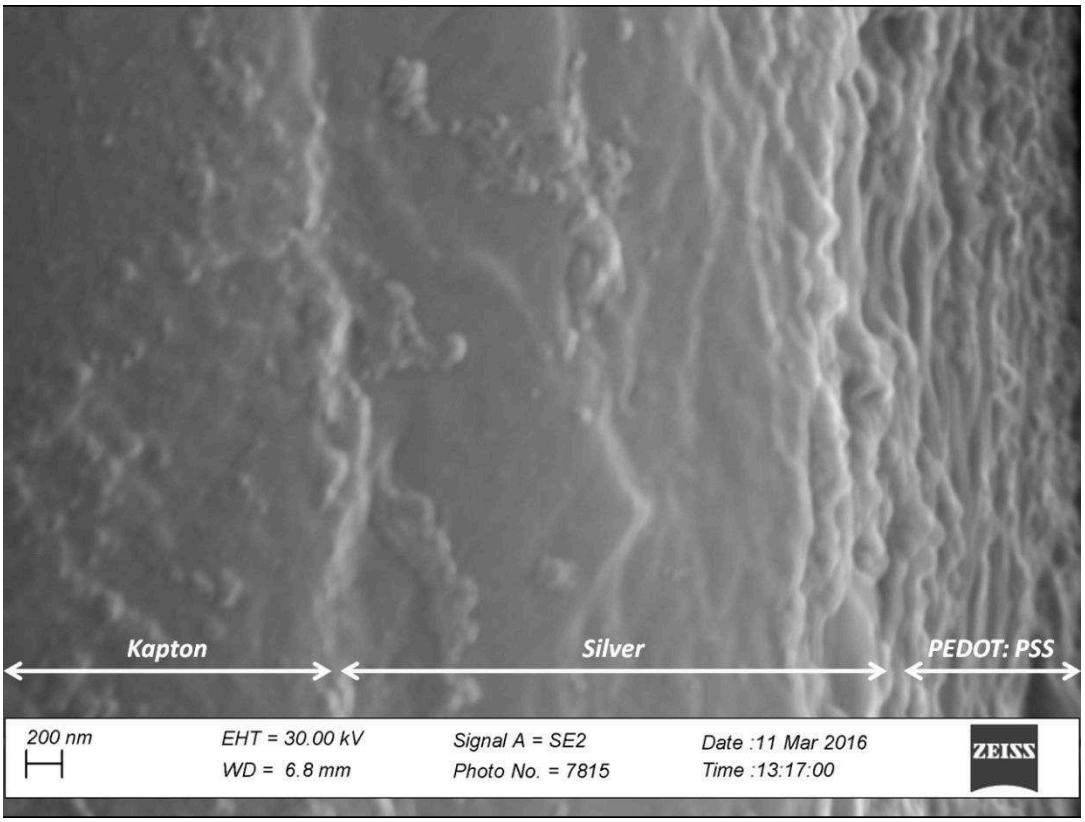

Figure S1: SEM cross-section of PEDOT : PSS MEAs. The arrows in the picture indicates the different layers.

Element	% mass	% atoms
Carbon	64.03	73.68
Oxygen	29.10	25.14
Sulphur	0.24	0.10
Chlorine	0.73	0.28
Calcium	0.17	0.06
Silver	5.72	0.73
Total	100	---

Table S1: Mass and atoms percentages of elements in the Kapton layer. Such percentages are measured by Energy Dispersive X-ray (EDX) microanalysis.

Element	% mass	% atoms
Oxygen	55.54	85.88
Sulphur	3.00	2.32
Chlorine	2.87	2.00
Calcium	2.45	1.52
Silver	36.14	8.29
Total	100	---

Table S2: Mass and atoms percentages of elements in the Silver (Ag) layer. Such percentages are easured by Energy Dispersive X-ray (EDX) micranalysis.

Element	% mass	% atoms
Carbon	57.66	67.99
Oxygen	33.67	29.81
Aluminium	0.60	0.31
Sulphur	1.62	0.72
Chlorine	0.50	0.20
Calcium	0.83	0.29
Silver	5.12	0.67
Total	100	---

Table S3: Mass and atoms percentages of elements in the PEDOT : PSS layer. Such percentages are measured by Energy Dispersive X-ray (EDX) microanalysis.

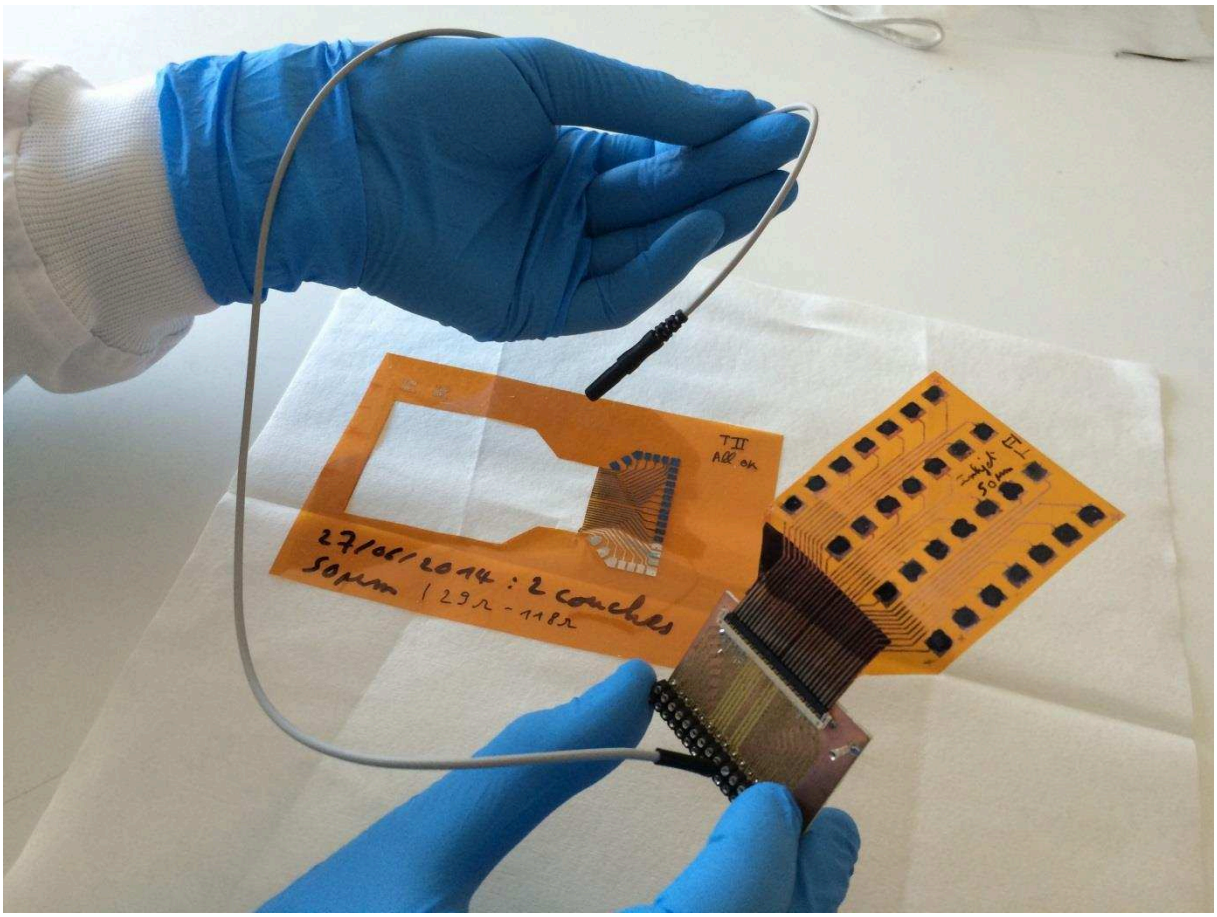

Figure S2: The inkjet-printed flexible multi-electrode arrays used for Electrochemical Impedance Spectroscopy (EIS) measurements, ElectroCardiography (ECG) and surface ElectroMyoGraphy (sEMG) recordings.

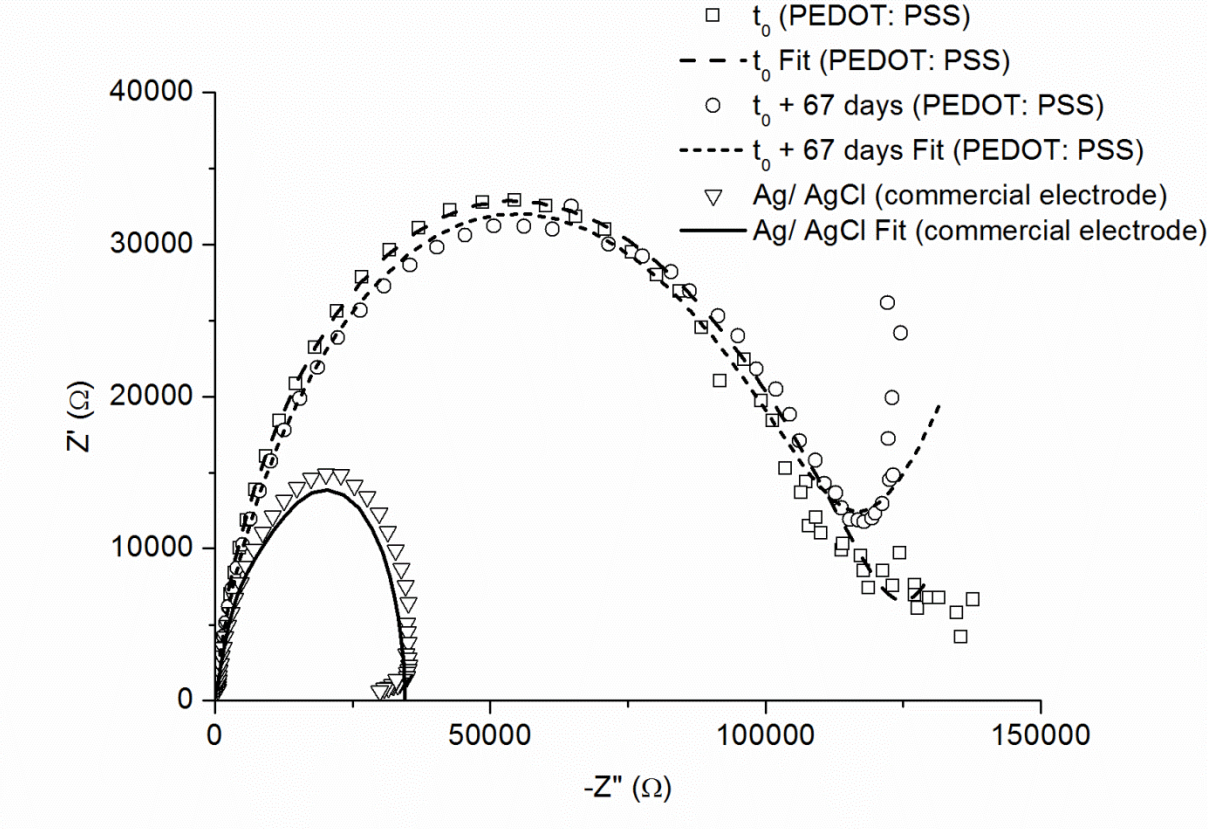

Figure S3: Electrochemical Bode phase plot as a function of frequency. Comparison of PEDOT: PSS electrodes (at different lifetimes) with wet Ag/AgCl commercial electrode.

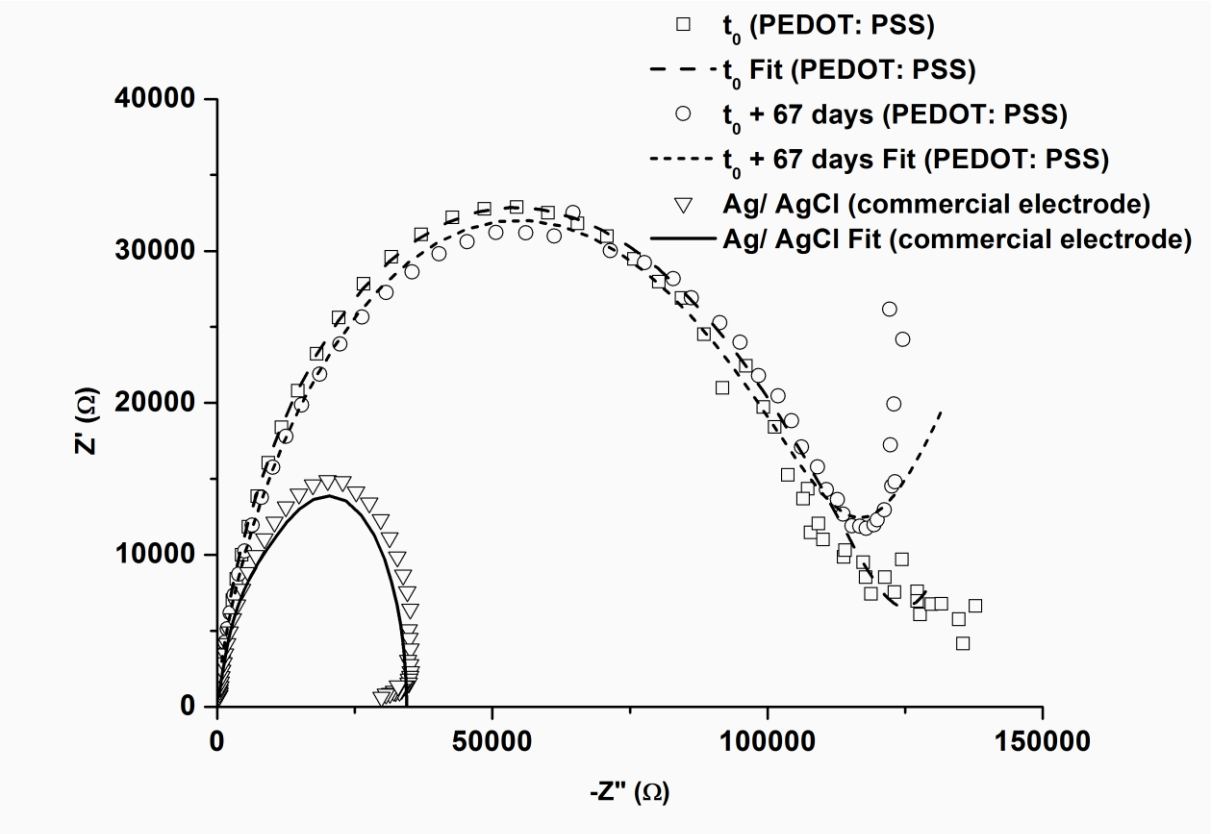

Figure S4: Nyquist plot as a function of frequency. Comparison of PEDOT: PSS electrodes (at different lifetimes with wet Ag/AgCl commercial electrode.

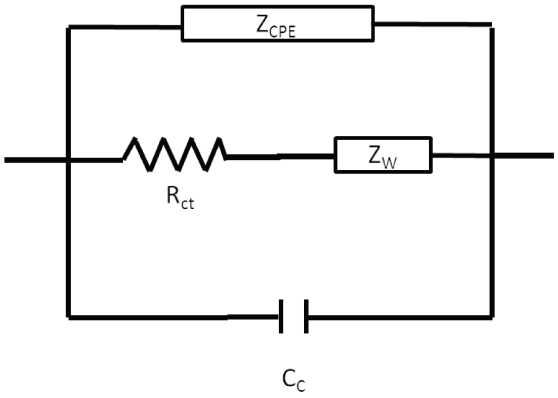

Figure S5: Schematic representation of the equivalent circuit model used to fit the Electrochemical Impedance Spectroscopy (EIS) data of the PEDOT: PSS electrode - skin interface. The global behavior is driven by the PEDOT: PSS electrochemical behavior. C_C: coating capacitance. Z_{CPE}: constant phase element ($Z_{CPE} = \frac{1}{Y_0(j\omega)^N}$) where Y_0 is the admittance (Ω^{-1}), N is the value of the exponent of the constant phase element and where $\omega=2\pi f$ is the angular frequency. Z_W: Warburg impedance ($Z_W = \frac{1}{Y_0\sqrt{j\omega}}$) where Y_0 is the admittance (Ω^{-1}) and $\omega=2\pi f$ is the angular frequency and f the frequency. R_{ct}: charge transfer resistance.

Working Electrode (W.E)						Reference Electrode (R.E)			χ^2
Conductive gel	Ag/AgCl electrode		Electrode/skin interface	Human body		Conductive gel	Ag/AgCl electrode		
R_{gel} (Ω)	$R_{electrode}$ (Ω)	$C_{electrode}$ (nF)	$R_{interface}$ (Ω)	R_{body} (kΩ)	C_{body} (nF)	R_{gel} (Ω)	$R_{electrode}$ (kΩ)	$C_{electrode}$ (nF)	
117	944	62.2	67	8.72	51.8	117	24.5	102	0.19

Table S4: Equivalent circuit model of a wet Ag/AgCl commercial electro-skin interface.

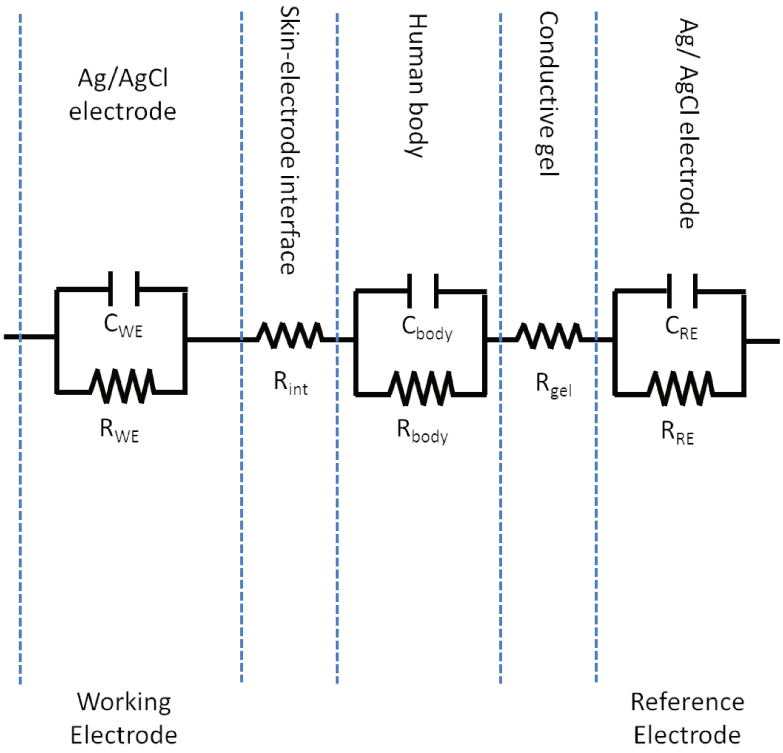

Figure S6: Schematic representation of the equivalent circuit model used to fit the Electrochemical Impedance Spectroscopy (EIS) data of commercial unitary wet Ag/agCl electrodes.

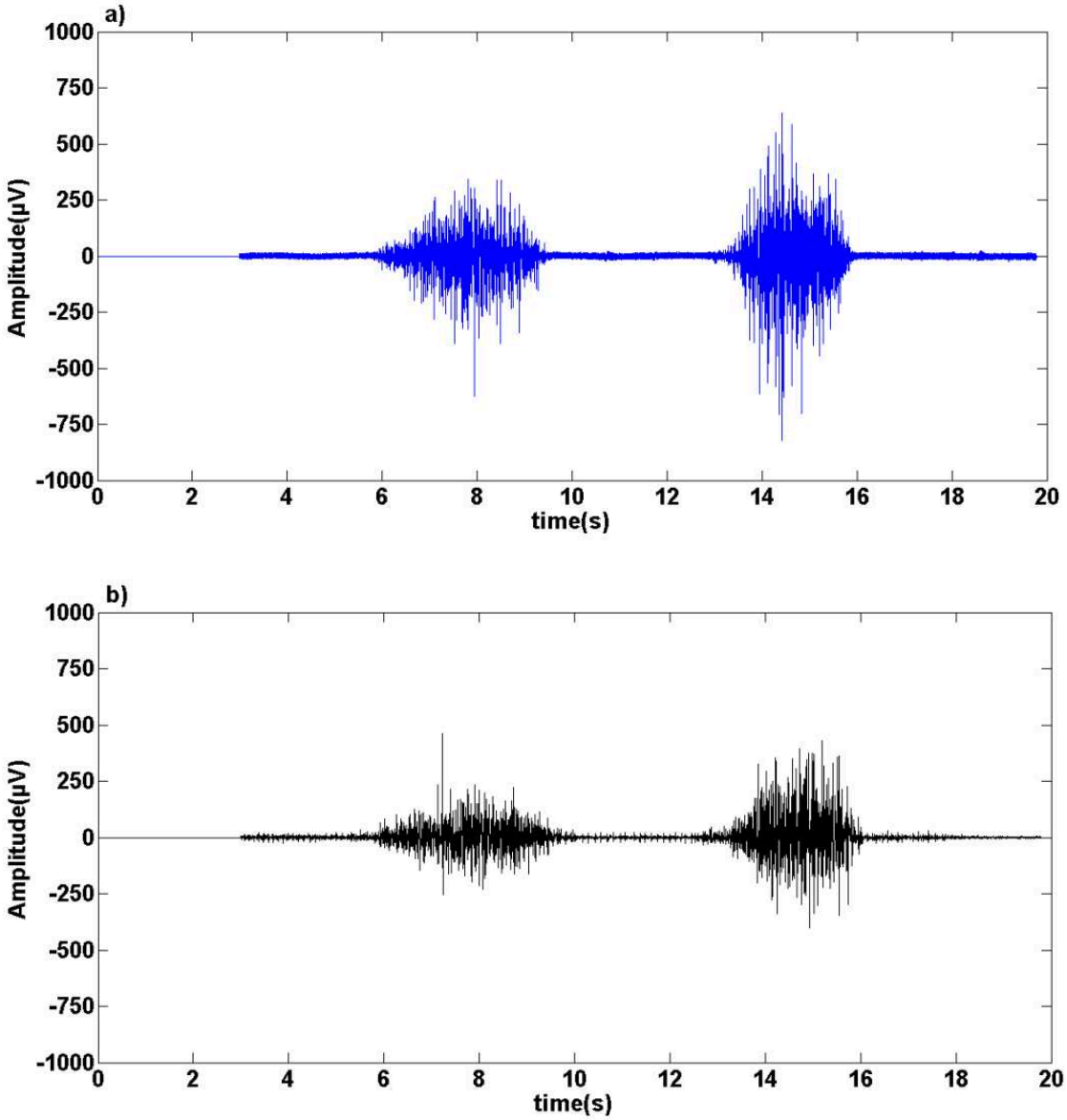

Figure S7: Surface ElectroMyoGraphy (sEMG) recordings with a PEDOT:PSS pair of electrodes (a), and with commercial wet Ag/AgCl control pair of electrodes (b).

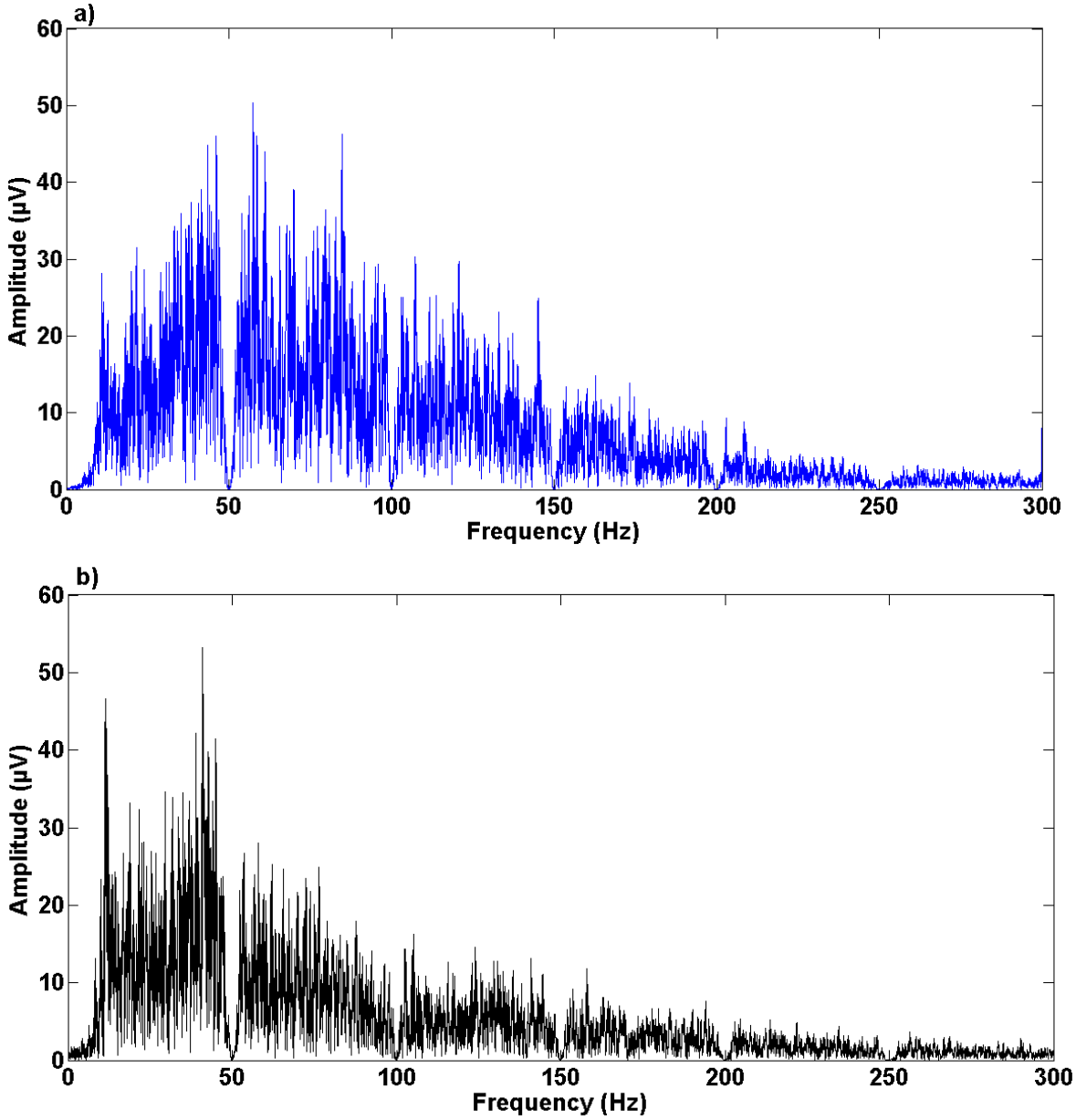

Figure S8: Fast Fourier Anlaysis (FFT) of the sEMG signals recorded with a PEDOT:PSS pair of electrodes (a), and with commercial wet Ag/AgCl control pair of electrodes (b)

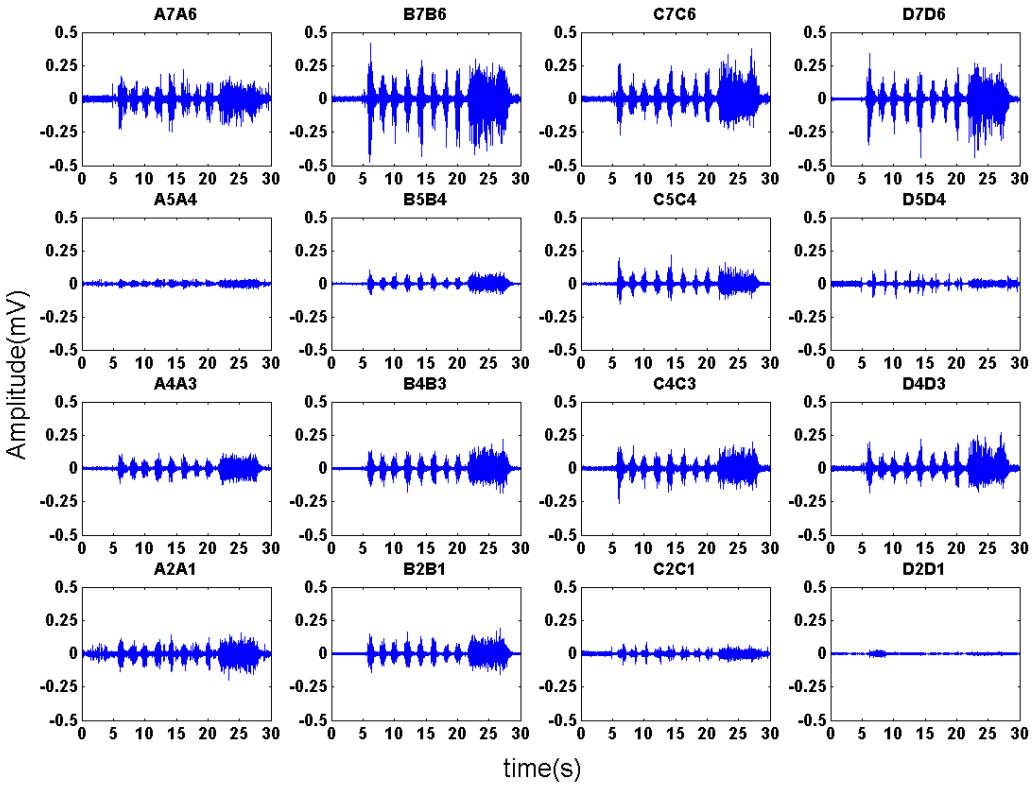

Figure S9: 16 simultaneous sEMG signals, recorded by using a 28 PEDOT: PSS multi-electrode arrays.

III. Impression d'électrodes à base de PEDOT : PSS sur du papier pour l'électrocardiographie

Dans ce chapitre, la fabrication d'électrodes par impression jet d'encre sur du papier sera abordée. Des tests mécaniques ont permis de vérifier la durabilité de telles électrodes. La mesure d'impédance électrochimique de ces électrodes et l'utilisation de ces électrodes pour mesurer des ECG ont permis de prouver leur viabilité pour mesurer des grandeurs électrophysiologiques en surface de la peau. Ces électrodes ont ensuite permis de mesurer des signaux ECG durant 3 mois sans pertes significatives de performance. Ces travaux suggèrent la fabrication simple d'électrode jetable peu coûteuse, sans métaux et avec un impact écologique potentiellement intéressant.

Inkjet-Printed PEDOT:PSS Electrodes on Paper for Electrocardiography

*Eloïse Bihar, Timothée Roberts, Mohamed Saadaoui, Thierry Hervé, Jozina B. De Graaf, and George G. Malliaras**

Cardiovascular diseases (CVDs) are the leading cause of deaths, with more than 610 000 cases per year in the United States alone, and are responsible for over 30% of the deaths in the world.[1] These illnesses are worldwide problems that concern both industrialized and developing countries. From 2010 to 2030, the associated medical costs are predicted to increase by a factor three.[2] This problem is compounded by other factors such as tobacco, alcohol or obesity, which increase the risks of developing CVDs. In many cases, early detection could prevent fatality but in many countries CVDs are detected late as a result of difficult access to preventative healthcare programs. Therefore, low cost, easy-to-use detection methods are of tremendous value in identifying early diseases such as heart failure. Currently, the detection of electrophysiological signals, including those stemming from cardiac activity, in clinical and research applications is realized using conventional electrodes. These are mostly made of Ag/AgCl layer, coated with conducting gel that is used to reduce the impedance at the electrode/skin interface. These electrodes are disposable, lead to a good recorded signal quality, but present several limitations.[3–5] For instance, the irritation coming from the adhesive used to ensure a good contact between the electrode and the skin can induce allergies/intolerances. Moreover, these electrodes exhibit poor performance in long-term monitoring mostly due to the drying of the gel. Finally, even the use of a gel does not adequately prevent motion artifacts in some applications.

E. Bihar, Prof. G. G. Malliaras
Department of Bioelectronics
Ecole Nationale Supérieure des Mines
CMP-EMSE
MOC, 880 Route de Mimet, 13541 Gardanne, France
E-mail: malliaras@emse.fr
E. Bihar, T. Roberts, Dr. T. Hervé
Microvitae Technologies
Hôtel Technologique
Europarc Sainte Victoire
Bâtiment 6 Route de Valbrillant, 13590 Meyreuil, France
E. Bihar, Dr. M. Saadaoui
Department of Flexible Electronics
Ecole Nationale Supérieure des Mines
CMP-EMSE
MOC, 880 Route de Mimet, 13541 Gardanne, France
T. Roberts, Dr. J. B. De Graaf
Aix Marseille Univ
CNRS, ISM
Marseille, France

DOI: 10.1002/adhm.201601167

Several works have focused on the development of dry electrodes that avoid problems associated with the drying of the gel.[4–7] These studies explored the feasibility of long-term measurements of cutaneous electrophysiological signals without inducing skin irritation,[4] and with a minimal influence from motion artifacts.[6] Other studies explored the feasibility of integrating conducting materials into textiles to fabricate wearable electrodes for electrocardiography (ECG) or electromyography.[8–10] Various technologies were used to pattern the conducting layer such as printing of metallic inks,[7,8] or a technique inspired by the dying of kimonos to deposit organic conductors.[9] Indeed, conducting polymers such as poly(3,4-ethylenedioxythiophene) doped with poly(styrene sulfonate) (PEDOT:PSS) are being widely studied these last few years for applications in bioelectronics due to their ease of processing, mixed electronic/ionic conductivity, and biocompatibility.[10,11] PEDOT:PSS, in particular, has been receiving a great deal of attention as a promising material for advanced transducers for cutaneous electrophysiology.[12,13]

Recently, the use of inkjet printing to make electrodes for ECG acquisition was reported.[14,15] These studies showed encouraging results using electrodes printed from metallic inks, opening new perspectives for printed electronics applications. Indeed, inkjet printing is an additive technology, which does not require the use of masks or additional manufacturing steps, and minimizes materials waste. It combines the possibilities to easily customize the printed pattern and to tune layer thickness by the deposition of single or multiple layers.[16] In this paper, we report the fabrication of fully inkjet-printed, metal-free electrodes using a commercial paper as an eco-friendly and recyclable substrate, and a biocompatible conducting polymer, PEDOT:PSS, as the active material. We show that printing a single layer of PEDOT:PSS ink on a commercial paper allows the measurement of ECG from a human volunteer by simply contacting the electrodes with his/her fingers. We compared the performance of electrodes consisting of one, two, and three printed layers in terms of recording quality over a period of three months, and in terms of electrochemical impedance to the skin. This work paves the way for the development of economical, ecological, and convenient-to-use ECG-based diagnostics.

We selected a commercial paper as the substrate for the electrode, as it is eco-friendly and recyclable. Three electrodes, consisting of one, two, and three layers of the conducting polymer PEDOT:PSS, were deposited side-by-side on a piece of paper as shown in **Figure 1**a. The corresponding average thicknesses were 85, 170, and 280 nm, while the roughness remained constant around 60 nm (same as for the uncoated

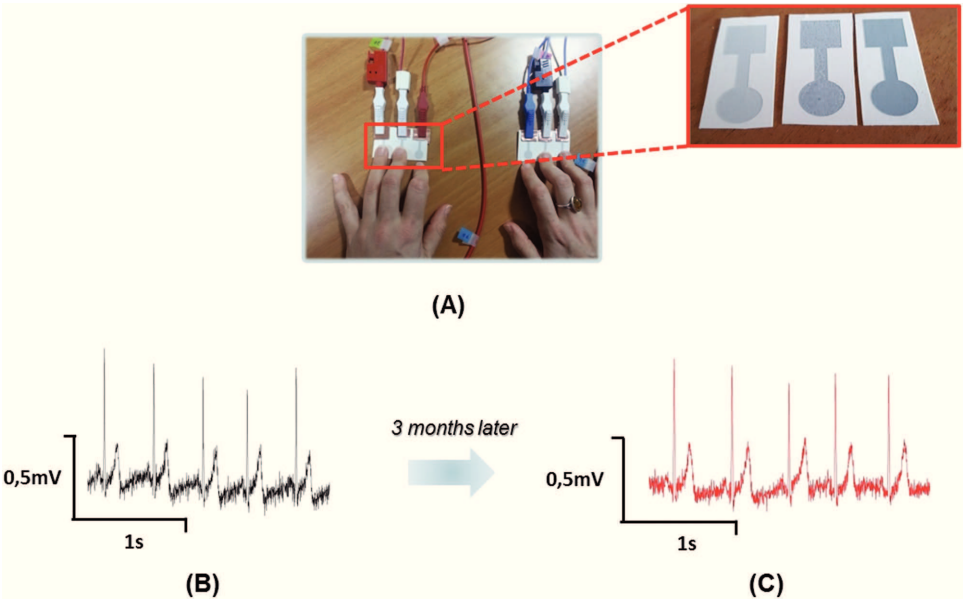

Figure 1. A) Photograph of printed PEDOT:PSS electrodes on a commercial paper with a zoom on individual electrodes consisting of one to three layers. Associated ECG measurements for a printed electrode (one layer) B) soon after fabrication and C) after three months.

paper). Each electrode consisted of a disk with a diameter of 1 cm (similar to the dimensions of a conventional Ag/AgCl electrode), connected to a 1×1 cm^2 contact pad area, as shown in Figure S1 (Supporting Information). The electrodes were connected to the acquisition system using toothless alligator clips and copper foil. A volunteer placed his/her hands on two pieces of paper containing electrodes, establishing contact with electrodes consisting of one layer with his/her ring fingers, electrodes consisting of two layers with his/her middle fingers, and electrodes consisting of three layers with his/her index fingers. Figure 1b shows the signal measured from a set of electrodes consisting of one printed layer (ring fingers), allowing to distinguishing clearly the specific electrical waves of the heartbeat such as the QT intervals. This signal is of adequate quality to detect CVD related anomalies such as arrhythmias. A measurement repeated three months later is displayed in Figure 1c, showing no visible signal deterioration during this period. It should be noted that the measured signal showed no significant variation on the force applied by the fingers. Indeed, signals recorded under two different conditions (quantified by a force sensing resistor, mounted under the electrodes and registering a weight of 10 g and 1 kg, respectively) were indistinguishable.

In order to better quantify the stability the electrodes, measurements were repeated approximately once a week for a period of three months. Three simultaneous recordings were conducted for each type of electrode (one, two, three layers) and repeated twice per session. In total, six ECG acquisitions of 1 min per electrode types were run every week. **Figure 2** shows the evolution of the mean signal-to-noise ratio (SNR) per electrode type. The data shows that the signal quality stays contrast as a function of time. At the same time, no visible changes to the electrodes were detected. The data also shows that SNR increases slightly with the number of depositions used to make the recording electrodes. Indeed, the mean SNR values that corresponds to all measurements obtained within a three months period by the electrode consisting of one layer was 10.28 ± 0.62 dB. This value increases to 10.79 ± 0.61 dB and to 11.01 ± 0.41 dB, for recordings obtained by electrodes consisting of two and three layers, respectively.

In order to understand this increase we performed electrochemical impedance spectroscopy measurements and characterized the contact between electrode and skin. We placed the electrodes on the arm of the volunteer as drawn in Figure S3 (Supporting Information). The printed electrode was used as the working electrode, while commercial wet Ag/AgCl electrodes were used as counter and reference electrodes. The data shows that the electrode/skin impedance decreases slightly with the number of layers printed. For example, at 1 Hz, the impedance drops from 1.40×10^6 Ohm for a one-layer electrode, to 1.26×10^6 Ohm for a two-layer electrode, to 1.17×10^6 Ohm for

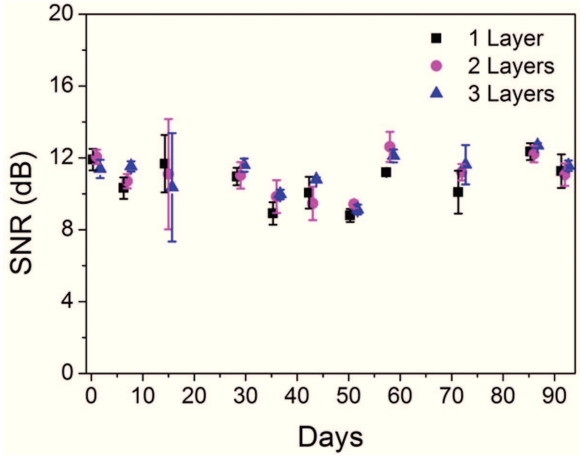

Figure 2. Mean signal-to-noise ratio (SNR) of ECG signals over time for PEDOT:PSS electrodes consisting of one, two, and three layers, $n = 6$.

a three-layer electrode. Decomposing the impedance in resistance and reactance, yields values of 1.22×10^6, 1.11×10^6, and 1.04×10^6 Ohm for the resistance, and -7.03×10^5, -5.87×10^5, and -5.26×10^5 Ohm for the reactance of films with one, two, and three printed layers, respectively. This analysis shows that the decrease in impedance with PEDOT:PSS thickness arises from a simultaneous decrease of sheet resistance (Figure S1, Supporting Information) and increase in capacitance. The latter is known to be volumetric in PEDOT:PSS.[17]

Compared to commercial and state-of-the-art textile electrodes reported in literature, the printed electrodes show an impedance that is approximately one order of magnitude higher (at 1 Hz).[9] This can be attributed to a combination of a lower conductivity, and poorer mechanical and electrical contact due to the limited flexibility of the paper substrate and the absence of a gel. Despite their high impedance, the electrodes provide high-quality ECG recordings in a convenient testing format. Moreover, this is a format that is resistant to deformation. Indeed, bending experiments of electrodes with dimensions of 5×1 cm^2 and consisting of one layer (Figure S2, Supporting Information) showed no significant change in electrode resistance after more than 2000 cycles.

In addition to applications in the diagnosis of CVDs, various other physiological phenomena/conditions can be extracted from the analysis of electrocardiograms. One example is breathing. This is done by monitoring variations in the RS amplitude, which increases and decreases during inhalation and exhalation, respectively.[18] Using the same electrodes and experimental setup, we lengthened the acquisition time to two minutes and asked the volunteer to stabilize his/her breathing. Typical data are displayed in **Figure 3**, showing the variation of the RS amplitude and of the corresponding signal envelope. Breathing is easily noticeable and shows that data obtained from the printed electrodes are of high enough quality to allow analysis of RS amplitudes.

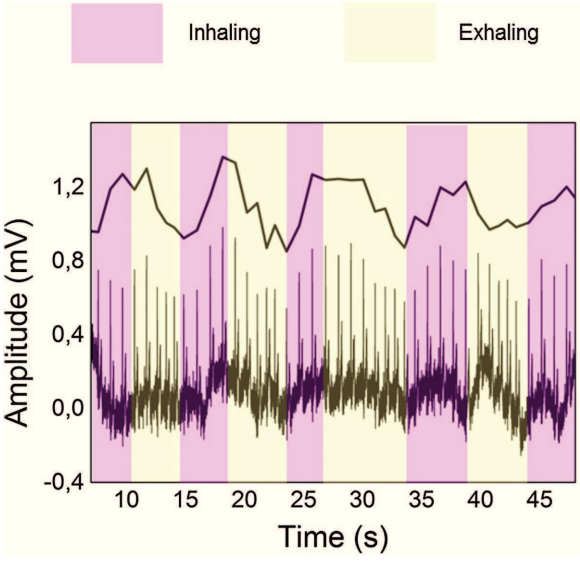

Figure 3. Breathing detection from ECG measurement using PEDOT:PSS electrodes consisting of one layer.

The electrodes described here could be easily used with an external device such as a smartphone to obtain electrophysiological signals. Their performance makes them suitable for a single or multiple uses. Being paper-based and metal-free, they could be easily integrated in a recycling process with a limited impact on the environment. Finally, a potential application of ECG that is currently receiving a great deal of attention is authentication.[19] Indeed, features extracted from electrocardiograms were shown to be independent of electrode location, invariant to the individual's anxiety state, and unique to the individual.[20] One, for example, can envision printing electrodes on a smart credit card that authenticating the owner based on the recorded ECG. Experiments that demonstrate this concept are ongoing.

In this work, we demonstrate inkjet-printed conducting polymer electrodes on paper for applications in electrocardiography. Electrocardiograms were obtained by simply placing two fingers on the electrodes. The recordings exhibited good signal quality, which remained stable over a period of three months. This work paves the way for the facile and cost-effective fabrication of metal-free medical electrodes on paper with a reduced number of manufacturing steps. As a result, it may help deliver convenient-to-use and inexpensive tools for the prevention of cardiovascular diseases.

Experimental Section

PEDOT:PSS Ink: The PEDOT:PSS ink was formulated from a commercially available PEDOT:PSS (Heraeus, Clevios PH1000) dispersion, with the addition of 20 wt% ethylene glycol (Sigma Aldrich) and organic solvents. 0.8 wt% glycidoxypropyltrimethoxysilane (Sigma Aldrich) and 0.3% proprietary surfactants were added to the ink to avoid delamination and to match the rheological requirements of the ink with the inkjet printer.

Inkjet Printing: A Dimatix DMP-2800 inkjet printer was used to print the electrodes onto a coated paper (Powercoat HD by Arjo-wiggins, Inc.) of thickness of 200 µm. We printed one, two, and three layers of PEDOT:PSS, and we cured the samples in a conventional oven for 30 min at 160 °C. The dimensions of the electrodes are shown in Figure S1 (Supporting Information). The thickness of the films was measured with a mechanical profilometer (Ambios Technology) and found to be 85 ± 5, 170 ± 5, and 280 ± 5 nm, for one, two, and three printed layers, respectively. Roughness was measured using an atomic force microscope (AFM) (Veeco/SP-II) over a 50×50 µm^2 area. Surface coverage was 100% as seen by optical micrographs.

Electrochemical Impedance Spectroscopy: Impedance measurements were performed using an Autolab potentiostat (Metrohm Autolab B.V.), and the associated software NOVA. No constant differential voltage was applied. A sinusoidal signal of 10 mV was used with a range of frequency between 0.1 and 100 Hz. The working and counter electrodes were placed 3 cm apart on the forearm. The reference electrode was placed on the elbow. The printed electrode was the working electrode while wet Ag/AgCl electrodes (Ambu Blue Sensor N, N-00-S/25, 0.95 cm diameter contact area) were used as counter and reference electrodes.

Physiological Data Acquisition: All volunteers provided informed signed consent to participate in this study. ECG data were acquired using an RHD2216 chip from Intan Technologies. The signals were sampled at 1.1 kHz at 16 bits. A first-order high pass at 0.1 Hz and a third-order low pass at 100 Hz analog filters were used. Three bipolar channels were used during the experiments, each channel connecting to with two electrodes of the same type (one, two, or three layers). A ground electrode was placed on the right leg. All measurements were carried out while the volunteer was not moving.

Force Sensitivity Measurements: A force-sensing resistor (Interlink FSR 402 short) was placed under a printed electrode and experiments were conducted under soft touch (sensor registering 10 g) and applied force (sensor registering 1 kg).

Bending Durability Measurements: A PEDOT:PSS rectangle with dimensions of 5×1 cm^2 and consisting of one printed layer was made to conform to a cylinder (of diameter of 2 or 5 cm) by applying a small load using a homemade machine. The experiment was performed at 30 cycles per minute.

Data Postprocessing: All postprocessing was carried out using National Instrument's LabVIEW software. The ECG data were first filtered using a forth-order Butterworth band pass, high passed at 0.5 Hz and low passed at 100 Hz, and a forth-order notch filter at 50 Hz. The SNR was then calculated for each measurement using the equation: $SNR(Sr) = 20 * \log\left(\sqrt{\frac{\sum_i Sf_i^2}{\sum_i (Sr_i - Sf_i)^2}}\right)$, Sr being the raw signal and Sf the filtered signal. The average value and its standard deviation were then calculated for the devices during periodic experiments. Breathing analysis was obtained using a simple algorithm that isolated the amplitudes of each RS complex of the ECG signal and then looked for a decrease or an increase in those amplitudes.

Supporting Information

Supporting Information is available from the Wiley Online Library or from the author.

Acknowledgements

E.B. and T.R. contributed equally to this work. This work was supported though grants by the ANR and MicroVitae Technologies. The prototyping and fabrication of the electrodes were performed at the Centre Microelectronique de Provence.

Received: October 13, 2016
Revised: December 11, 2016
Published online:

[1] J. Q. Xu, S. L. Murphy, K. D. Kochanek, B. A. Bastian, *Hyattsville, MD: Natl. Cent. Health Stat.* **2016**, *64*, 2.
[2] P. A. Heidenreich, J. G. Trogdon, O. A. Khaviou, J. Butler, K. Dracup, M. D. Ezekowitz, E. A. Finkelstein, Y. Hong, S. C. Johnston, A. Khera, D. M. Lloyd-Jones, S. A. Nelson, G. Nichol, D. Orenstein, P. W. F. Wilson, Y. J. Woo, *Circulation* **2011**, *123*, 933.
[3] A. Searle, L. Kirkup, *Physiol. Meas.* **2000**, *21*, 271.
[4] J.-Y. Baek, J.-H. An, J.-M. Choi, K.-S. Park, S.-H. Lee, *Sens. Actuators, Phys.* **2008**, *143*, 423.
[5] K. P. Hoffmann, R. Ruff, *IEEE Eng. Med. Biol. Soc.* **2007**, 5739.
[6] C.-T. Lin, L.-D. Liao, Y.-H. Liu, I.-J. Wang, B.-S. Lin, J.-Y. Chang, *IEEE Trans. Biomed. Eng.* **2011**, *58*, 1200.
[7] T. Roberts, J. B. De Graaf, C. Nicol, T. Hervé, M. Fiocchi, S. Sanaur, *Adv. Healthcare Mater.* **2016**, *5*, 1462.
[8] N. Matsuhisa, M. Kaltenbrunner, T. Yokota, H. Jinno, K. Kuribara, T. Sekitani, T. Someya, *Nat. Commun.* **2015**, *6*, 7461.
[9] S. Takamatsu, T. Lonjaret, D. Crisp, J.-M. Badier, G. G. Malliaras, E. Ismailova, *Sci. Rep.* **2015**, *5*, 15003.
[10] J. Rivnay, R. M. Owens, G. G. Malliaras, *Chem. Mater.* **2013**, *26*, 679.
[11] M. Berggren, A. Richter-Dahlfors, *Adv. Mater.* **2007**, *19*, 3201.
[12] A. Campana, T. Cramer, D. T. Simon, M. Berggren, F. Biscarini, *Adv. Mater.* **2014**, *26*, 3874.
[13] P. Leleux, J.-M. Badier, J. Rivnay, C. Bénar, T. Hervé, P. Chauvel, G. G. Malliaras, *Adv. Healthcare Mater.* **2014**, *3*, 490.
[14] A. P. Alves, J. Martins, H. P. da Silva, A. Lourenço, A. L. Fred, H. Ferreira, in *PhyCS*. **2014**, 275.
[15] J. C. Batchelor, A. J. Casson, *IEEE Eng. Med. Biol. Soc.* **2015**, 4013.
[16] Z. Xiong, C. Liu, *Org. Electron.* **2012**, *13*, 1532.
[17] J. Rivnay, P. Leleux, M. Ferro, M. Sessolo, A. Williamson, D. A. Koutsouras, D. Khodagholy, M. Ramuz, X. Strakosas, R. M. Owens, C. Benar, J.-M. Badier, C. Bernard, G. G. Malliaras, *Sci. Adv.* **2015**, *1*, e1400251.
[18] G. B. Moody, R. G. Mark, A. Zoccola, S. Mantero, *Comput. Cardiol.* **1985**, *12*, 113.
[19] "The heartbit vs the fingerprint in the battle for biometric authentication", https://www.washingtonpost.com/news/innovations/wp/2014/11/21/the-heartbeat-vs-the-fingerprint-in-the-battle-for-biometric-authentication/, accessed: September 2016.
[20] S. A. Israel, J. M. Irvine, A. Cheng, M. D. Wiederhold, B. K. Wiederhold, *Pattern Recognit.* **2005**, *38*, 133.

ADVANCED HEALTHCARE MATERIALS

Supporting Information

for *Adv. Healthcare Mater.,* DOI: 10.1002/adhm.201601167

Inkjet-Printed PEDOT:PSS Electrodes on Paper for Electrocardiography

*Eloïse Bihar, Timothée Roberts, Mohamed Saadaoui, Thierry Hervé, Jozina B. De Graaf, and George G. Malliaras**

Supporting Information

Inkjet-printed PEDOT:PSS electrodes on paper for electrocardiography

*Eloïse Bihar†, Timothée Roberts†, Mohamed Saadaoui, Thierry Hervé, Jozina B. De Graaf, and George G. Malliaras**

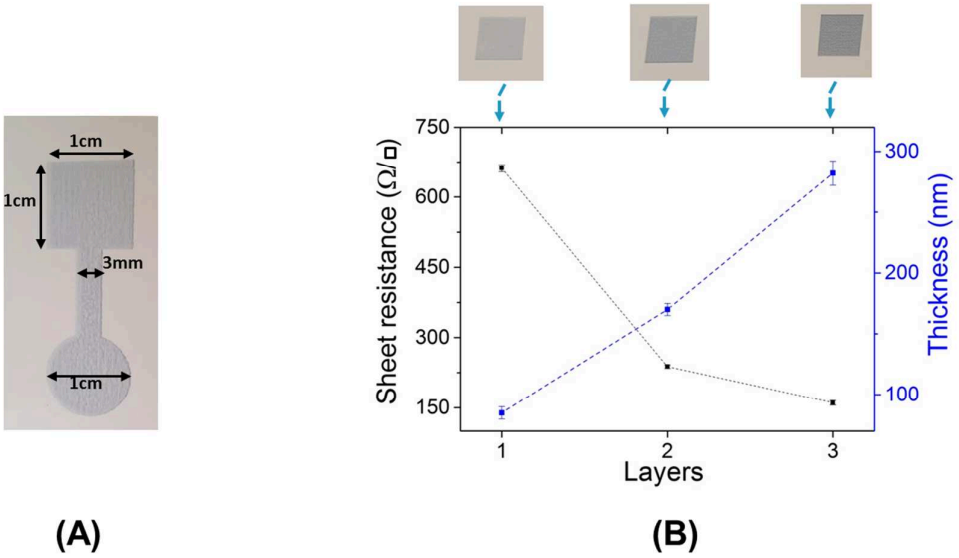

Figure S1. (A) Photograph showing the dimensions of the PEDOT:PSS electrode (B) Sheet resistance of printed PEDOT:PSS electrodes on paper consisting of 1, 2 and 3 layers, n=3.

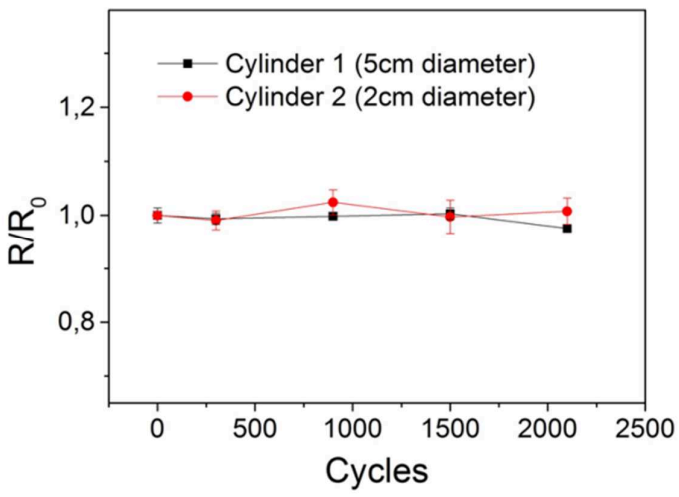

Figure S2. Relative change in resistance of a PEDOT:PSS electrode on paper subjected to different number of bending cycles on cylinders of diameter of 2 and 5 cm.

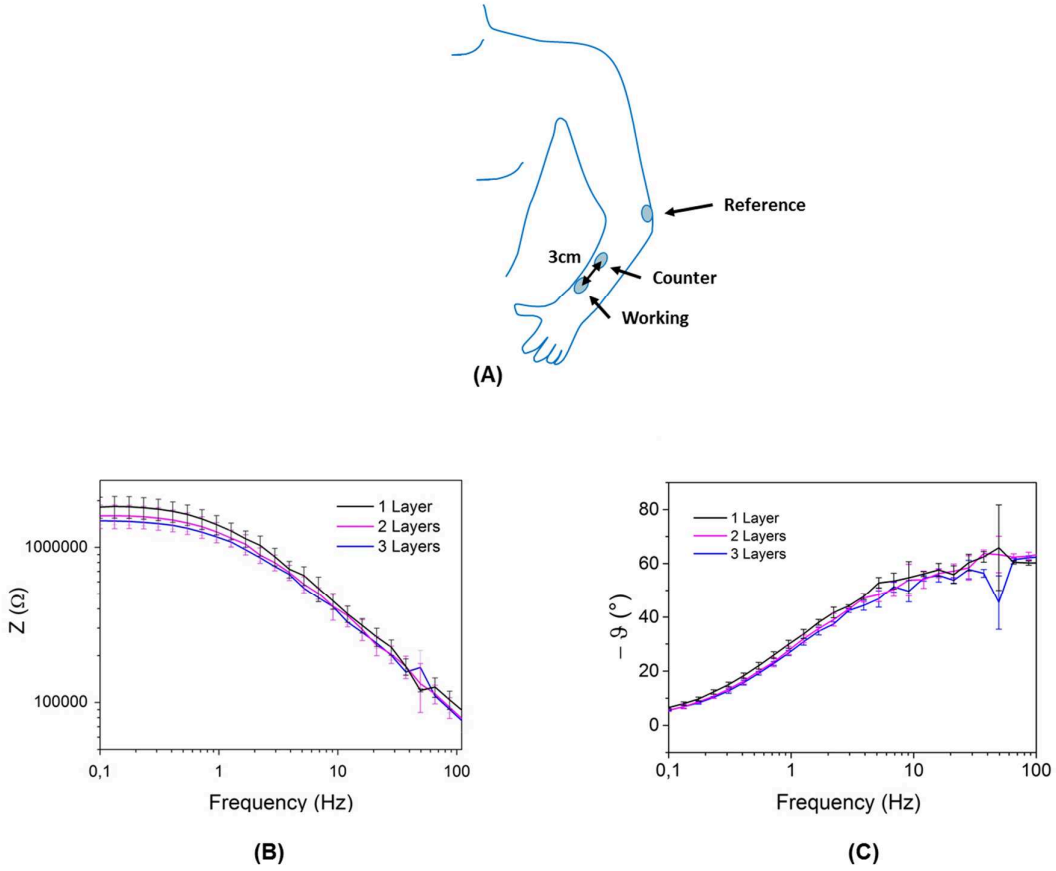

Figure S3. (A) Schematic of the experiment for electrode/skin impedance measurements. (B) and (C) Electrochemical impedance spectra measured from printed PEDOT:PSS electrodes consisting of 1, 2 and 3 layers, n=3.

IV. Impression d'électrodes sur du textile étirable pour des mesures électrophysiologiques de longue durée

Après avoir créé des électrodes sur du Kapton et sur du papier, je me suis intéressé au textile. Le chapitre qui suit, présente la fabrication grâce à l'impression jet d'encre d'électrode en PEDOT :PSS avec du gel ionique solide sur un support textile. Des tests mécaniques ont été réalisés pour vérifier la détérioration due aux manipulations de l'électrode. L'impédance électrochimique de ces électrodes a été mesurée dans le but de comparer les performances du PEDOT :PSS avec ou sans gel ionique solide sur du textile. Des mesures électrophysiologiques ont ensuite été réalisées sur une période de 40 jours. L'impact des artefacts de mouvement a été observé dans le cadre de l'utilisation d'électrode textile PEDOT :PSS (avec ou sans gel) et d'électrode AMBU classique. Cette étude présente : i) la possibilité d'imprimer en jet d'encre du gel ionique solide, ii) la capacité du PEDOT :PSS et du gel ionique solide a imprégner de façons stable des fibres de textile, et iii) les performances d'électrodes PEDOT :PSS avec ou sans gel sur textile sur le long terme.

Fully Printed Electrodes on Stretchable Textiles for Long-Term Electrophysiology

*Eloïse Bihar, Timothée Roberts, Esma Ismailova, Mohamed Saadaoui, Mehmet Isik, Ana Sanchez-Sanchez, David Mecerreyes, Thierry Hervé, Jozina B. De Graaf, and George G. Malliaras**

Fully printed electrodes consisting of a conducting polymer and an ionic liquid gel are fabricated on a stretchable textile. They are shown to record cardiac activity while the wearer is moving and for long periods of time, paving the way for the development of low-cost devices for continuous health monitoring.

Cutaneous devices for health monitoring are attracting a great deal of interest in both industry and academia. Recent advances on the deposition of electronic materials onto textiles are generating a considerable effort focused on the integration of electrical health monitoring systems into clothing.[1–3] Such autonomous, wearable monitoring systems allow a better patient comfort during daily use. They aim to provide early diagnosis of cardiovascular diseases (CVDs), such as arrhythmias and can be used for prevention of heart-related problems and related deaths.[4]

Existing commercial devices for infant and adult health monitoring use wet (gel-assisted) Ag/AgCl electrodes but these electrodes cause discomfort, and in some cases, skin irritation and allergic reactions from the adhesive used to fix them on the skin.[5] They are also not suitable for long-term measurements due to the drying of the gel.[6] To find alternatives, many studies explored electrodes embedded in or deposited on textiles.[7] Textile electrodes can be fabricated by integrating conducting yarns into the textile,[8,9] by dip-coating the fibers,[10] or by deposition of conducting materials on the textile.[11] The latter approach, coupled with a direct deposition technique such as inkjet printing, offers great versatility and has the potential to lead to customizable electrodes for health monitoring. To date, however, only a few studies reported the use of inkjet for the fabrication of wearable electrodes for health monitoring.[12,13] Inkjet technology is an additive technology which permits to design customizable electrodes with reduced manufacturing costs. It offers many advantages such as compatibility with a wide range of substrates, small number of fabrication steps, low materials waste, and the possibility to integrate this technique in a roll-to-roll process, making production efficient and inexpensive.

In this work we report the fabrication of fully printed, wearable electrodes using inkjet technology by printing the conducting polymer PEDOT:PSS on a commercial stretchable textile. A commercially available pantyhose (100 wt% polyamide) was chosen as the substrate, as it offers a high level of stretchability. We chose PEDOT:PSS as the conducting layer due to its biocompatibility,[14] and its mixed ionic/electronic conductivity, which yields high quality cutaneous contacts.[15] We further printed an ionic liquid gel to improve the contact between the conducting polymer and skin, as such gels have been shown to lead to high quality contacts with excellent long-term stability.[16] We record electrocardiograms (ECG) from a volunteer and demonstrate recordings that are stable and rather insensitive to motion artifacts, paving the way for the fabrication of low cost, customizable electrodes for cutaneous electrophysiology.

The printed electrode geometry (**Figure 1**) consists of a round disk with a diameter of 1 cm, similar to that of a commercial Ag/AgCl electrode, connected to a square contact pad with area of 1 cm^2. We inkjet-printed several layers of the conducting ink (**Figure 2**) and obtained electrodes with a color that became more apparent as the quantity of conducting material added onto the textile increased. As seen in Figure 2b, the electrical resistance of a 1 cm^2 PEDOT:PSS square decreased with

Dr. E. Bihar, Dr. E. Ismailova, Prof. G. G. Malliaras
Department of Bioelectronics
Ecole Nationale Supérieure des Mines
CMP-EMSE
MOC, 880, route de Mimet, 13541 Gardanne, France
E-mail: malliaras@emse.fr
Dr. E. Bihar, T. Roberts, Dr. T. Hervé
Microvitae Technologies
Hôtel Technologique
Europarc Sainte Victoire
Bâtiment 6 Route de Valbrillant, 13590 Meyreuil, France
Dr. E. Bihar, Dr. M. Saadaoui
Department of Flexible Electronics
Ecole Nationale Supérieure des Mines
CMP-EMSE
880, route de Mimet, 13541 Gardanne, France
T. Roberts, Dr. J. B. De Graaf
Aix Marseille Univ
CNRS, ISM, Marseille, France
Dr. M. Isik, Dr. A. Sanchez-Sanchez, Prof. D. Mecerreyes
POLYMAT
University of the Basque Country UPV/EHU
Joxe Mari Korta Center
Avda. Tolosa, 72, 20018 Donostia-San Sebastian, Spain

DOI: 10.1002/admt.201600251

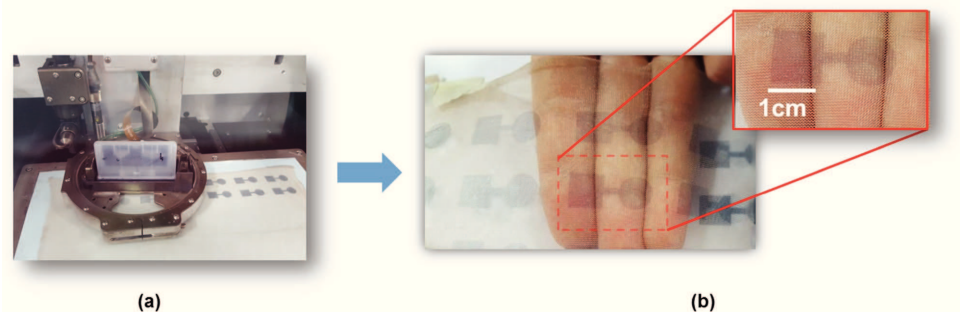

Figure 1. a) Photograph of the inkjet printing process. b) Photograph of printed electrodes on a commercial textile with a zoom on an individual electrode.

the number of printed layers, reaching a plateau at 8 layers. Mechanical deformation tests showed that PEDOT:PSS rigidified slightly the textile, yet the electrodes could be stretched at least up to 200% (Figure S1, Supporting Information). The resistance of electrodes consisting of 4, 6, 8, and 10 layers increased only by a factor of 6.0 ± 0.4, 2.7 ± 0.5, 1.4 ± 0.2, and 1.5 ± 0.2 times, respectively, at 100% strain (Figure 2c). Compared to literature, these values are close to the state-of-the-art and validate the choice of textile as a substrate.[17–19]

Based on the results above, electrodes consisting of 8 printed layers of PEDOT:PSS were chosen for further investigation. When taken up to 200% strain, their resistance increased only by a factor of 3.48 ± 0.05 (Figure S1c, Supporting Information). The high degree of stretchability is consistent with recent work from the Bao group that shows that surfactants allow changes of conformation of PEDOT:PSS chains during stretching.[18] Such high excursions, though, were found to eventually cause delamination of the PEDOT:PSS (Figure S2, Supporting Information). Thus, cyclic tests were performed at lower values of strain in order to evaluate durability during repetitive deformation. Figure 2d shows that after a slight initial increase of ≈1.05, resistance remains constant after 50 cycles at 30% strain, proving the stability of the printed polymer electrical properties under mechanical stress. Scanning Electron Microscopy (SEM) images of the fibers after the experiment provided no evidence of cracking or delamination for the fibers coated with ionic liquid, though some delamination was visible in the samples without ionic liquid when stretched at 200% (Figure S2, Supporting Information).

In order to improve the contact between the skin and the dry electrode interface, we used a gel formulation based on the biocompatible cholinium lactate ionic liquid.[19] The main

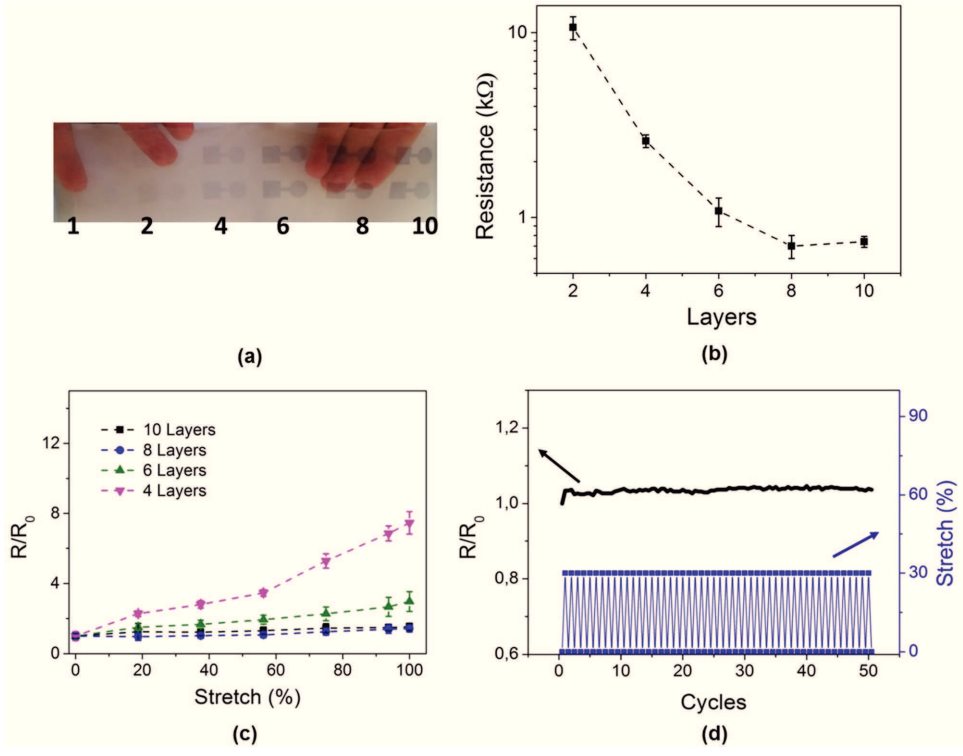

Figure 2. a) Photograph of electrodes with a different number of printed layers (1, 2, 4, 6, 8, 10). b) Resistance of a printed square (1 × 1 cm^2). c) Normalized resistance (R/R_0) of printed squares as a function of stretching. d) Normalized resistance (R/R_0) during stretching cycles ($n = 3$).

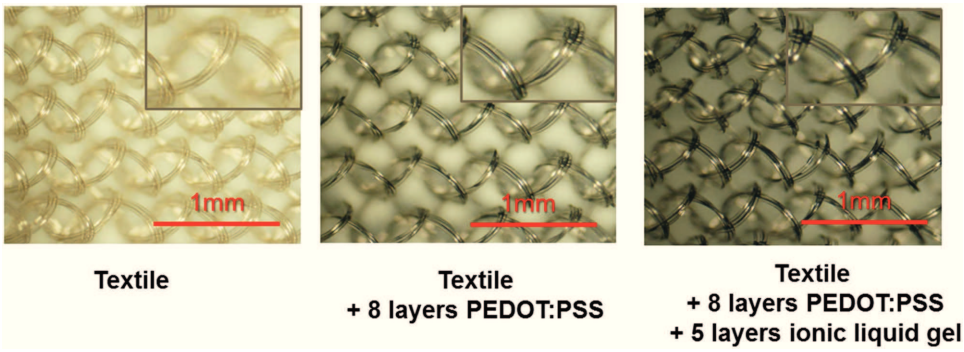

Figure 3. Images of the pristine textile, the textile with 8 layers of PEDOT:PSS, and the textile with 8 layers of PEDOT:PSS and 5 layers of ionic liquid gel.

advantage of this ionic liquid is its low toxicity, which is an attractive feature for prolonged skin contact. As reported previously, its ionic conductivity improves with temperature, while the gel maintains its mechanical properties.[19] We printed the ionic liquid ink on the PEDOT:PSS active electrode area and photopolymerized it as discussed in the experimental section. The ink penetrated directly into the yarns to form a thin transparent encapsulation layer around PEDOT:PSS coated fibers (**Figure 3**). Electrochemical impedance measurements of the electrode/skin interface were performed on a volunteer, as shown in **Figure 4**, using the textile one as the working electrode, and wet Ag/AgCl electrodes as counter and reference. The data shows that the addition of the ionic liquid gel lowers impedance, as expected due to the extended contact with skin. The addition of five layers of ionic liquid gel decreases impedance by two orders of magnitude in the frequency range of 0.1–10 Hz, and one order of magnitude in the range of 10–1000 Hz (Figure 4b). Indeed, the gel-assisted textile electrode with 5 layers of ionic liquid gel shows an impedance spectrum that is similar to that of a commercial wet Ag/AgCl electrode (Figure 4c). This is despite the fact that the textile electrode forms a contact with a smaller effective area (even after possible "squeezing" of the ionic liquid due to the conformal textile/skin contact), which implies a high quality interface both in terms of mechanical and electrical properties. A coating consisting of 5 printed layers of ionic liquid gel was, therefore, selected and used to make gel-assisted PEDOT:PSS textile electrodes for the remainder of this study. It should be noted that the addition of the ionic liquid gel has a positive impact on stretchability (Figure S1, Supporting Information)

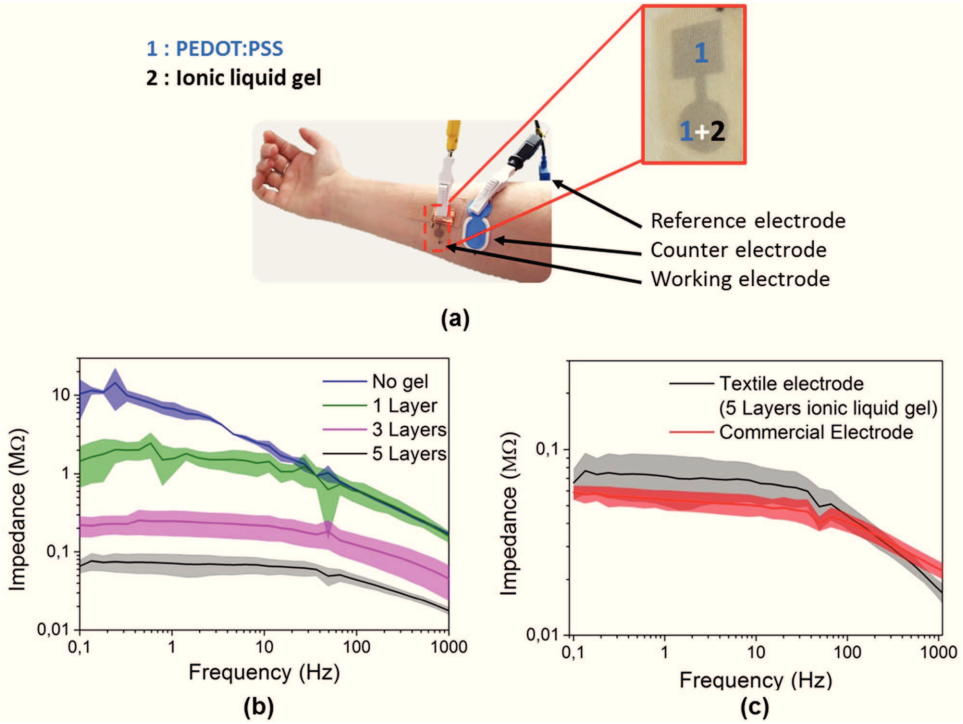

Figure 4. a) Photograph showing the electrode configuration for the impedance measurements. b) Impedance spectra measured from a PEDOT:PSS electrodes made of 8 printed layers with and without an ionic liquid gel consisting of various number of layers. c) Impedance spectra of a commercial electrode and a printed electrode consisting of 8 layers of PEDOT:PSS and 5 layers of ionic liquid gel ($n = 3$).

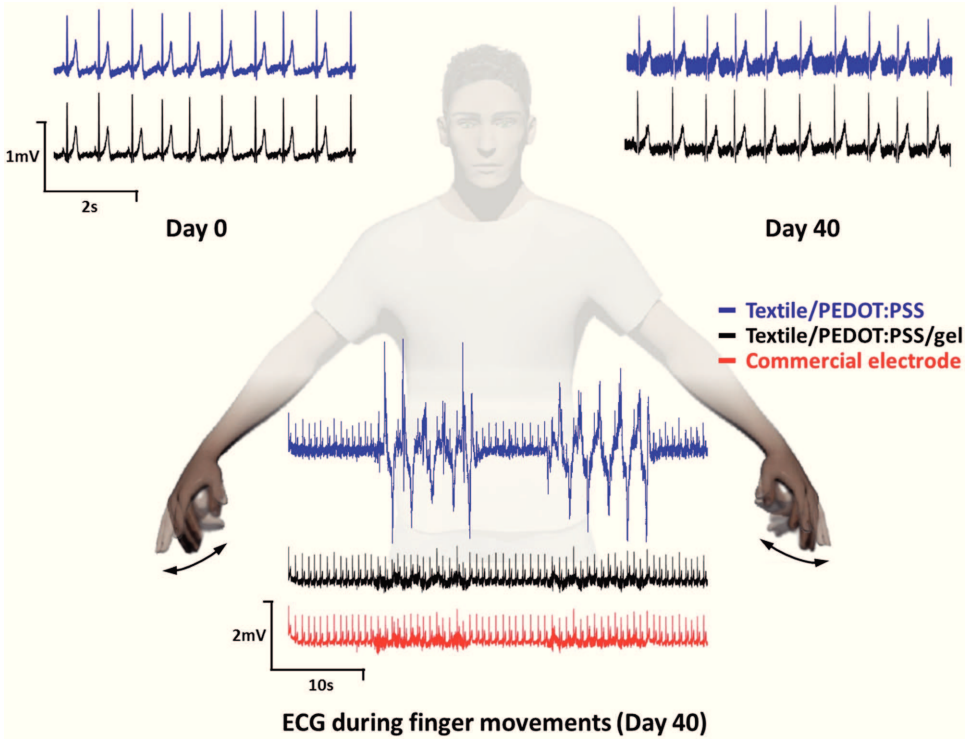

Figure 5. ECG data acquired under different conditions: (i) static recoding at t_0 in the top left corner, (ii) static recording at t_0 + 40 d in the top right corner, (iii) dynamic recording under repeated hand motion at t_0 + 40 d in the bottom center.

and decreases the change in electrical resistance at large elongations (Figure 2c).

In order to validate the use of the textile electrodes in electrophysiology we measured the ECG of a volunteer. ECG signals were simultaneously acquired with the three electrode types: dry and gel-assisted textile electrodes and commercial wet Ag/AgCl electrodes. Measurements were conducted between the two forearms, over a period of 40 days (d) at four different times: t_0, t_0 + 4 h, t_0 + 8 h, t_0 + 24 h, and t_0 + 40 d. Typical ECG recordings at t_0 and t_0 + 40 d are shown in **Figure 5**. The characteristic waves of ECG, essential to establish CVD diagnostics, are clearly recorded by both the dry and the gel-assisted textile electrodes. The mean signal-to-noise ratio (SNR), calculated at t_0 for three different recordings, was 12.93 ± 0.80 and 13.75 ± 0.26 dB, for the dry and the gel-assisted electrodes, respectively, and remained constant for the first 24 h of recording (Figure S3, Supporting Information). 40 d later, the performance of the printed electrodes exhibited signs of slight degradation, characterized by a decrease in SNR to 7.28 ± 5.28 and 10.37 ± 2.53 dB, for the dry and the gel-assisted electrodes, respectively. It should be noted that the impedance of the gel-assisted textile electrode at 10 Hz increased from 0.06 MΩ at t_0 to 1.15 MΩ at t_0 + 14 d, pointing toward changes at the electrode due to uptake of sweat.

To evaluate the impact of motion artifact generated on the ECG signals, we asked the volunteer to repeatedly open and close his/her hands to induce movement artifacts on the recordings. Figure 5 shows typical recordings for each electrode type. While the signal was clearly affected on the dry textile electrodes, it was affected considerably less on both the gel-assisted textile and the commercial electrodes. During movement, the ECG complex recorded by these two electrodes was still detectable, while in recordings from the dry textile electrode, the characteristic peaks were indiscernible. The advantage of the gel-assisted textile electrode, compared to the commercial one, is that it does not dry out. Indeed, the commercial electrode lost its ability to record after ≈12 h. Therefore, the use of an ionic liquid gel printed on textile electrodes improved the signal stability over time and under motion.

We used inkjet printing to make electrodes from PEDOT:PSS on a commercial stretchable textile. Contact with the skin was improved by the addition of a cholinium lactate-based ionic liquid gel that was also inkjet-printed directly on the textile. These gel-assisted electrodes made low impedance contacts to the skin and yielded recordings that were of comparable quality than those of commercial wet Ag/AgCl electrodes, but without drying and using a format that is more compatible with wearable diagnostics. As such, they pave the way for the fabrication of customizable health monitoring devices for cutaneous applications.

Experimental Section

Ink Formulations: To formulate the conducting ink, the authors added in a commercially available dispersion (Heraeus, Clevios PH1000), 20% of ethylene glycol (Sigma Aldrich), and other organic solvents to enhance electrical conductivity, 0.8 wt% of glycidoxypropyltrimethoxysilane (Sigma Aldrich) to prevent delamination, and 0.3% of surfactants to achieve suitable rheological properties for inkjet printing. The viscosity of the ink was adjusted to 12.2 mPa·s and the surface tension to 29 mN m^{-1}. To create the ionic liquid ink, the authors mixed a solution

containing cholinium lactate and 2-cholinium lactate methacrylate monomer with the crosslinker (ethyleneglycol dimethacrylate) and a photoinitiator, (2-hydroxy-2-methyl propiophenone 97%, Aldrich).[19] The authors added ethanol to achieve adequate viscosity for inkjet printing.

Inkjet Printing: The authors used a Dimatix DMP-2800 inkjet printer to fabricate the electrodes, using ten pL droplets. The authors printed successively 1, 2, 4, 6, 8, and 10 layers of PEDOT:PSS ink on a commercial, stretchable polyamide textile (Dim, knee highs) and cured the samples 60 min at 110 °C in a conventional oven. To crosslink the ionic liquid gel, the authors placed the samples in the oven for 10 min (100 °C) for solvent evaporation, and exposed the printed textiles to UV light (from a UVGL-58 hand-held UV lamp, $\lambda = 365$ nm).

Surface Characterization: SEM images were taken by CARL ZEISS Ultra 55 with an accelerating voltage of 10 kV.

Electrical Characterization: Electrical resistance was measured on 1×1 cm^2 squares by placing pogo pin connectors at the edges and using a Fluke 175 multimeter. Electrical tests during stretching were performed using an Instron tabletop model 3665. The samples in this case were larger for experimental convenience, consisting of printed rectangles (1.5×3 cm^2) on textile. The authors connected the conducting textile via a copper tape attached to the Instron's jaws and measured resistance using a multimeter (Fluke 175).

Electrochemical Impedance Spectroscopy: The authors used an Autolab potentiostat (Metrohm Autolab B.V.), and the associated software NOVA to perform the impedance measurements using the fabricated and commercial electrodes placed on the skin of a volunteer. The frequency range was between 0.1 and 100 Hz and the sinusoidal signal was 10 mV. The authors placed the reference electrode on the elbow. The working and counter electrodes were placed on the forearm, 3 cm apart. The working electrode was the electrode under study, while the reference and counter electrodes were wet Ag/AgCl electrodes (Ambu Blue Sensor N, N-00-S/25, 0.95 cm diameter contact area).

Physiological Data Acquisition: Informed consent was signed by the volunteer. A RHD2216 amplifier chip from Intan Technologies was used to record the ECG signal. The chip was configured to use a high-pass filter at 0.1 Hz and a low-pass filter at 1000 Hz. After filtering, the signals were sampled on 16 bits at 1.1 kHz. ECGs were recorded between the two forearms with a ground electrode on the right leg. The textile electrodes were attached halfway on the forearm of the participants with a sports bracelet. They were then connected to the recording electronics using a copper tape and a metal wire.

Data Post-Processing: Labview software from National Instrument was used to process the signal. The "raw" ECG signal (Sr) were obtained by filtering the output of the RHD2216 using a fourth-order Butterworth band-pass filter. The high- and low-pass frequencies were 0.5 and 100 Hz, respectively. A 50 Hz Notch filter was added to obtain the filtered signal (Sf). The SNR was then calculated for each measurement using the following equation

$$\mathrm{SNR(Sr)} = 20 \times \log\left(\frac{\mathrm{RMS(Sf)}}{\mathrm{RMS(Sr-Sf)}}\right)$$

Supporting Information

Supporting Information is available from the Wiley Online Library or from the author.

Acknowledgements

E.B. and T.R. contributed equally to this work. This work was supported though grants by the ANR, and MicroVitae Technologies. The prototyping and fabrication of the electrodes were performed at the Centre Microelectronique de Provence. The authors would like to thank Marc Ramuz and Bastien Marchiori for their help with the mechanical properties testing.

Received: October 27, 2016
Revised: January 15, 2017
Published online:

[1] S. Park, S. Jayaraman, *MRS Bull.* **2003**, *28*, 585.
[2] D. Marculescu, R. Marculescu, N. H. Zamora, P. Stanley-Marbell, P. K. Khosla, S. Park, S. Jayaraman, S. Jung, C. Lauterbach, W. Weber, T. Kirstein, D. Cottet, J. Grzyb, G. Troster, M. Jones, T. Martin, Z. Nakad, *Proc. IEEE* **2003**, *91*, 1995.
[3] P. Lukowicz, T. Kirstein, G. Troster, *Methods Inf. Med.* **2004**, *43*, 232.
[4] WHO Cardiovascular diseases (CVDs), http://www.who.int/media-centre/factsheets/fs317/en/, accessed: October, 2016.
[5] N. Mazzaro, Risk of skin reaction when using ECG electrodes, http://www.ambu.es/files/billeder/es/micro/cardiologia/the_risk_of_skin_reactions_using_ecg_electrodes_0711.pdf, accessed: July, 2016.
[6] A. Gruetzmann, S. Hansen, J. Müller, *Physiol. Meas.* **2007**, *28*, 1375.
[7] M. Catrysse, R. Puers, C. Hertleer, L. Van Langenhove, H. van Egmond, D. Matthys, *Sens. Actuators, A* **2004**, *114*, 302.
[8] M. S. Lebby, K. E. Jachimowicz (Motorola Inc.), US 5906004 A, **1998**.
[9] L. Hu, M. Pasta, F. L. Mantia, L. Cui, S. Jeong, H. D. Deshazer, J. W. Choi, S. M. Han, Y. Cui, *Nano Lett.* **2010**, *10*, 708.
[10] D. Pani, A. Dessì, J. F. Saenz-Cogollo, G. Barabino, B. Fraboni, A. Bonfiglio, *IEEE Trans. Biomed. Eng.* **2016**, *63*, 540.
[11] S. Takamatsu, T. Lonjaret, D. Crisp, J.-M. Badier, G. G. Malliaras, E. Ismailova, *Sci. Rep.* **2015**, *5*, 15003.
[12] Y. Li, R. Torah, S. Beeby, J. Tudor, *Sensors, 2012 IEEE*, IEEE, **2012**, 1–4.
[13] T. Roberts, J. B. De Graaf, C. Nicol, T. Hervé, M. Fiocchi, S. Sanaur, *Adv. Healthcare Mater.* **2016**, *12*, 1462.
[14] M. Berggren, A. Richter-Dahlfors, *Adv. Mater.* **2007**, *19*, 3201.
[15] S. Takamatsu, T. Lonjaret, E. Ismailova, A. Masuda, T. Itoh, G. G. Malliaras, *Adv. Mater.* **2016**, *28*, 4485.
[16] D. J. Lipomi, J. A. Lee, M. Vosgueritchian, B. C.-K. Tee, J. A. Bolander, Z. Bao, *Chem. Mater.* **2012**, *24*, 373.
[17] T. S. Hansen, K. West, O. Hassager, N. B. Larsen, *Adv. Funct. Mater.* **2007**, *17*, 3069.
[18] M. Vosgueritchian, D. J. Lipomi, Z. Bao, *Adv. Funct. Mater.* **2012**, *22*, 421.
[19] M. Isik, T. Lonjaret, H. Sardon, R. Marcilla, T. Herve, G. G. Malliaras, E. Ismailova, D. Mecerreyes, *J. Mater. Chem. C* **2015**, *3*, 8942.

ADVANCED MATERIALS TECHNOLOGIES

Supporting Information

for *Adv. Mater. Technol.*, DOI: 10.1002/admt.201600251

Fully Printed Electrodes on Stretchable Textiles for Long-Term Electrophysiology

*Eloïse Bihar, Timothée Roberts, Esma Ismailova, Mohamed Saadaoui, Mehmet Isik, Ana Sanchez-Sanchez, David Mecerreyes, Thierry Hervé, Jozina B. De Graaf, and George G. Malliaras**

Supporting Information

Fully-printed electrodes on stretchable textiles for long-term electrophysiology

*Eloïse Bihar[1,2,3]†, Timothée Roberts[2,4]†, Esma Ismailova[1], Mohamed Saadaoui[3], Mehmet Isik[5], Ana Sanchez-Sanchez[5], David Mecerreyes[5], Thierry Hervé[2], Jozina B. De Graaf[4],and George G. Malliaras[1]**

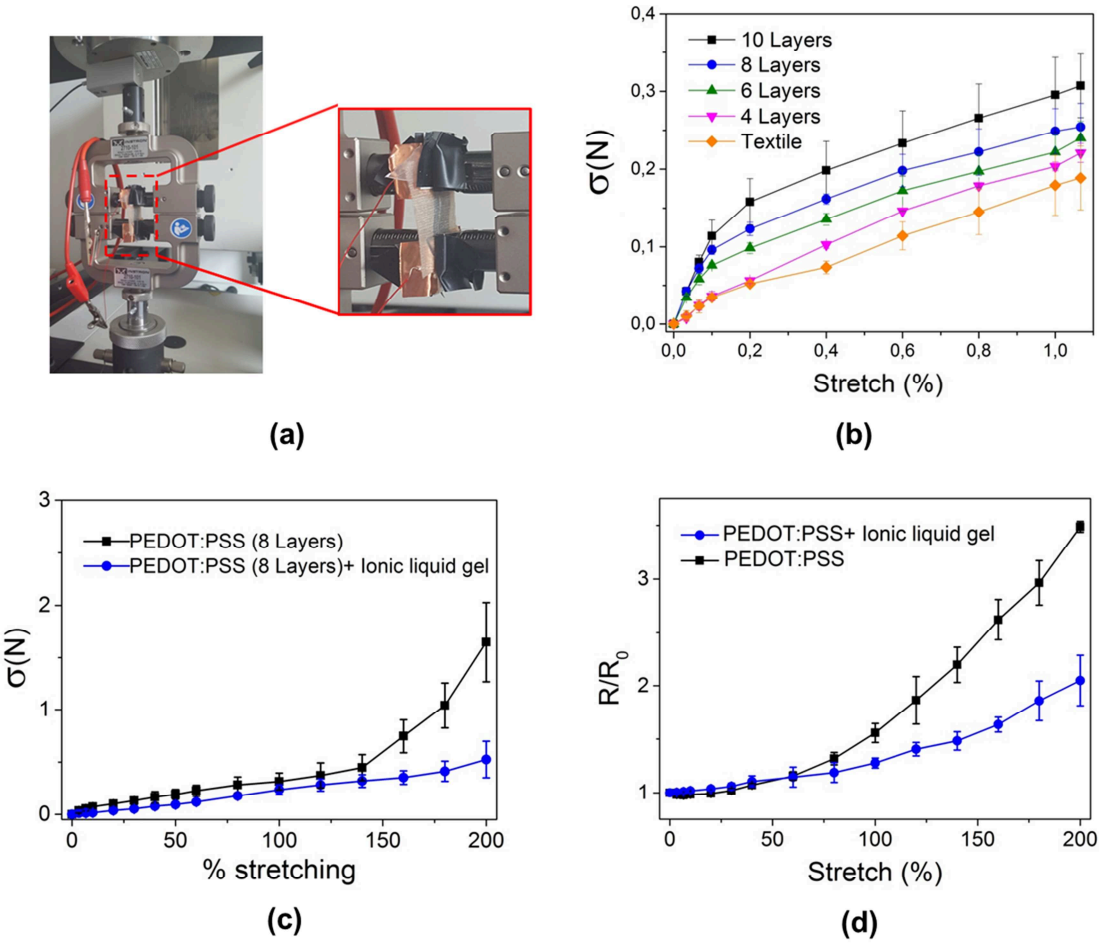

Figure S1: (a) Setup of the mechanical properties testing experiment with a zoom on the printed textile. **(b)** Stress-strain curve of a virgin textile and a textile with a different number of PEDOT:PSS layers (4, 6, 8, 10). The increase in the slope of the load extension curve (from 0 to 15%) shows that the textile is rigidified by the PEDOT:PSS. **(c)** Stress-strain curves of a PEDOT electrode with and without the ionic liquid **(d)** Normalized resistance (R/R_0) of a PEDOT:PSS textile electrode with and without the ionic liquid versus stretch.

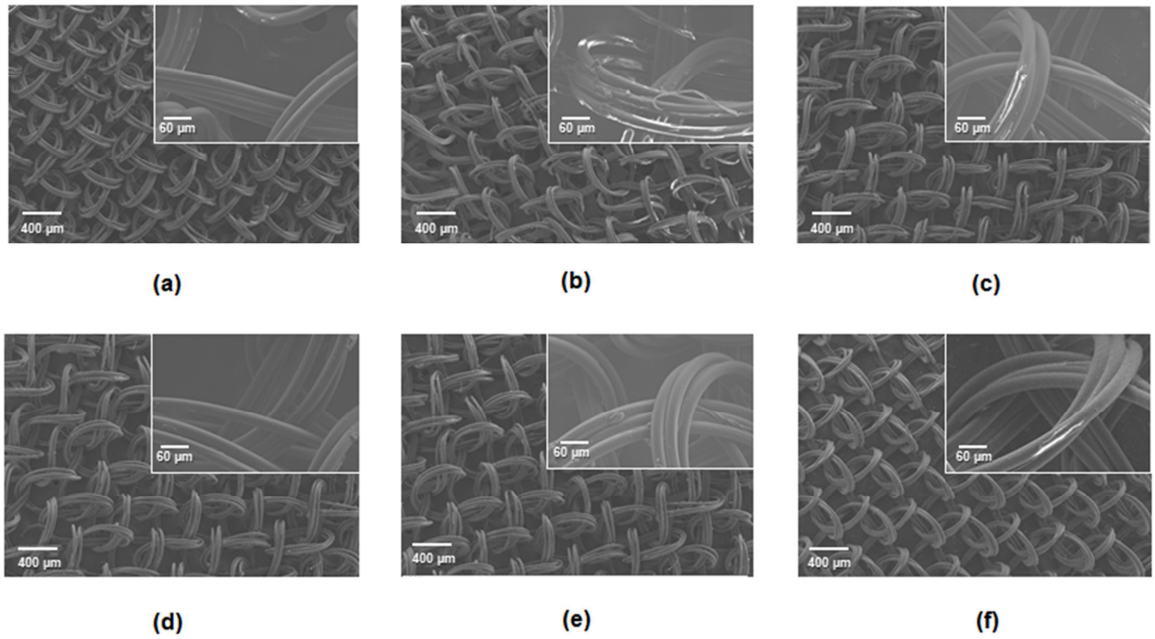

Figure S2: SEM images of electrodes consisting of 8 layers of PEDOT:PSS as fabricated (a), after 200% strain (b), and after 50 cycles at 30% strain (c). SEM images of electrodes consisting of 8 layers of PEDOT:PSS and 5 layers of ionic liquid gel as fabricated (d), after 200% strain (e), and after 50 cycles at 30% strain (f).

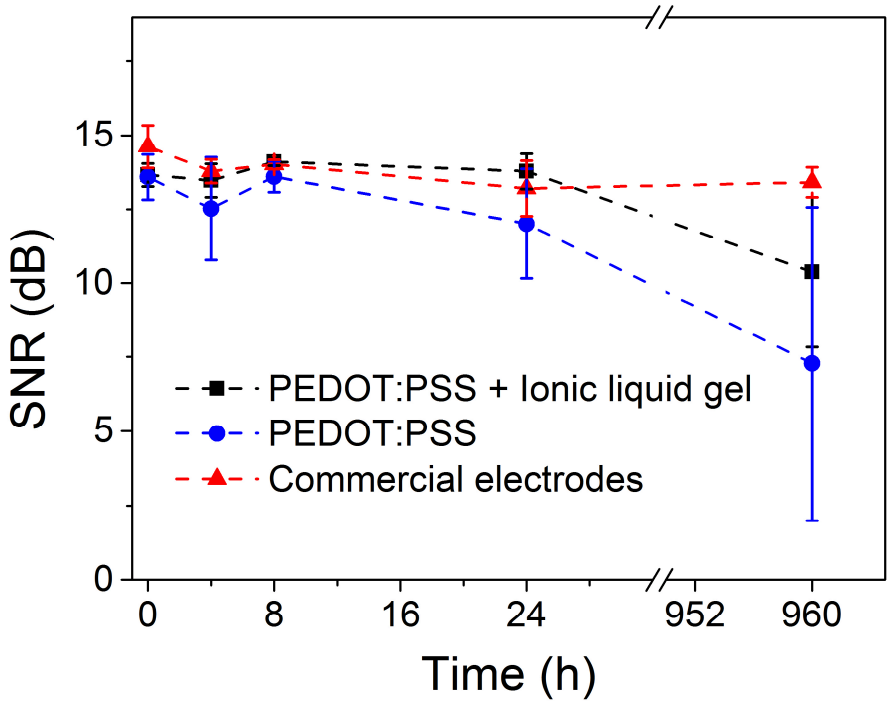

Figure S3: Mean signal-to-noise ratio (SNR) over time (40 days) for textile electrodes with 8 layers of PEDOT:PSS, with and without ionic liquid gel (n=6). For comparison, the SNR of a commercial wet Ag/AgCl electrode is also shown, where a new electrode is used for each measurement.

V. Impression d'électrodes Tattoo/textiles pour des mesures électro-myographiques

Dans l'industrie du médical embarqué, une forte demande de patchs et de textiles intelligents émerge. Pour aborder les possibilités sur ces thématiques, je me suis intéressé à la création d'électrodes sur des papiers tattoo temporaires. Je présente dans ce chapitre la création, grâce à l'impression jet d'encre et à l'utilisation du PEDOT : PSS, d'électrodes tattoo temporaires. Ces dernières sont ici connectées par un simple contact avec une électrode textile. Classiquement, un fil de cuivre aurait été utilisé. Cependant, si une tension est appliquée à ce fil de cuivre, le tattoo temporaire risque de s'arracher. Je montre ici la possibilité de mesurer des signaux EMG durant 6 heures grâce à ces électrodes. Des tests mécaniques et d'impédance électrochimique ont aussi été réalisés pour caractériser les performances de ces électrodes. Ce travail démontre la possibilité de déposer grâce à l'impression jet d'encre du PEDOT : PSS sur des substrats extrêmement fins et fragiles. De plus, une méthode de connexion alternative au fil de cuivre est proposée pouvant être utile pour diverses applications.

Fully printed all-polymer tattoo/textile electronics for electromyography

Eloïse Bihar[1,2,3,5]†, Timothée Roberts[3,4]†, Yi Zhang[5], Esma Ismailova[1], Thierry Hervé[3], George G. Malliaras[1], Jozina B. De Graaf[4], Sahika Inal[5]* and Mohamed Saadaoui[2]*

[1] Department of Bioelectronics, Ecole Nationale Supérieure des Mines, CMP-EMSE, MOC, 13541 Gardanne, France

[2] Department of Flexible Electronics, Ecole Nationale Supérieure des Mines, CMP-EMSE, MOC, 13541 Gardanne, France

[3] Microvitae Technologies, Hôtel Technologique, Europarc Sainte Victoire, Bâtiment 6, Route de Valbrillant, Meyreuil, 13590, France

[4] Institut des Sciences du Mouvement, CNRS, Aix Marseille Université, ISM UMR 7287, 163, Avenue de Luminy, CP 910, 13288 Marseille Cedex 9, France

[5] Division of Biological and Environmental Sciences and Engineering, King Abdullah University of Science and Technology (KAUST), Thuwal 23955, Kingdom of Saudi Arabia

*Corresponding author: saadaoui@emse.fr and sahika.inal@kaust.edu.sa

†These authors contributed equally to this work.

Keywords

Inkjet, printing, PEDOT:PSS, electromyography, tattoo, textile, electrophysiology

Abstract

Driven by the ever-growing needs for developing low cost, easy-to-use, noninvasive diagnostic tools, biomedical devices that can be integrated on human skin or textiles have begun to emerge. These "wearable" devices should couple electronics directly to the human skin and detect a variety of biologically relevant signals such as the neuro-muscular activity. In this work, we present a simple, low cost and customizable device to perform electromyography (EMG) measurements based on electronics fabricated on a tattoo paper. The electrodes are based on the conducting polymer poly(3,4-ethylenedioxythiophene) doped with polystyrene sulfonate (PEDOT:PSS) and inkjet-printed on the

conformable tattoo paper. Addressing the integration challenge common for such flexible electronic devices, we connect the tattoo electrodes to the acquisition system through a textile in the form of a wristband comprising printed PEDOT:PSS contacts. While the textile wristband conforms around the "tattooed" skin, it enables a reliable contact with the electrodes beneath due to its conformability around the limb. We show that this tattoo/textile electronics system is able to detect the biceps activity of the arm during muscle contraction for a period of seven hours, with comparable performance to conventional biopotential electrodes without the use of gels and expensive metallic materials. Combining the tattoo electronics with the electronic textile constitutes a versatile solution for the integration of skin-like electrodes with the external electronics, renders a reliable system for detecting biopotential signals critical for myoelectric prosthesis, muscle injury prevention and/or detection.

Introduction

One of the greatest endeavors of current medical diagnostics research is to develop devices that can record vital signals from the body in real time whilst being minimally invasive[1]. The sensor technologies move from lab-on-chip platforms to wearable electronics, indicating that sensors should be integrated with the skin or clothes that surround the skin, allowing for personal health monitoring as well as drug delivery systems[2–8]. Electrically interfacing the skin with electrodes for monitoring the electrical activity related to functioning of cells is a well-established practice in clinic, albeit performed with electronics that are neither high performance nor comfortable to wear. For instance, nonpolarizable Ag/AgCl electrodes are used as standard devices to record muscle activity, i.e., electromyography (EMG), typically applied on the skin with gels that allow for ion/water penetration to lower skin/electrode impedance. As such, the performance of these electrodes are gel-material dependent and they pose several limitations including discomfort, allergies or irritation when in contact with the human skin, as well as limited stability which is related to gel drying out during long-term applications[9]. New materials and concepts have emerged in order to address the aforementioned limitations, aiming for

devices that can adhere seamlessly to human skin as well as adapt to movements of the skin. Conformable electrodes based on smart textiles [10–13] have been investigated recently. For instance, Someya's group developed recently new conductors made of highly stretchable and conductive materials composed of Ag flakes mixed with fluorines and by the use of screen printing they realized electrodes matrix integrated into garments for electrophysiology recordings[12]. Graphene has also been under the scope of investigation for the development of new conductive textiles. Lately, Yapici et al[13] integrated a cladding layer composed of graphene into the textile to record electrocardiograms (ECG). A new generation of devices that can be even fully conformable ones also known as electronic skin (e-skin)[7,14,15] have emerged as more patient-compliant devices. One example was reported by Kim et al, who developed systems incorporating electrophysiological, temperature and strain sensors made of gold, silicon, gallium arsenide forming nanoribbons and nanomembranes deposited directly on the surface of the skin by dissolving a water soluble film of PVA, the electronics were attached to the skin by van der Walls interactions and they successfully recorded electrical activities from heart, brain etc. They also suggested the possibility to use a commercial temporary transfer tattoo as the substrate. Indeed an interesting substrate material for device integration has been the commercially available tattoo papers. If the electronics can be integrated on the paper, it can be transferred onto the skin by dissolution of the water soluble sacrificial layer (typically made of starch-dextrin) of the paper. As such, the paper and thereof the electronic on it conforms to the skin and represents an ideal disposable system for performing noninvasive daily diagnostics of a variety of markers through the skin integrating both sensors and acquisition systems into a fully autonomous platform[2,16,17]. Such platforms, used for electrophysiological signal recordings, exhibit excellent skin conformation, resistance to deformation and good biocompatibility with the human skin.

Conducting polymers have come to the fore as promising electronic materials in interfacing the tissue due to the mechanical softness and biocompatibility as well as low impedance of their films[18]. Amongst these materials, poly(3,4-ethylenedioxythiophene) doped with polystyrene sulfonate

(PEDOT:PSS) has been the standard organic electronic coating, owing its popularity mostly to its electrochemical stability (no degradation in aqueous environments rich in oxidative species) and being readily available as a dispersion in water through commercial vendors[19]. Another reason for the current popularity of PEDOT:PSS in bioelectronics is that the dispersion can be processed through various means[20], allowing for integration into a wide range of pre-existing fabrication protocols/procedures. Co-solvents, secondary dopants, and crosslinkers are often added to the dispersion to modulate the film conductivity, mechanical properties as well as viscosity so that it is ideal for printing and coating over large areas[21–26]. All these properties render PEDOT:PSS a promising candidate as an electrode material on substrates that can conform with the skin. In fact, PEDOT:PSS has recently been integrated as the electrode material on tattoo paper for recording electrophysiological signals. Recently, Zucca et al presented different techniques for the realization of conductive tattoo nanosheet electrodes made of PEDOT:PSS, first by spin coating the conducting polymer on a commercial tattoo paper, and later inkjet printed a NaClO solution for the subtractive patterning of the tattoo[27], secondly by coating poly(D,L-lactic acid) (PDLLA) and PEDOT:PSS on a plastic substrate (Polypropylene) with a gravure roll, process that can be adapted for large area and then using an adhesive for the detachment of the electrode (PDLLA+ PEDOT:PSS) [28]. In both cases, after placing the tattoo electrode on the skin, they successfully recorded EMG recordings. However the integration of stable interconnections needs to be advanced for stability and use for long term measurements. Another interesting approach was suggested by Bareket et al who developed tattoo electrodes for oculography measurements (EOG). They patterned the electrodes by screen printing a carbon ink and for the second step, plasma polymerized PEDOT:PSS for enhancing the impedance of the electrodes. [29] They successfully managed to record an EOG signal for 3 hours, however the overall thickness of the electrodes (ca. 100μm) was a concern for the conformal contact between the skin and the electrode.

For such disposable organic electronics based on-tattoo electrodes to be ever commercialized, the fabrication of the electronics should be cost and time effective. Emergent solution processing

technologies such as spraying techniques[30], screen printing,[31,32] or inkjet printing[25,33] not only require a reduced number of fabrication steps, but they are also compatible to produce electronics on large-area flexible substrates. Inkjet printing, in particular, allows for the digital fabrication of customizable designs at atmospheric conditions, with patterns that can be easily modified on demand, ideal for fabricating diagnostic devices on flexible substrates.[34,35] We and some others have already shown inkjet-printed flexible electrodes comprising PEDOT:PSS[21,22], and applied these electrodes printed either on paper substrates[25] or on stretchable textiles for long-term electrocardiography recordings.[23] A recent work of Ferrari et al demonstrated PEDOT:PSS electrodes printed on a tattoo paper which could measure muscular activity with high precision on limbs and face[36]. The electrode allows for hair growth underneath, a great advantage over conventional systems promising for long-term recordings on areas with high hair density. For practical applications, however, when the tattoo electronics is envisaged to be carried on the skin for longer periods, the integration of the tattoo with the acquisition system is as a challenge that needs to be addressed. Design solutions should exclude adhesives, insulating layers and metallic interconnects in order to reduce fabrication costs and involve a user friendly interface for these disposable systems. In this work, we present a simple method for the fabrication and integration of an inkjet-printed e-skin device based on tattoo technology. Using PEDOT:PSS both as the active electrode material as well as contact material, we record high quality EMG signals from the arm's biceps over 7 hours. Replacing conventional electrical wires or any contact fabricated by metal evaporating deposition that limit the feasibility of e-skin technologies, we utilize PEDOT:PSS contacts inkjet-printed on a conformable textile wristband. We characterized the tattoo/textile electronics system and investigated the performance of the device compared to commercial electrodes. Thickness and roughness for the tattoo electrodes and electrical properties for the tattoo/electronics were evaluated. The tattoo/textile electronics-skin impedance in the relevant frequency range for the recording of electrophysiological activities was measured. We show that with the band conforming on the skin and the intimate adhesion of the tattoo, we are able to record stable EMG signals

with comparable performance to conventional wet (gelled) Ag/AgCl electrodes. The proposed platform paves the way towards easy-to-fabricate and use, conformable, all-polymer biopotential electrodes that can be utilized in a wide range of diagnostics and as well as therapy applications.

Experimental

Fabrication of PEDOT:PSS based electronics on tattoo and textile: PEDOT:PSS ink was prepared using a mixture containing PEDOT:PSS dispersion (conducting polymer, Heraeus, Clevios PH1000), 20 wt% ethylene glycol (EG, co-solvent, Sigma Aldrich) and 0.8 wt% glycidoxypropyltrimethoxysilane (GOPS, crosslinker, Sigma Aldrich). While EG increases the conductivity of the films deposited, GOPS prevents the delamination of the conductive pattern during the tattoo deposition on skin. In this mixture, we also included 0.3wt% of commercially available surfactants and a combination of organic solvents to render rheological properties of the ink suitable for inkjet process without compromising softness and electrical conductivity. We used a Dimatix DMP-2800 inkjet printer to fabricate the tattoo/textile electronics. 1cm^2 square pattern of PEDOT:PSS (single layer) was printed on a commercially available temporary tattoo sheet (Tattoo 2.1, the Magic Touch Ltd., 123 Applications) composed of a single decal transfer paper (including 3 layers : a paper carrier, a starch–dextrin water soluble sacrificial layer, and a layer of ethylcellulose (thickness ca. 400nm). We printed up to 8 layers of PEDOT:PSS ink on a commercially available satin ribbon (Ideatiss). The metallic snaps buttons were installed to the ribbon via a snap plier. The drop spacing for all printing procedures was 15 µm. Once the ink was printed, the samples were placed in a conventional oven to cure the films at 110°C for 60 min.

Electrical characterization of the tattoo electrodes: The thickness of one PEDOT:PSS layer printed on the tattoo substrate was measured by using a mechanical profilometer (Ambios Technology). The sheet resistance of the printed PEDOT:PSS pattern was determined using a four point probe system (Jandel). The electrical resistance of the PEDOT:PSS contact on the textile as well as the one between the tattoo electrode and the textile contact were measured using a digital Multimeter (Amprobe 37XR-A Tru-rms).

Electrode–skin contact impedance measurements were performed as shown in Figure 2. The working electrode (the tattoo/textile electronics) and the counter electrode (wet Ag/AgCl, Ambu blue sensor) were placed on the forearm of a volunteer, keeping 3 cm distance from each other. The reference electrode (wet Ag/AgCl, Ambu blue sensor) was placed on the elbow. The experiments were conducted by applying a sinusoidal potential of 10 mV at the working electrode (tattoo electrode) with no constant differential voltage on the skin using a potentiostat (Metrohm Autolab B.V.). The impedance of the electrodes was screened for a frequency range between 0.1 and 1000 Hz and the data were analyzed using NOVA software. We evaluated the electrical stability of the tattoo electrode upon mechanical deformation. The tattoo electronics was placed across the distal phalange of the index finger that is exposed to multiple flexions/extensions. The electrical connection was made using two copper tapes adhering to the printed PEDOT:PSS electrode on opposite edges. The flexion/extension was repeated 250 times at 30° and at 90° angle of closure. The resistance was measured at every 10 repetitions.

EMG recordings and data acquisition: An able-bodied subject (male, 25 years old) participated in this study with informed consent acquired before conducting the experiments. All protocols and procedures were approved by the direction of research of the Ecole des Mines de St. Etienne. Two tattoo electrodes were placed 2 cm apart from each other at the center of the biceps of the left arm. The contacts printed on the textile wristband were placed on top of the tattooed areas of the skin in order to connect the recording and counter electrodes to the acquisition system. The second recording was done on the biceps of the right arm using 2 wet Ag/AgCl electrodes (Metrohm Autolab B.V.). In order to have comparable signals, the volunteer was asked to lift 1 kg of a standard weight with each arm simultaneously. A ground electrode was placed on the right leg. Each recording has been repeated at least 6 times one every 3 hours over 7 hours (T_0=1h, T_0+3h and T_0+6h). A RHD2216 chip from Intan Technologies has been used to acquire EMG data. The data were encoded on 16 bits at 1.1 kHz per channels. The on-chip filters were set as follows: the first order high pass was set at 10 Hz and the third order low pass filter was set at 300 Hz.

Processing of EMG data: Labview software was used to filter the signal and calculate the signal-to-noise-ratio (SNR). A first order Butterworth band-pass (10-300 Hz) was applied to all recordings. Then the SNR value of each signal was calculated using the following equation: $SNR(Sr) = 20 * \log\left(\sqrt{\frac{\sum_i Sc_i^2}{\sum_i Sr_i^2}}\right)$, where S_c is a portion of 5 s of the signal during a contraction and S_r is a portion of 5 s of the signal during a resting position.

Results and Discussion

Figure 1a shows a layer schematic of the tattoo electronics integrated with the textile contacts. The tattoo involves one layer of PEDOT:PSS ink inkjet-printed onto the temporary tattoo paper. PEDOT:PSS coating increases the roughness (RMS) of the substrate from 1.35nm to 3.77nm (figure S1). The electrical conductivity of a 95±5 nm thick printed PEDOT:PSS electrode (single layer) is 240±10 S/cm. The thickness and the associated sheet resistance can be further controlled by varying the number of printed layers of PEDOT:PSS. However, the tattoo substrate is not compatible with printing multiple layers of aqueous ink due to aqueous instability of the sacrificial layer. We estimated the conductivity of a single layer of the film (ca. 95±5 nm in thickness) to be adequate to acquire EMG signals. As inkjet offers freedom of form and design, different patterns can be realized (Figure 1b). Following the fabrication, the electronics printed on the paper was transferred onto the skin by simply wetting the tattoo transfer paper and gently pressing the tattoo against the skin. As the transfer paper is wetted, it dissolves and the conducting polymer pattern remains on the skin. The electrode conforms well to the skin and is in fact reported to enter deeply inside the creases of the skin[36] (Figure 1c). As the skin is crumbled or stretched due to muscle movements, the electrodes move with the skin, acting as its natural component (Figure 1d.). The electrodes tattooed on the skin have an intimate contact with the tissue and by using a conducting material which has a young's modulus of ca. 150MPa in wet state[24], similar to that of skin- 0.002-500 MPa[37], we overcome the inherent mechanical mismatch (Figure 1e).

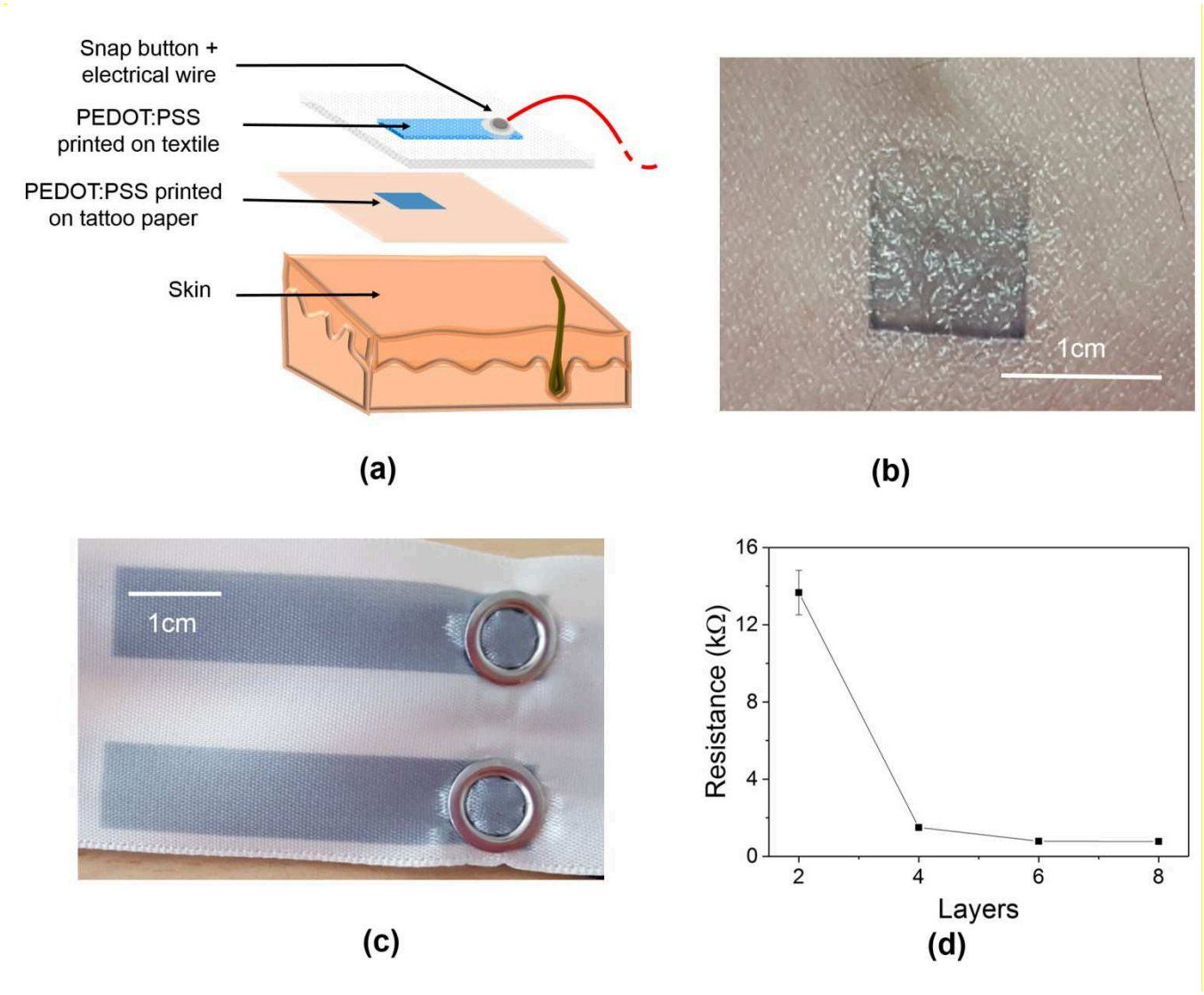

Fig. 1. (**a) Schematic of the Tattoo-textile electrodes**. The conducting polymer electrode printed on the tattoo paper is transferred to the skin. The textile containing the printed conducting polymer contacts is wrapped around the tattooed electrode on the skin replacing the wires connecting the skin adhered electrodes with the acquisition system allowing for detection of EMG signals, **(b) Photograph of customized printed tattoo electrodes deposited on the skin, Photographs of printed tattoo electrodes on the skin: undeformed (c), compressed (d), and after compression (e),** the tattoo electrode shows a good resistance to mechanical deformation, **(f) Electrical resistance of the printed squares on textile (1.5x1.5 cm^2) measured by a digital multimeter, (g) Photograph of the printed electrodes on textiles used for EMG (6 Layers) with the snap button.**

The conducting polymer was also printed on the textile wristband made of knitted conformable fabric (i.e. satin) using the same printing principles as for the tattoo paper. In order to optimize the electrical performance of the PEDOT:PSS contacts on the textile, we investigated the impact of the

number of the PEDOT:PSS layers on the conductivity of printed areas (1.5x1.5 cm^2). In particular, the electrical resistance of textile contacts decreased with the number of printed layers, reaching a plateau upon 6 layers of PEDOT:PSS (Figure 1f). The saturation is due to complete impregnation of the fabric with the conducting polymer. Following the fabrication of electrodes, we inserted metal snaps buttons to the textile on top of the conducting polymer pattern. With the snaps attached, the textile is now in the form of a wristband which could can be comfortably wrapped around the target skin area where the tattoo electrodes were transferred, and fixed using the snap closure (Figure 1g,). As such, we directly interface the tattooed electrodes with the contacts on the textile. The metal snaps on the wristband enable to connect the tattoo electrodes to the acquisition system while recording the electrophysiological activity. The electrical resistance between the tattooed electrodes on the skin and the metal snap on the textile is measured to be ca. 52±5 kΩ (Figure S2). This configuration obviates the need to use external wires in contrast to other studies with EMG electrodes relying on external connectors such as silver cotton wires,[27] gold coated plastic foils,[28] or polyimide films[29] which tend to cause unstable measurements due to motion artefacts and discomfort to the user.

We compared the electrode-skin contact impedance of the tattoo/textile electronics with the conventional wet (gelled) Ag/AgCl electrodes 1 hour after they have been in contact with skin (Figure 2a). Figure 2b shows the configuration of the measurement on the forearm of a volunteer. The commercial electrodes displayed impedance values two orders of magnitude lower than the tattoo/textile electronics for low frequencies (from 0.1 Hz to 100 Hz) and one order of magnitude lower for higher frequencies (from 100 Hz to 1000 Hz). This difference is due to the presence of the gel electrolyte applied with the Ag/AgCl electrodes, which lowers the impedance dramatically.[38] The tattoo/textile system, on the other hand, shows reduced impedance values for all the frequencies explored, as well as a smaller sample to sample deviation compared to the printed textile electrode only. At the frequency range where the significant EMG signals occur (5-450 Hz)[39], the tattoo/textile electronics display an impedance of ca. 1.835+/-0.007 MΩ at 5 Hz and 225+/-10 kΩ at 450 Hz. Albeit with impedance higher

than conventional electrodes (15.4+/-0.5 kΩ at 5 Hz and 9.1+/-0.1 kΩ at 450 Hz.for the wet Ag/AgCl electrodes), we and others postulate that the dry electrodes have the advantage of being more stable[40].

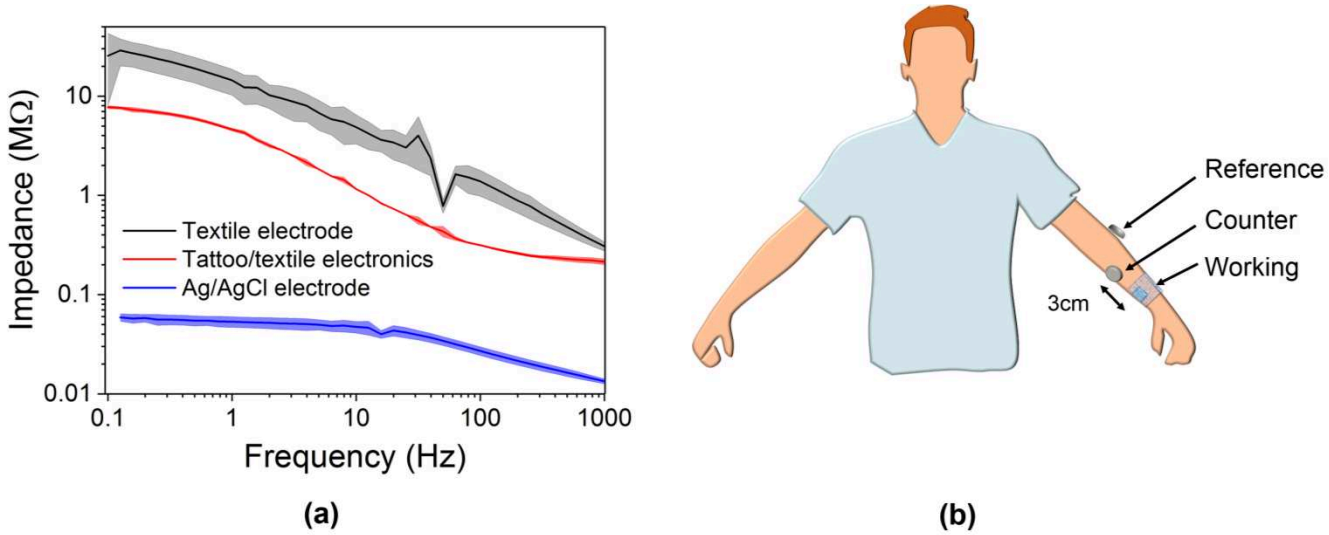

Fig. 2. (a) Electrochemical impedance spectra of the textile, tattoo/textile electronics and wet (gelled) Ag/AgCl electrodes after 1 hour of contact on the skin. The evaluation includes 3 samples, the shaded areas represent the standard deviation. (b) Schematic representation of the electrode positions on the forearm for characterization of the electrodes that electrically interface skin: working electrode is the textile, tattoo/textile electronics or wet (gelled) Ag/AgCl, while counter and reference electrodes are Ag/AgCl.

Compared to the conventional gelled electrodes, tattoo electrodes conform and bend with the skin. In order to demonstrate the stability of the tattoo electrode, we measured its electrical resistance under deformation. The tattoo is deposited between the distal and intermediate phalanges of the index finger of the volunteer who was asked to perform repetitive flexions/extensions (Figure 3a and b). We recorded the electrical resistance of the electrode, as the tattoo was subject to different bending angles (30° and 90°) up to 250 cycles. While we do not observe a significant variation in the electrical resistance at a flexion to 30°, there is a slight increase of resistance for flexion to 90°, attributed to the failure of the thicker metallic adhesives used to contact the tattoo. This hypothesis, similar to the one proposed by Zucca and colleagues,[28] is confirmed by the cracks observed at the adhesive-tattoo interface (Figure S3). In parallel, we examined the electrical stability of the contact printed on the textile electrode worn for a period of 7 hours. We observed no fluctuation in the polymer conductivity, proving the stability of the contact over time.

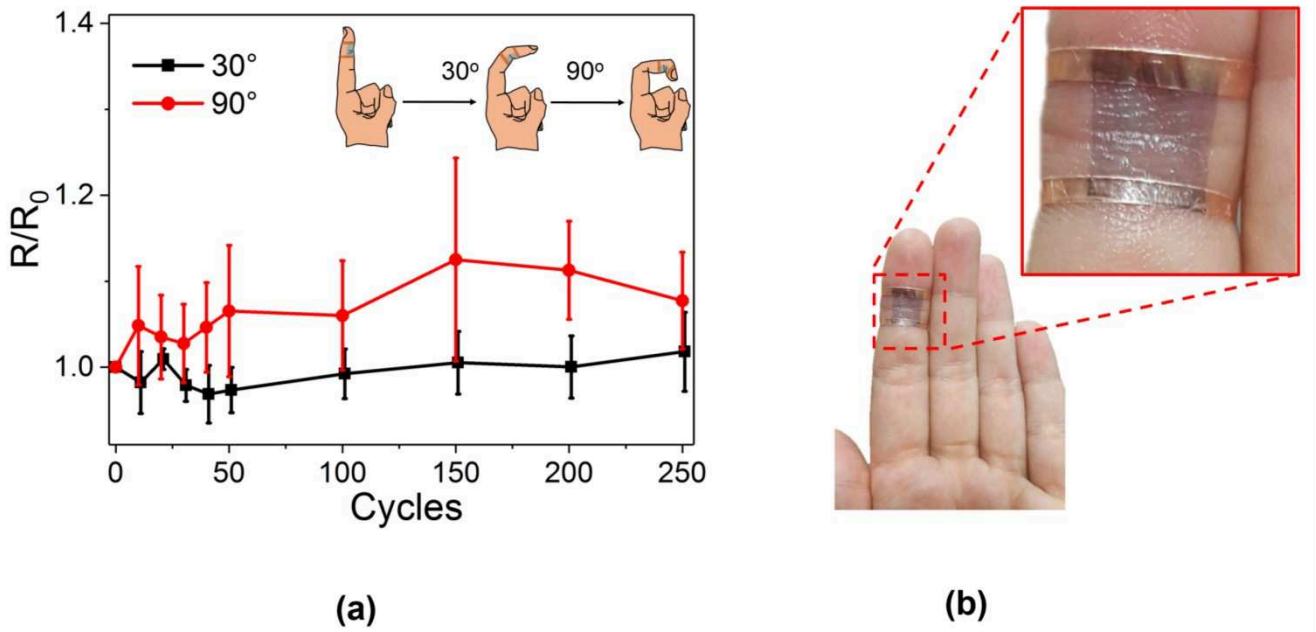

Fig. 3. Evaluation of the functionality of the tattoo electronics on the skin. (a) Variation of the electrical resistance of the printed tattoo electrode after repeated contractions of the index finger at 30° and 90° bending angle, (b) Photograph of the tattoo on the index finger of the volunteer and the bending experiment. The tattoo electrode is this time connected to the acquisition system with copper adhesives placed underneath at the edges of the conducting pattern.

To validate the use of our tattoo/textile electronics for acquiring EMG signals, we transferred the tattoo onto the forearm of a volunteer and connected the tattoo electrode to the acquisition system using the electronic wristband as shown in Figure 4a. The tattoo electrodes (working and counter) were positioned 2 cm apart from each other on the lower part of the left arm's biceps and EMG signals were recorded over a 6 hour period once in every 3 hours. The signals acquired from the tattoo/textile electronics were compared to those acquired with wet Ag/AgCl electrodes. These electrodes were positioned on the exact same locations this time on the right arm exposed to the same experimental conditions.

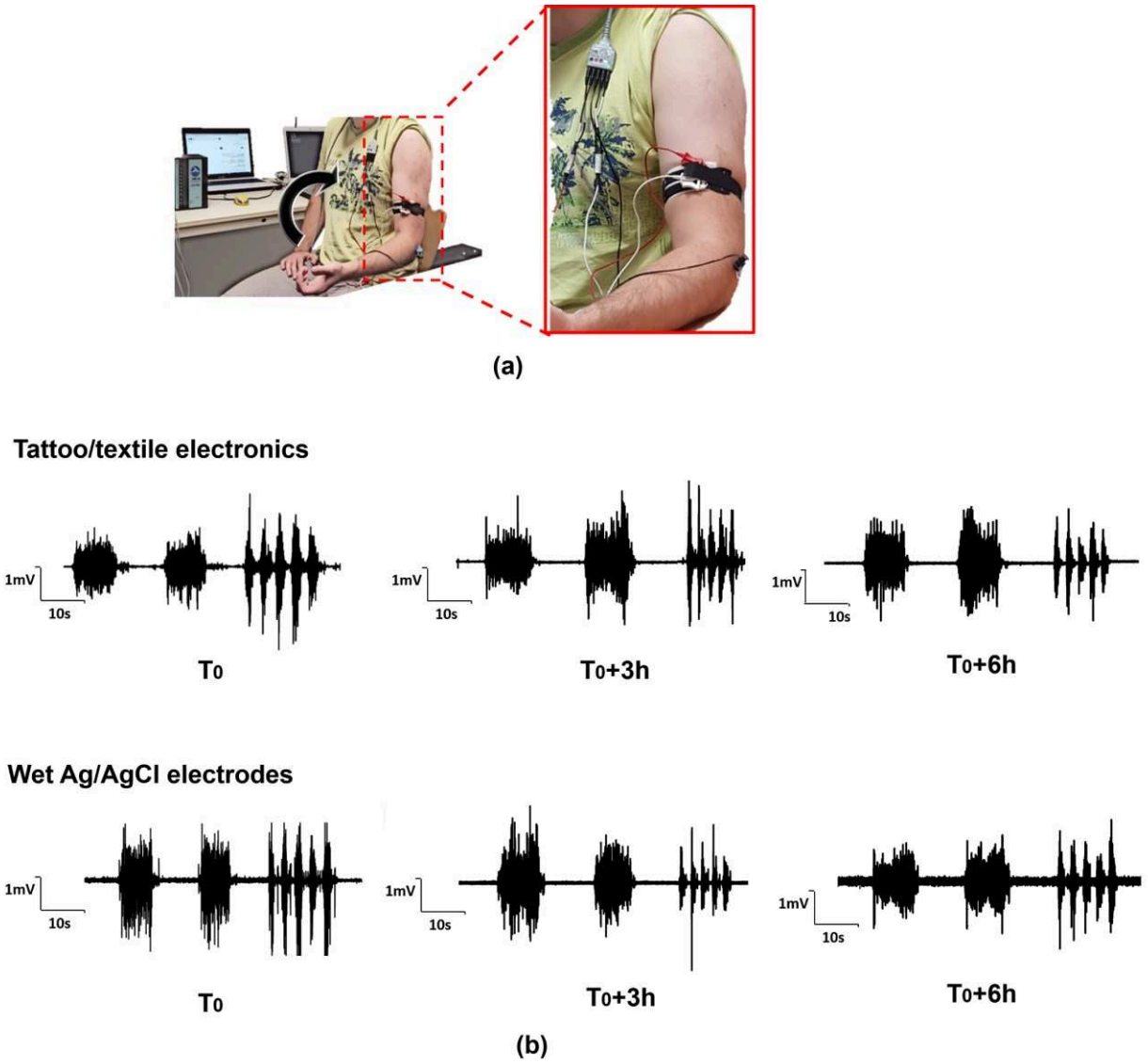

Fig. 4. EMG recordings of the biceps contraction on a volunteer. (a) Photograph of the EMG experiment with a loop on the arm, the textile was placed underneath a black adjustable sweatband and the tattoo electrodes were deposited below the textile, (b) Comparison between the EMG signals measured tattoo-textile electrodes after 2 long contractions (10 s) and 5 short contractions (1 s) at T_0+1h at T_0+3h and finally T_0+6h or tattoo-textile electronics and for wet Ag/AgCl electrodes The working and counter electrodes were positioned 2 cm apart on the lower part of the left arm's biceps and EMG signals were recorded over a 7 hour period once in every 3 hours (The SNR were 11+/-2dB, 26+/-2dB, 21+/-1dB for the tattoo/textile electronics vs 29+/1dB, 25+/-1dB, 20+/-5 dB for the wet Ag/AgCl electrodes respectively at T_0, T_0+3h, T_0+6h).

Figure 4b shows the EMG recordings acquired with tattoo/textile electronics as well as Ag/AgCl electrodes during the biceps activity for both short (1 s) and long (10 s) voluntary muscle contractions over 6 hours. Each experiment was repeated 6 times. The recordings used to extract the signal to noise ratio (SNR) consisted of 10 seconds long muscle contractions during which the volunteer was asked to

lift a 1 kg of standard weight with an elbow angle of ca. 90°, with a resting period of 10 seconds. As the electrodes are placed on the skin (t_0=1h), the tattoo/textiles electronics exhibited a mean SNR of 11±2 dB compared to a mean SNR of 29±1 dB for the wet Ag/AgCl electrodes. The lower quality of the recordings with the dry tattoo after its adherence with the skin is attributed to the high electrode-skin contact impedance of these electrodes (Figure 2a). Despite the lower SNR, the tattoo/textiles electronics could measure the EMG activity. Interestingly, after 4 hours of contact with the skin ($t=T_0$+3h), the performance of the electronics was substantially improved: SNR increased to 26±2 dB while the one from Ag/AgCl electrodes decreased to 25±1 dB. We postulate that the quality of the contact of the tattoo/textile electronics with the skin increased due to the sweat-gland activity. The sweat produced by the body wets the tattoo, thus enhances the ionic conductivity at the skin-electrode interface and leads to a decrease of the contact impedance between the skin and the PEDOT:PSS.[41] Another factor that contributed to reduce impedance is the improved quality of contact between the tattoo and the textile as shown is fig 1a there is thin layer of ionic conductor ethyl cellulose between 2 PEDOT:PSS layers as the skin get wet the layer becomes more permeable to ions allowing the current to pass easier form the skin to the textile contact. Finally, 7 hours after the first recordings ($t=T_0$+6h), the tattoo-textile electrodes displayed similar performance (SNR=21±1 dB) compared to the wet Ag/AgCl electrodes (SNR=20±5 dB).These results demonstrate the stability of the tattoo-textile electronics over time their easy fabrication, integration and the absence of a gel electrolyte.

Conclusions

We designed an inkjet-printed tattoo/textile electronics system for facile EMG recordings utilizing the biocompatible conducting polymer PEDOT:PSS both as the transducer and the contact to the acquisition system. The polymer electrode printed on the tattoo showed excellent adherence to the skin with no evident side effects such as skin irritation or allergies. The electrodes exhibited sufficient conductivity for acquiring muscle activities from the skin. The same conducting polymer was printed on a textile

used as a wristband around the skin and acted as a bridge between the tattoo electrode and the external electronics. The integration of the conducting polymer both as the electrode and contact material minimizes the cost while improving the feasibility of such skin-adhering electronics envisaged to be applied as diagnostics or therapy tools. The intimate contact of the tattooed electronics with the skin, its conformability and bending with the movements of the limbs is a great advantage over other cutaneous systems. Our approach for interfacing the external electronics avoids the use of inorganic rigid wires and presents a wearable solution. We show that over 7 hours of EMG recordings (biceps contraction), the tattoo/textile electronics showed similar performance to conventional wet Ag/AgCl electrodes without the use of gel electrolytes. These results pave the way toward a new class of easy-to-use, easy-to-fabricate, low cost, skin adhering electronics that involve a wearable connection. Due to the versatility of the materials and the processes employed, such systems can encompass a variety of applications such as myoelectric prosthesis or detection of muscle functioning.

Acknowledgments: The authors acknowledge Dr. Anna Maria Pappa (University of Cambridge) for fruitful discussions. This work was supported though grants by the ANR, and MicroVitae Technologies.

References

[1] Gambhir S S, Ge T J, Vermesh O and Spitler R 2018 Toward achieving precision health *Sci. Transl. Med.* **10** eaao3612

[2] Yeo W-H, Kim Y-S, Lee J, Ameen A, Shi L, Li M, Wang S, Ma R, Jin S H, Kang Z, Huang Y and Rogers J A 2013 Multifunctional Epidermal Electronics Printed Directly Onto the Skin *Adv. Mater.* **25** 2773–8

[3] J. Bandodkar A, S. Hung V W, Jia W, Valdés-Ramírez G, R. Windmiller J, G. Martinez A, Ramírez J, Chan G, Kerman K and Wang J 2013 Tattoo-based potentiometric ion-selective sensors for epidermal pH monitoring *Analyst* **138** 123–8

[4] Kim J, Valdés-Ramírez G, Bandodkar A J, Jia W, Martinez A G, Ramírez J, Mercier P and Wang J 2014 Non-invasive mouthguard biosensor for continuous salivary monitoring of metabolites *Analyst* **139** 1632–6

[5] Parrilla M, Cánovas R, Jeerapan I, Andrade F J and Wang J 2016 A Textile-Based Stretchable Multi-Ion Potentiometric Sensor *Adv. Healthc. Mater.* **5** 996–1001

[6] Imani S, Bandodkar A J, Mohan A V, Kumar R, Yu S, Wang J and Mercier P P 2016 A wearable chemical–electrophysiological hybrid biosensing system for real-time health and fitness monitoring *Nat. Commun.* **7** 11650

[7] Tee B C-K, Wang C, Allen R and Bao Z 2012 An electrically and mechanically self-healing composite with pressure- and flexion-sensitive properties for electronic skin applications *Nat. Nanotechnol.* **7** 825–32

[8] Wang S, Xu J, Wang W, Wang G-J N, Rastak R, Molina-Lopez F, Chung J W, Niu S, Feig V R and Lopez J 2018 Skin electronics from scalable fabrication of an intrinsically stretchable transistor array *Nature*

[9] N, Mazzaro 2016 Risk of skin reaction when using ECG electrodes

[10] Tao X M 2001 *Smart Fibres, Fabrics and Clothing: Fundamentals and Applications* (Elsevier)

[11] Park S and Jayaraman S 2003 Smart textiles: Wearable electronic systems *MRS Bull.* **28** 585–91

[12] Matsuhisa N, Kaltenbrunner M, Yokota T, Jinno H, Kuribara K, Sekitani T and Someya T 2015 Printable elastic conductors with a high conductivity for electronic textile applications *Nat Commun* **6**

[13] Yapici M K, Alkhidir T, Samad Y A and Liao K 2015 Graphene-clad textile electrodes for electrocardiogram monitoring *Sens. Actuators B Chem.* **221** 1469–74

[14] Wagner S, Lacour S P, Jones J, Pai-hui I H, Sturm J C, Li T and Suo Z 2004 Electronic skin: architecture and components *Phys. E Low-Dimens. Syst. Nanostructures* **25** 326–34

[15] Kim D-H, Lu N, Ma R, Kim Y-S, Kim R-H, Wang S, Wu J, Won S M, Tao H, Islam A, Yu K J, Kim T -i., Chowdhury R, Ying M, Xu L, Li M, Chung H-J, Keum H, McCormick M, Liu P, Zhang Y-W, Omenetto F G, Huang Y, Coleman T and Rogers J A 2011 Epidermal Electronics *Science* **333** 838–43

[16] Huang X, Liu Y, Cheng H, Shin W-J, Fan J A, Liu Z, Lu C-J, Kong G-W, Chen K, Patnaik D, Lee S-H, Hage-Ali S, Huang Y and Rogers J A 2014 Materials and Designs for Wireless Epidermal Sensors of Hydration and Strain *Adv. Funct. Mater.* **24** 3846–54

[17] Kim J, Banks A, Cheng H, Xie Z, Xu S, Jang K-I, Lee J W, Liu Z, Gutruf P, Huang X, Wei P, Liu F, Li K, Dalal M, Ghaffari R, Feng X, Huang Y, Gupta S, Paik U and Rogers J A 2015 Epidermal Electronics with Advanced Capabilities in Near-Field Communication *Small* **11** 906–12

[18] Rivnay J, Owens R M and Malliaras G G 2013 The rise of organic bioelectronics *Chem. Mater.* **26** 679–85

[19] Elschner A, Kirchmeyer S, Lovenich W, Merker U and Reuter K 2010 *PEDOT: principles and applications of an intrinsically conductive polymer* (CRC Press)

[20] Strakosas X, Wei B, Martin D C and Owens R M 2016 Biofunctionalization of polydioxythiophene derivatives for biomedical applications *J. Mater. Chem. B* **4** 4952–68

[21] Mannerbro R, Ranlöf M, Robinson N and Forchheimer R 2008 Inkjet printed electrochemical organic electronics *Synth. Met.* **158** 556–60

[22] Vuorinen T, Niittynen J, Kankkunen T, Kraft T M and Mäntysalo M 2016 Inkjet-Printed Graphene/PEDOT:PSS Temperature Sensors on a Skin-Conformable Polyurethane Substrate *Sci. Rep.* **6** 35289

[23] Bihar E, Roberts T, Ismailova E, Saadaoui M, Isik M, Sanchez-Sanchez A, Mecerreyes D, Hervé T, De Graaf J B and Malliaras G G 2017 Fully Printed Electrodes on Stretchable Textiles for Long-Term Electrophysiology *Adv. Mater. Technol.* **2** 1600251

[24] ElMahmoudy M, Inal S, Charrier A, Uguz I, Malliaras G G and Sanaur S 2017 Tailoring the electrochemical and mechanical properties of PEDOT: PSS films for bioelectronics *Macromol. Mater. Eng.* **302**

[25] Bihar E, Roberts T, Saadaoui M, Hervé T, De Graaf J B and Malliaras G G 2017 Inkjet-Printed PEDOT:PSS Electrodes on Paper for Electrocardiography *Adv. Healthc. Mater.* 1601167

[26] Håkansson A, Han S, Wang S, Lu J, Braun S, Fahlman M, Berggren M, Crispin X and Fabiano S 2017 Effect of (3-glycidyloxypropyl) trimethoxysilane (GOPS) on the electrical properties of PEDOT: PSS films *J. Polym. Sci. Part B Polym. Phys.* **55** 814–20

[27] Zucca A, Cipriani C, Tarantino S, Ricci D, Mattoli V and Greco F 2015 Tattoo Conductive Polymer Nanosheets for Skin-Contact Applications *Adv. Healthc. Mater.* **4** 983–90

[28] Zucca A, Yamagishi K, Fujie T, Takeoka S, Mattoli V and Greco F 2015 Roll to roll processing of ultraconformable conducting polymer nanosheets *J. Mater. Chem. C* **3** 6539–48

[29] Bareket L, Inzelberg L, Rand D, David-Pur M, Rabinovich D, Brandes B and Hanein Y 2016 Temporary-tattoo for long-term high fidelity biopotential recordings *Sci. Rep.* **6** 25727

[30] Pitsalidis C, Pappa A-M, Hunter S, Payne M M, Anthony J E, Anthopoulos T D and Logothetidis S 2015 Electrospray-Processed Soluble Acenes toward the Realization of High-Performance Field-Effect Transistors *ACS Appl. Mater. Interfaces* **7** 6496–504

[31] Scheiblin G, Aliane A, Strakosas X, Curto V F, Coppard R, Marchand G, Owens R M, Mailley P and Malliaras G G Screen-printed organic electrochemical transistors for metabolite sensing *MRS Commun.* 1–5

[32] Ersman P A, Westerberg D, Tu D, Nilsson M, Åhlin J, Eveborn A, Lagerlöf A, Nilsson D, Sandberg M and Norberg P 2017 Screen printed digital circuits based on vertical organic electrochemical transistors *Flex. Print. Electron.* **2** 045008

[33] Roberts T, De Graaf J B, Nicol C, Hervé T, Fiocchi M and Sanaur S 2016 Flexible Inkjet-Printed Multielectrode Arrays for Neuromuscular Cartography *Adv. Healthc. Mater.* **5** 1462–70

[34] Bihar E, Deng Y, Miyake T, Saadaoui M, Malliaras G G and Rolandi M 2016 A Disposable paper breathalyzer with an alcohol sensing organic electrochemical transistor *Sci. Rep.* **6** 27582

[35] Batchelor J C and Casson A J 2015 Inkjet printed ECG electrodes for long term biosignal monitoring in personalized and ubiquitous healthcare 2015 37th Annual International Conference of the IEEE Engineering in Medicine and Biology Society (EMBC) pp 4013–6

[36] Ferrari L M, Sudha S, Tarantino S, Esposti R, Bolzoni F, Cavallari P, Cipriani C, Mattoli V and Greco F 2018 Ultraconformable Temporary Tattoo Electrodes for Electrophysiology *Adv. Sci.*

[37] Kalra A, Lowe A and Jumaily A A 2016 An Overview of Factors Affecting the Skins Youngs Modulus *J. Aging Sci.* **4** 1–5

[38] Searle A and Kirkup L 2000 A direct comparison of wet, dry and insulating bioelectric recording electrodes *Physiol. Meas.* **21** 271

[39] Van Boxtel A 2001 Optimal signal bandwidth for the recording of surface EMG activity of facial, jaw, oral, and neck muscles *Psychophysiology* **38** 22–34

[40] Leleux Pierre, Badier Jean-Michel, Rivnay Jonathan, Bénar Christian, Hervé Thierry, Chauvel Patrick and Malliaras George G. 2013 Conducting Polymer Electrodes for Electroencephalography *Adv. Healthc. Mater.* **3** 490–3

[41] Gruetzmann A, Hansen S and Müller J 2007 Novel dry electrodes for ECG monitoring *Physiol. Meas.* **28** 1375

Supplementary Materials

Fully printed all-polymer tattoo/textile electronics for electromyography

Eloïse Bihar[1,2,3,5]†, Timothée Roberts[3,4]†, Yi Zhang[5], Esma Ismailova[1], Thierry Hervé[3], George G. Malliaras[1], Jozina B. De Graaf[4], Sahika Inal[5]* and Mohamed Saadaoui[2]*

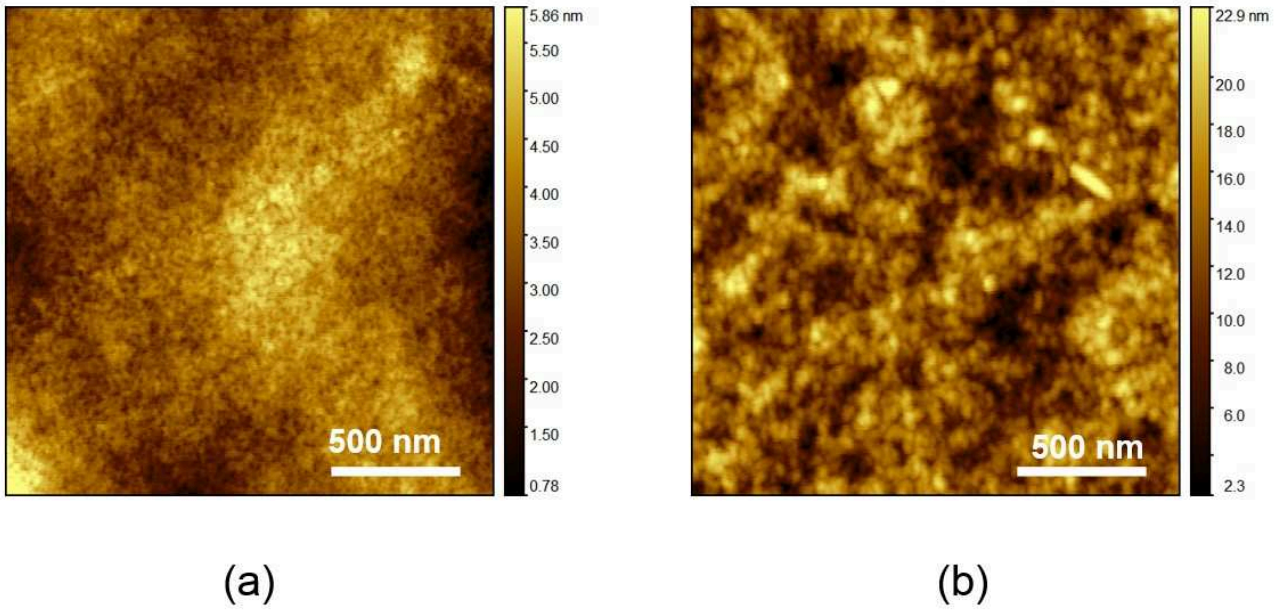

Fig. S1. AFM image (2x2um) of the tattoo substrate (a) and PEDOT:PSS printed on tattoo (b)

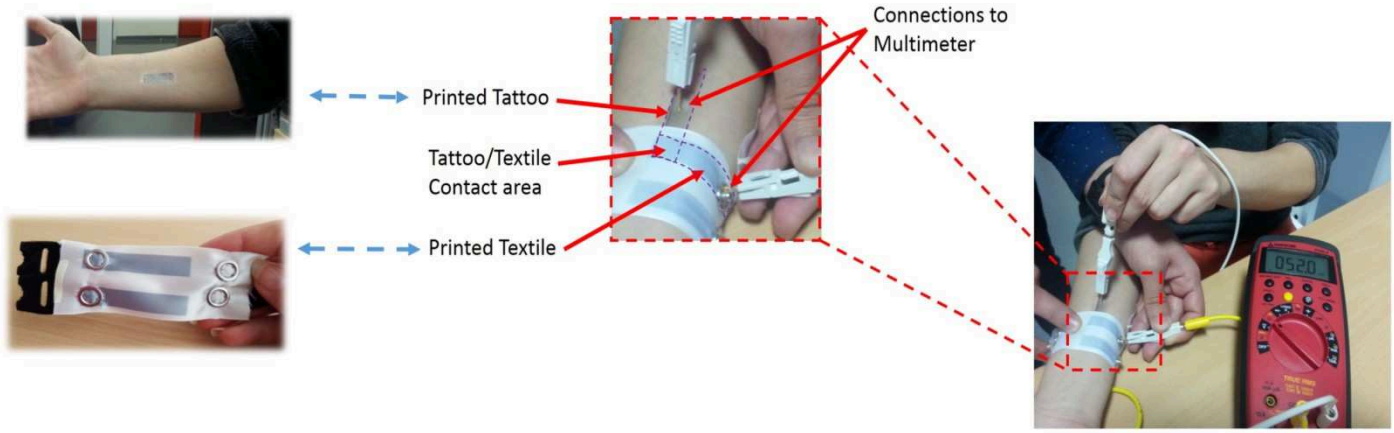

Fig. S2. Fig. 1. Photograph of the tattoo-textile electronics. The printed tattoo electrode (1cm x 5cm) is deposited on the skin after humidification with water. A printed stretchable textile electrode wristband is placed on top of the tattoo. The electrical resistance of the tattoo-textile system is measured by connecting the tattoo and the electrode extremities to the digital multimeter

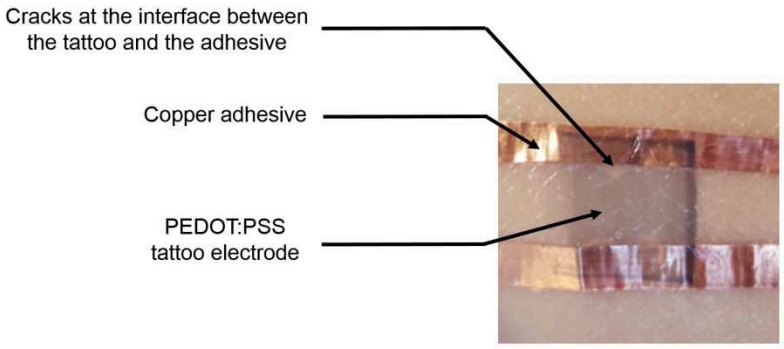

Fig. S3. Photograph of the cracks observed at the tattoo/copper adhesive interface. The tattoo is connected with copper adhesives placed underneath at the edges of the conducting pattern on the skin of the volunteer.

VI. Analyses de signaux sEMG pour la localisation de zones d'innervations

Comme présenté dans l'introduction, je me suis intéressé à deux thématiques : la création d'électrodes intégrables dans le manchon d'une prothèse myoélectrique et l'étude de la réorganisation neuromusculaire post-amputation via l'étude des zones d'innervations. Nous allons dans ce chapitre nous intéresser à la deuxième thématique.

Pour revenir sur ce qui a été abordé dans le chapitre d'introduction, les zones d'innervations sont les zones où les axones issus de motoneurones projettent sur les fibres musculaires. Lors d'une contraction musculaire, les motoneurones génèrent des potentiels d'action qui vont se propager dans les axones pour atteindre les zones d'innervations. À partir de là, une vague de polarisation va se propager à partir de la zone d'innervation vers les extrémités des fibres musculaires. En sEMG, on mesure en surface de la peau la somme de tous ces potentiels d'actions dans le volume de détection du couple d'électrodes. Pour détecter les zones d'innervations, il nous faut donc nous intéresser aux phénomènes physiques autour de la propagation de ces potentiels d'actions.

De nombreuses méthodes électro-physiologiques ont été expérimentées durant les 40 dernières années pour pouvoir remonter à la position de ces zones d'innervation [51,52]. Les premières techniques utilisaient des électrodes piquées qui permettaient de faire un mapping des potentiels d'action le long des fibres permettant la localisation des jonctions neuromusculaires. Ensuite, même si cela est plus complexe analytiquement, des techniques de décomposition du signal sEMG ont permis de reconstituer la propagation de potentiels d'action le long des fibres du muscle. Ces méthodes sont précises mais sont trop lourdes analytiquement pour être implémentées sur des systèmes embarqués et ont besoin d'une certaine expertise pour être utilisées.

D'autres méthodes calculent des grandeurs mathématiques à partir des signaux sEMG et comparent les résultats suivant la position des électrodes placées parallèlement aux fibres musculaires. Beck et collègues (2010) nous présentent certaines de ces techniques [53]. Une de ces techniques est basée sur la valeur RMS (« root mean square ») qui correspond à l'aire sous la courbe d'un signal. On parle aussi de puissance du signal. La formule utilisée est la suivante :

$RMS(X) = \sqrt{\frac{\sum_i^n {X_i}^2}{n}}$, avec *X* l'ensemble des points de mesure sEMG, et *n* le nombre total de points de mesure sEMG.

L'amplitude du signal sEMG est directement liée au nombre de potentiels d'action qui sont détectés par la paire d'électrodes. Or, dû à l'enregistrement bipolaire, on ne garde que la différence locale entre les deux électrodes. Lorsqu'une paire d'électrodes est positionnée sur les deux côtés d'une zone d'innervation, l'amplitude du signal diminue car les signaux détectés ont la même polarité pour les deux électrodes. Par conséquent, autour de la zone d'innervation, la valeur RMS du signal est plus faible. J'ai utilisé cette méthode dans le cadre de la fabrication et du test de matrice Kapton présenté dans le chapitre II (Image 5b). Cette expérience a permis de compléter la validation de la capacité des matrices d'électrodes en Kapton à acquérir des données électrophysiologiques exploitables. Cette méthode est facile à automatiser et à réaliser. Cependant, elle est très sensible à la qualité du signal, et peu précise par rapport à d'autres techniques.

Une autre méthode classique, reprise par Beck et al. 2010 [53], s'intéresse au domaine fréquentiel des signaux sEMG en utilisant la « Mean Power Frequency » (MPF). Pour cela, on prend le spectre fréquentiel d'un signal donné et on le découpe en deux aires égales sous la courbe. Cette technique se base sur le fait que la composante fréquentielle des signaux est plus puissante dans les hautes fréquences lorsque l'on approche la paire d'électrodes des zones d'innervation. Il a donc été proposé de comparer les valeurs MPF, la valeur la plus élevée correspondant à la position supposée des zones d'innervation. Cette technique est tout aussi simple analytiquement que la méthode RMS mais souffre des mêmes défauts.

La dernière méthode présentée par Beck et al. 2010 [53] utilise la technique de cross-corrélation entre les différents signaux obtenus par des couples d'électrodes successifs. Cette dernière technique se base sur le fait que l'on devrait détecter un changement de phase au niveau de la zone d'innervation étant donné le changement de sens de conduction des potentiels d'action à ce niveau-là. Pour cela, on calcule les courbes de cross-corrélation entre deux signaux consécutifs le long des fibres musculaires et on récupère l'amplitude du pic de corrélation. Beck et collègues (2010) ont montré que les méthodes utilisant les méthodes RMS et MPF ont moins de 50% de réussite, alors qu'avec cette méthode utilisant la cross-corrélation, ils ont localisé les zones d'innervation dans 90% du temps.

D'autres méthodes ont été recherchées [54–57]. Parmi celles-ci, une méthode proposée par Östlund et al. (2007) [49] nous a particulièrement intéressés. Ces auteurs ont proposé d'utiliser un algorithme appliqué au traitement d'image basé sur les travaux de Horn et Schunk en 1981 [58] qui permet initialement d'analyser les déplacements d'intensité lumineuse sur deux images successives dans le temps. Cette méthode permet donc d'identifier des objets en mouvement. L'hypothèse sur laquelle elle se base est qu'entre deux images successives, les intensités lumineuses sont les mêmes mais légèrement déplacées. De façon intéressante, Ötslund et al [49] ont utilisé cette technique (que l'on nommera ici H&S du nom de ses inventeurs) pour détecter les zones d'innervations musculaires. L'hypothèse ici, est que les intensités du signal sEMG entre t et t+dt sont les mêmes. Elles sont seulement légèrement déplacées spatialement. Ce qui n'est pas exactement correct étant donné la somme de potentiels d'action de sources diverses et le bruit. C'est pourquoi Östlund et al. proposent de calculer le champ médian des résultats de l'algorithme HS. L'hypothèse sur l'intensité nous donne donc l'équation suivante:

$$I(x + dx, y + dy, t + dt) = I(x, y, t)$$

Puis, en faisant les approximations mathématiques nécessaires, on obtient la contrainte à résoudre suivante :

$-I_t = I_x u + I_y v$, où u et v sont les vitesses de déplacement de l'intensité lumineuse respectivement dx/dt et dy/dt.

Horn et Schunk [58] proposent une résolution de cette équation. Ce que l'on obtient finalement est grossièrement le résultat d'une différence locale permettant d'observer les petits déplacements d'intensité sur une image sous la forme de champ de vecteur (U, V). Pour l'appliquer à la détection de zone d'innervation [49], Östlund et al. proposent de prendre les points de mesure enregistrés à un instant t par une matrice d'électrodes, comme les pixels d'une image. Les points de mesure enregistrés par la même matrice à l'instant t+1 composeront donc l'image succédant à la précédente image dans le temps. L'intensité lumineuse étudiée dans l'algorithme de base sera ici l'amplitude du signal sEMG. En appliquant l'algorithme à la totalité du temps d'enregistrement (du mouvement), nous récupérerons le champ de vecteurs médians. La dispersion des vecteurs vers l'extrémité du muscle étudié reflète la position des zones d'innervation. On cherche alors à voir une zone autour de laquelle tous les vecteurs environnants pointent vers l'extérieur. Dans la publication en question, cet algorithme est comparé à l'analyse RMS, présentée précédemment, en termes d'efficacité de détection des zones d'innervation. Pour cela, un

écart moyen par rapport à une référence est défini comme l'écart entre la position des zones d'innervations trouvées grâce aux algorithmes étudiés et grâce à une méthode témoin. Par rapport à une référence définie par un expert (utilisant des techniques de décomposition), la méthode RMS a un écart moyen de 13.6 ± 11 mm alors que la méthode H&S a un écart moyen de 2.4 ± 3.4 mm. De plus, ces auteurs montrent que même si la matrice d'électrode n'est pas dans le sens des fibres musculaires, il est toujours possible de détecter les zones d'innervation ou à minima de détecter le sens des fibres musculaires sous-jacentes, ce qui a été confirmé par Mesin en 2015 [59]. Ce dernier aspect de l'algorithme est très important dans notre cas étant donné la méconnaissance du placement de la musculature dans le membre résiduel après une amputation. De plus, cette méthode semble très prometteuse en termes de temps de calcul. Nous avons donc décidé de nous intéresser également à cette technique dans notre étude.

Pour évaluer l'algorithme H&S, nous l'avons comparé aux méthodes RMS, MPF et de cross-corrélation qui sont plus faciles à mettre en place. Pour des raisons de temps, il n'a malheureusement pas été possible d'aller jusqu'au bout de l'application de cet algorithme à l'étude de la réorganisation neuromusculaire chez l'amputé de bras. Des résultats préliminaires pour évaluer les algorithmes vont donc être présentés ici. Pour cela, 3x8 électrodes commerciales Ambu Blue Sensor ont été positionnées sur le biceps d'un sujet sain, comme présenté sur la figure 3.

Figure **3.** Placement de 3x8 électrodes ambu sur le biceps d'un participant sain pour la comparaison d'algorithmes de détection de zone d'innervation. On remarque les deux électrodes proximales qui sont la référence ainsi que l'électrode de terre. L'électrode de référence est nécessaire pour le système d'enregistrement utilisé dont nous utilisons l'entrée EEG pour l'enregistrement de l'EMG.

Les signaux ont été échantillonnés à 1000 Hz grâce au système eego^{TM}sports (ANT-neuro, Pays-Bas). Les signaux ont ensuite été filtrés par un filtre passe-bande d'ordre 2 autour des fréquences 0.1-500 Hz ainsi qu'un filtre coupe bande autour de 50 Hz. Les signaux bipolaires ainsi obtenus sont présentés dans la figure 4.

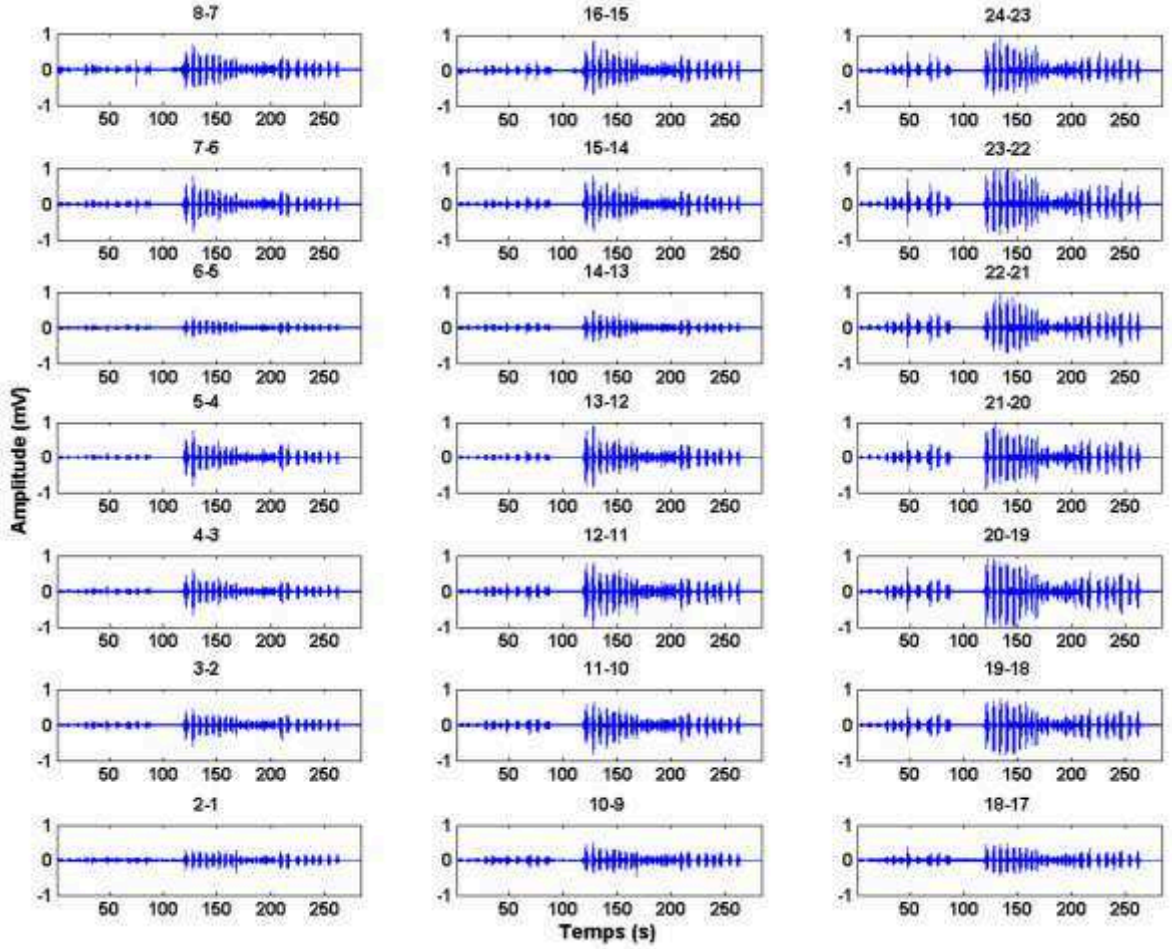

Figure 4. Signaux bipolaires du biceps d'un participant sain pour chaque paire d'électrodes. Le positionnement de bas en haut correspond aux positions des électrodes sur le bras de distal à proximal ; les positions à gauche correspondent à la colonne de gauche sur le bras. Au-dessus de chaque signal sont indiquées les deux électrodes dont la différence de signal a été calculée.

Ces signaux ont ensuite été traités en utilisant respectivement les algorithmes RMS, MPF, de cross-corrélation et H&S. La figure 5 montre la représentation topographique des résultats obtenus par l'algorithme RMS. On peut y voir un minima se former au niveau du couple d'électrodes (6-5) pour chaque colonne. Des effets de bords[2] sont cependant assez importants au niveau du couple d'électrodes (2-1).

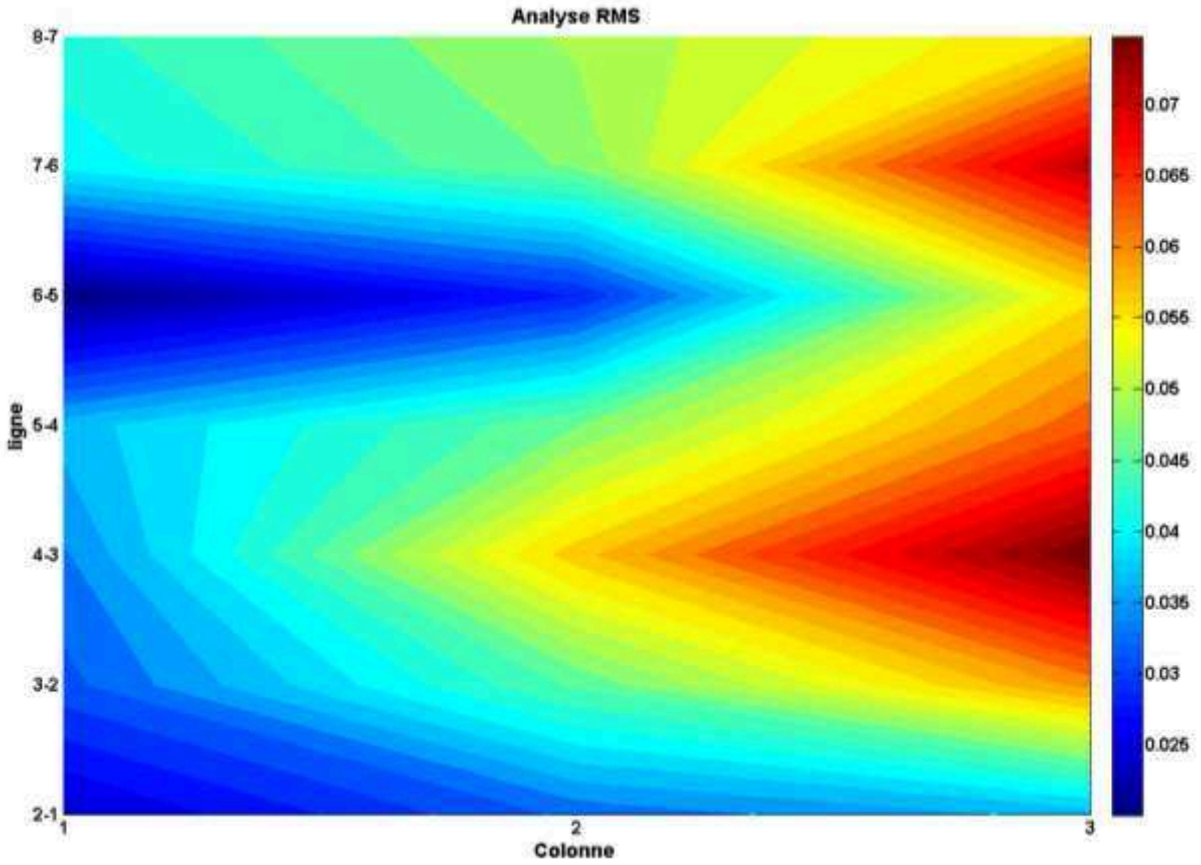

Figure **5**: Topographie des résultats de l'analyse avec la technique RMS avec la matrice de 3x8 électrodes. Le positionnement des électrodes correspond à celle de la Figure 5. La couleur correspond à l'amplitude du signal, indiquée dans l'échelle à droite dans la figure. On remarque une ligne horizontale minimum au niveau de l'électrode 5 ainsi qu'au niveau de l'électrode 1.

[2] Effet de bord : Changement de propriété à l'approche d'une zone modifiant le résultat attendu.

Les résultats pour l'algorithme MPF, présentés dans la figure 6 montrent une séparation du spectre fréquentiel en deux parties avec une aire sous la courbe égale.

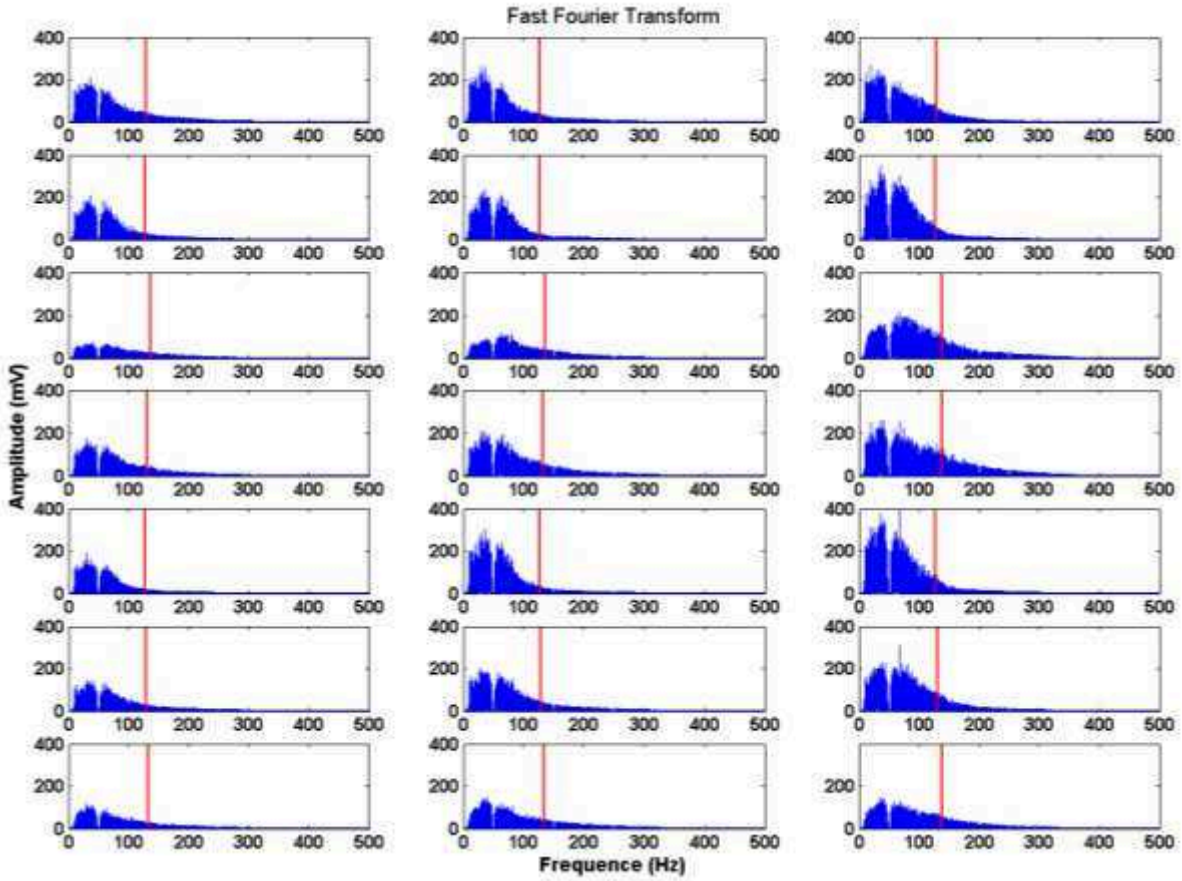

Figure 6: Spectre fréquentiel séparé en deux parties avec une aire sous la courbe égale. Le trait rouge situe cette séparation. Chaque spectre est le résultat pour une paire d'électrodes correspondant à la distribution sur le bras de la Figure 5.

Les valeurs ainsi obtenues par le calcul du MPF sont présentées dans la figure 7 sous forme de topographie. On voit apparaître des valeurs maximales autour du couple d'électrodes (6-5) ce qui coïncide avec les résultats de l'analyse RMS. De même que pour l'analyse RMS, des effets de bords sont à noter au niveau de la ligne distale (2-1).

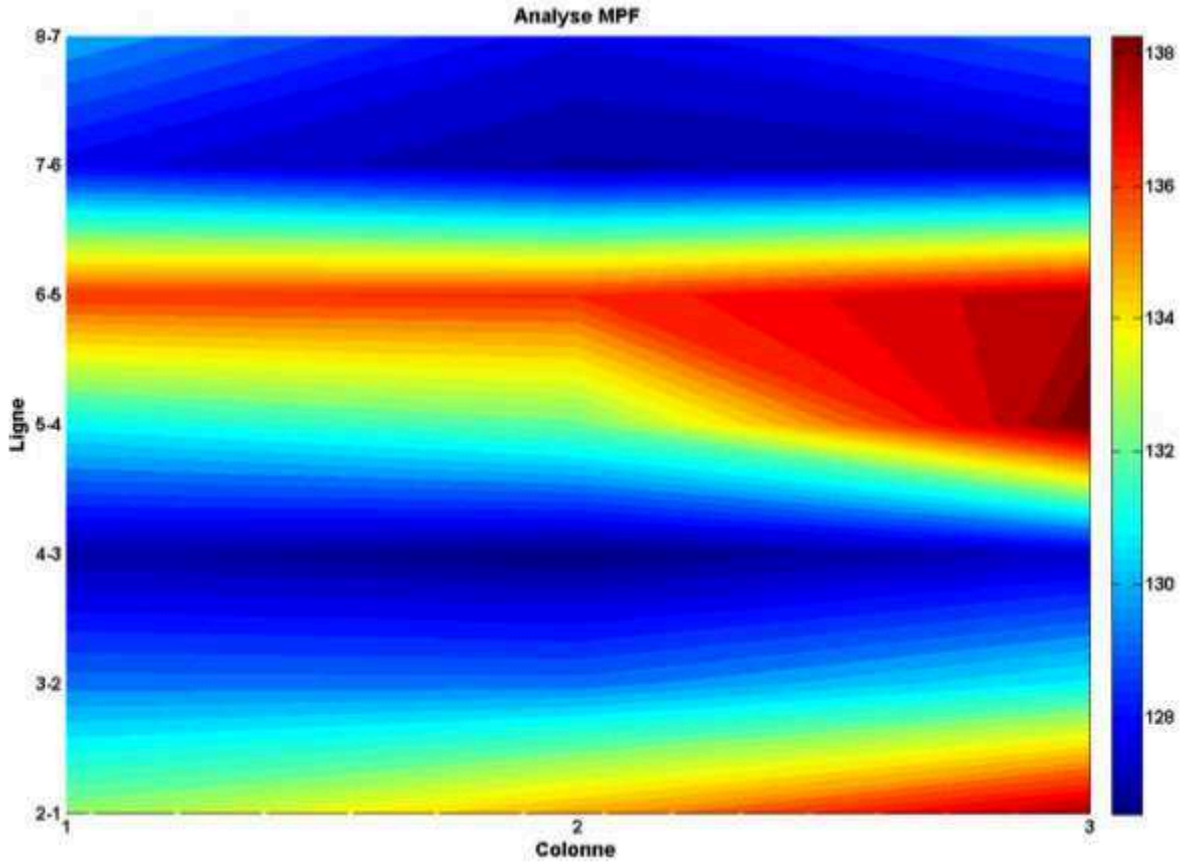

Figure 7: Topographie des résultats de l'analyse MPF obtenus avec la matrice de 3x8 électrodes de la Figure 4. Le positionnement des électrodes correspond à celle de la Figure 5. La couleur correspond à la valeur RMS obtenue du signal, indiquée dans l'échelle à droite dans la figure.

Ensuite, l'algorithme de cross-corrélation a été utilisé. La figure 8 ci-dessous montre le résultat de la cross-corrélation entre deux signaux bipolaires successifs sur chaque colonne dans le sens descendant. Par exemple, la première ligne de résultat correspond à la cross-corrélation de la première ligne de mesure EMG comparé à la deuxième ligne. On peut y voir une inversion du pic de corrélation au niveau de la comparaison entre les couples d'électrodes (6-5) et (5-4) sur chaque colonne.

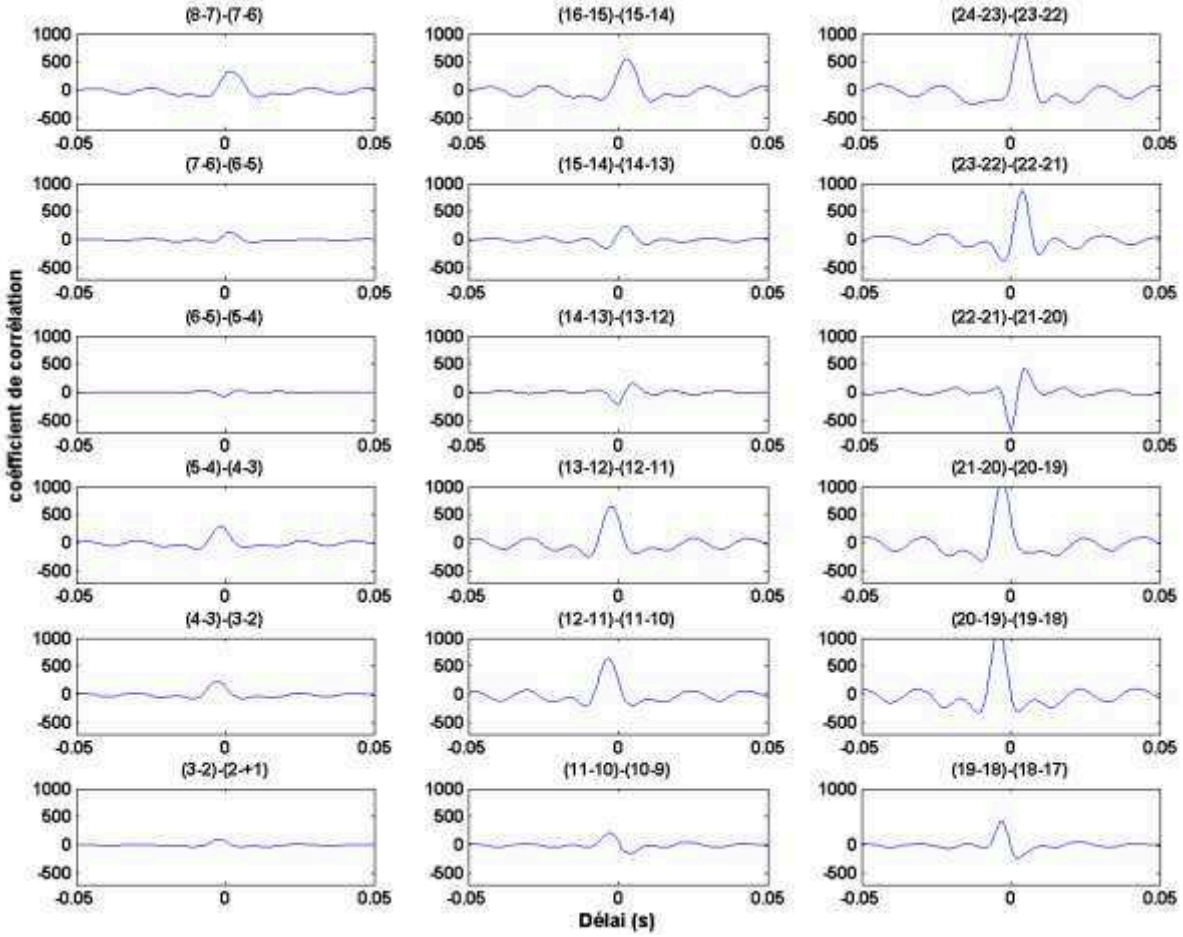

Figure 8. Cross-corrélation de deux mesures sur des paires d'électrodes successives en allant de proximal à distal sur chaque colonne d'électrodes.

En récupérant le pic de corrélation et en le présentant comme pour les algorithmes utilisés précédemment, on obtient la figure 9 ci-dessous illustrant une valeur minimale au niveau de la cross-corrélation entre les couples d'électrodes (6-5) et (5-4).

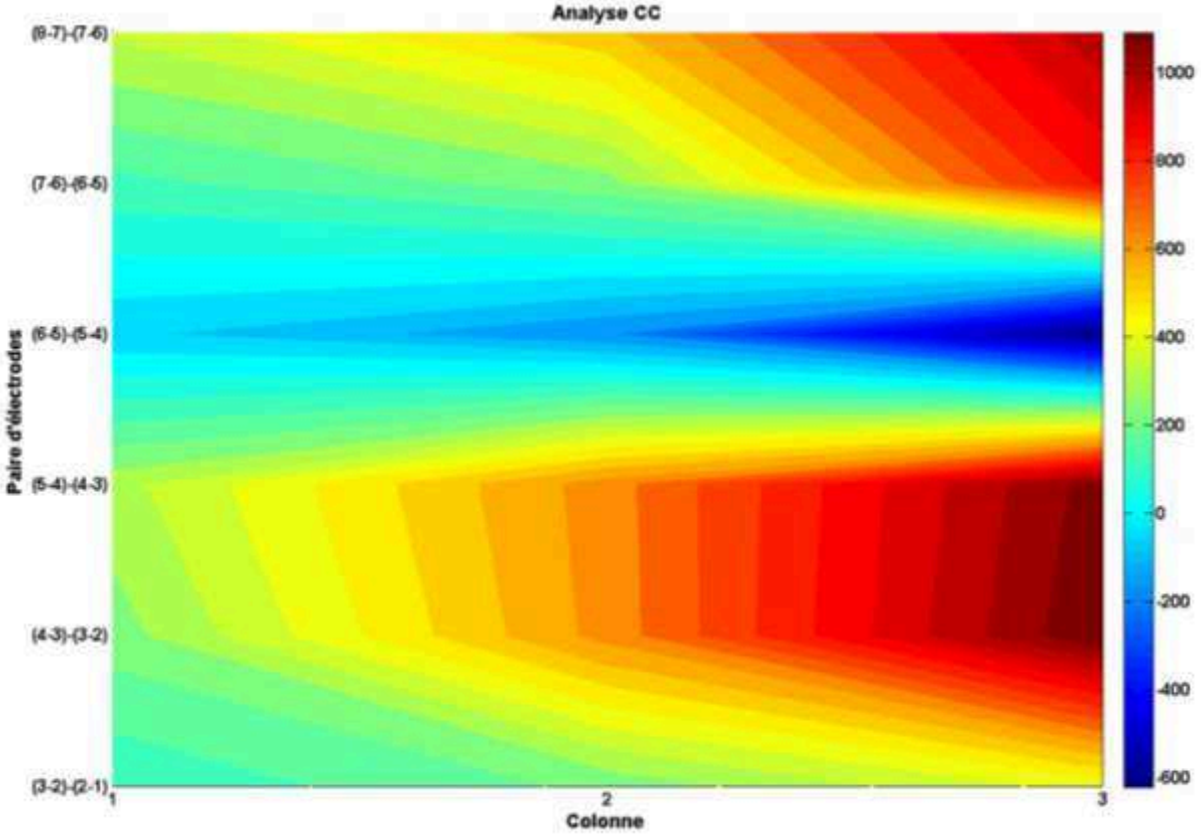

Figure 9: Topographie des résultats de l'algorithme de cross-corrélation obtenus avec la matrice de 3x8 électrodes de la Figure 4. Le positionnement des électrodes correspond à celle de la Figure 9. La couleur correspond à la valeur maximale de la cross-corrélation suivant l'échelle à droite dans la figure.

Enfin, j'ai appliqué l'algorithme H&S aux mêmes mesures sEMG. On peut voir sur la figure 10 que les vecteurs en dessous du couple d'électrodes (6-5) sont dirigés vers le bas alors que ceux au-dessus du couple (7-6) sont dirigés vers le haut de la matrice. Cela pousse à penser que les jonctions neuromusculaires se situent entre ces couples d'électrodes.

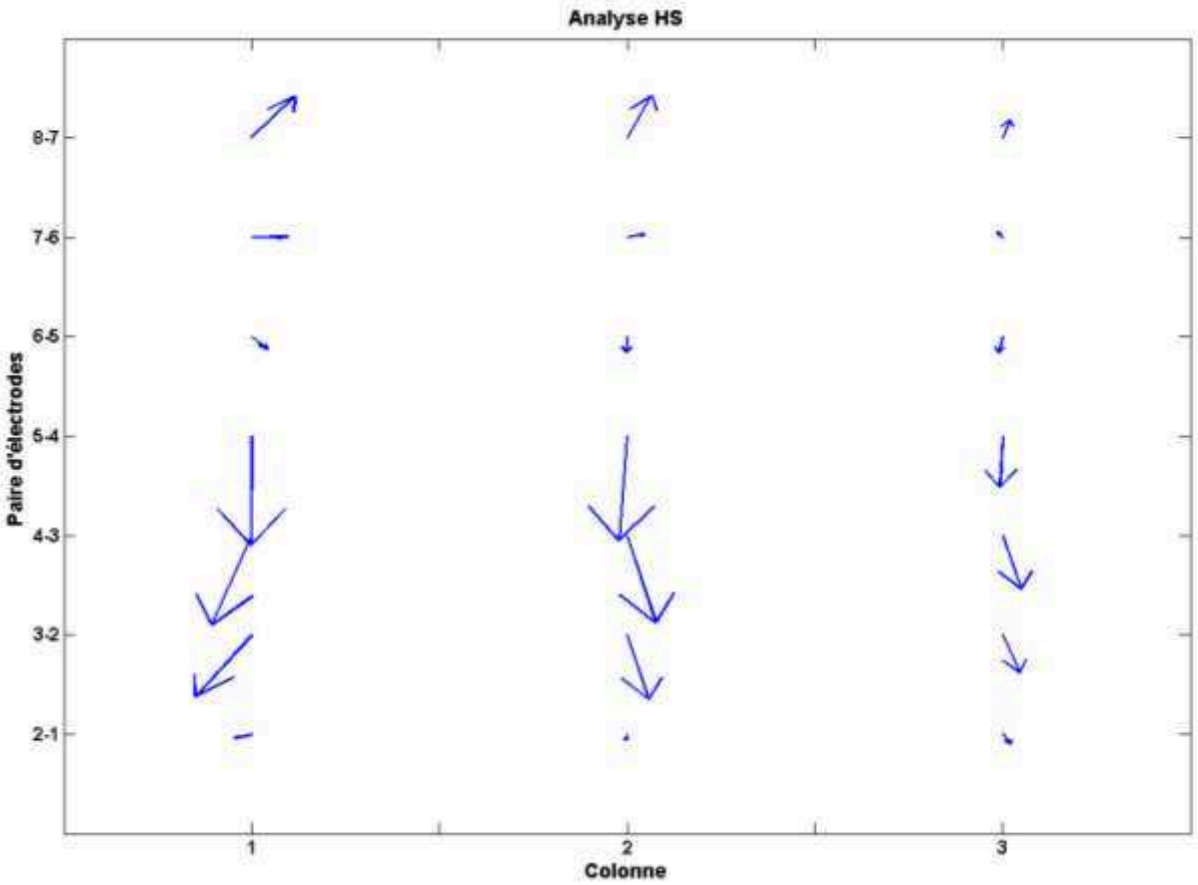

Figure 10: Champ de vecteurs obtenu en appliquant l'algorithme H&S aux mesures sEMG de 3x8 électrodes. Le sens des vecteurs indique le sens du déplacement des potentiels d'action sur les fibres musculaires.

Au vu des résultats, les différents algorithmes semblent tous indiquer la présence d'une jonction neuromusculaire aux alentours du couple d'électrodes (6-5) de chaque colonne. De forts effets de bords sur le bas de la matrice sont cependant à noter sur les résultats des analyses RMS et MPF. Pour l'analyse H&S, malgré la réduction de l'amplitude des vecteurs en bord de matrice, l'orientation de ceux-ci reste inaffectée par ces effets de bords. Dans le cadre de la cross-corrélation, l'inversion attendue au niveau des zones d'innervations reste uniquement localisée au niveau du couple d'électrodes (6-5)-(5-4). Au vu de la position des couples d'électrodes de la ligne (2-1), une hypothèse pourrait être que les signaux seraient perturbés par l'arriver en limite du muscle.

Aujourd'hui, ces enregistrements ne permettent pas de conclure sur la capacité à répondre à la question posée dans le projet : est-il possible de valider l'hypothèse d'une réorganisation neuromusculaire périphérique post-opératoire chez une personne amputée en utilisant ces techniques pour la détection de zones d'innervation? Pour répondre à cette question, il reste d'abord à valider la force de chacun de ces algorithmes pour différencier les jonctions neuromusculaires en utilisant nos matrices d'électrodes Kapton dans les conditions similaires à celles de l'enregistrement traité ci-dessus. Il sera en effet intéressant de se pencher sur l'impact de la diminution de la distance inter-électrode sur les résultats des algorithmes, ce qui est un point central de la justification de l'utilisation de matrice en plus de la praticité à l'usage par rapport aux électrodes commerciales dans le cadre de la détection de zones d'innervations. Ensuite, il serait primordial de valider que le niveau de bruit des signaux acquis avec des matrices d'électrodes sèches ne perturbe pas l'analyse des signaux via les divers algorithmes présentés dans ce chapitre. Finalement, il va falloir tester si l'ensemble de ces techniques (matrices et traitements) peuvent nous permettre d'explorer les zones d'innervation de muscles résiduels après une amputation du bras.

Concernant le protocole, il nous semble pertinent d'étudier le résultat des algorithmes lors de différentes contractions musculaires du membre intact et le membre résiduel chez l'amputé de bras. En effet, s'il y a eu une réinnervation de la musculature résiduelle par les axones axotomisés par amputation, il pourrait en résulter une poly-innervation, comme j'avais élaboré dans le Chapitre 1. Ceci impliquerait qu'un *mouvement du bras résiduel* active les « anciennes » innervations du muscle (zones classiquement trouvées), similaires à celles du même muscle du bras intact. Par contre, un *mouvement fantôme de la main* utiliserait les nouvelles innervations qui seront probablement placées plus distales sur le même muscle. Nous envisageons donc de placer des matrices d'électrodes sur les muscles du bras intact ainsi que du bras résiduel et d'explorer les zones

d’innervations musculaires dans 3 conditions expérimentales : exécution d’une contraction du biceps du bras intact, contraction du biceps résiduel, et finalement exécution d’un mouvement fantôme de la main.

Il reste cependant des questions importantes. La taille du muscle résiduel est-elle suffisante pour permettre une détection de zones d’innervations ? Le sens des fibres musculaires change-t-il après une amputation transhumérale ? Et enfin, sera-t-il possible de différencier les zones d’innervations si la réinnervation supposée s’est effectuée proche de la zone d’innervation native du muscle ? La réponse aux deux dernières questions va dépendre de la résolution spatiale de nos matrices d’électrodes. Une résolution élevée permettra la détection des zones d’innervations même si le sens des fibres a changé [59] et si les zones de réinnervations sont proches des zones des anciennes innervations. Les tests pour répondre à toutes ces questions seront faits dans les mois qui suivent.

VII. Discussion

Mes travaux de thèse ont été motivés par deux objectifs : la validation embarquée d'un concept innovant de contrôle de prothèse myoélectrique, et l'approfondissement des connaissances sur la réorganisation neuromusculaire au niveau des muscles du membre résiduel d'une personne amputée. Ces deux thématiques m'ont amené à me pencher sur l'étude de la fabrication de matrices d'électrodes sèches et de l'analyse des données sEMG permettant de localiser les zones d'innervations musculaires.

J'ai commencé par fabriquer 4 types d'électrodes innovantes de par les matériaux utilisés et les méthodes de fabrication employées : une matrice d'électrodes en PEDOT : PSS sur un support Kapton, une électrode PEDOT : PSS sur du papier, une électrode PEDOT : PSS sur du textile avec et sans gel ionique solide, et enfin une électrode PEDOT : PSS sur un support tattoo temporaire en utilisant un textile comme connecteur. J'ai testé ces électrodes mécaniquement, électriquement et d'un point de vue applicatif. Je me suis ensuite intéressé aux algorithmes de détection de zones d'innervations. J'ai testé 4 algorithmes proposés dans la littérature, dans le but de les appliquer à l'exploration de la réorganisation neuromusculaire postopératoire dans un futur proche.

Au vu des résultats, les électrodes avec un **support Kapton** (Chapitre II), semblent présenter les caractéristiques les plus intéressantes vis-à-vis de nos deux objectifs. En effet, celles-ci présentent les meilleures impédances, elles sont résistantes aux efforts mécaniques et peuvent facilement être connectées sous forme de matrice, contrairement aux autres substrats proposés. De plus, des perspectives de procédés de fabrication industrielle sont facilement envisageables étant donné que des PCB (Printed Circuit Board) flexibles en support Kapton sont déjà proposés sur le marché. Seul le PEDOT : PSS serait à déposer. L'intérêt d'une chaîne d'impression jet d'encre dans ce cas d'application particulier serait à étudier économiquement. En effet, un simple dépôt à la pipette pourrait aussi déposer le PEDOT :PSS étant donné la précision du dépôt nécessaire. Ces électrodes ne sont cependant pas étirables et ne se conforment donc pas parfaitement au membre à mesurer, ce qui peut poser problème sur une matrice de grande taille. Ce problème pourrait être résolu en incorporant des électrodes sur Kapton dans un support textile, améliorant la conformation de l'ensemble.

Les électrodes **sur support papier**, chapitre III, présentent des potentialités dans le cadre d'électrodes jetables étant donné le faible coup de fabrication et la durée limitée de vie mécanique du papier. De plus, cette électrode pourrait potentiellement être

biodégradable. Cependant, il faudra étudier la dégradation du PEDOT :PSS dans un milieu organique classique, comme cela commence a être fait pour d'autres polymères [60,61]. Le support papier est cependant trop fragile pour une utilisation dans la prothèse.

Les électrodes en **support textile** présentées dans le chapitre IV ne me semblent, à l'expérience de leurs utilisations, pas exploitables dans notre cas sans l'ajout de gel ionique solide pour la création de petite surface de contact nécessaire à la fabrication de matrice. En effet, la faible surface de contact des électrodes d'une matrice rendrait le signal trop instable sauf si une pression mécanique est appliquée pour forcer le contact des électrodes avec la peau. Dans le cadre de la prothèse, il faudrait tester si la pression à l'intérieur de l'emboiture est suffisamment homogène au niveau des électrodes. De plus, dans le but de créer une matrice, la connexion de chaque électrode est un problème, ce qui n'a pas été abordé dans mes travaux. Une solution potentielle pour ce problème serait l'insertion de fibres en cuivre dans les fibres textiles, mais cela pourrait significativement compliquer la fabrication de ces matrices. Le gel ionique solide présente par contre des caractéristiques remarquables et permettrait d'assurer le bon contact avec la peau de n'importe quelle électrode sèche. Enfin, les résultats de mon étude, comme le montrent aussi d'autres publications [32,62,63], en particulier la qualité de l'incorporation du PEDOT :PSS dans du textile, restent intéressants vis-à-vis de la demande du marché des textiles connectés dans le loisir et l'e-santé. Ces applications amènent la problématique de lavage de ces électrodes. Une piste a été abordée récemment en proposant une formulation de PEDOT : PSS utilisant un additif rendant le résultat résistant à l'eau [64]. Enfin, un dernier problème est l'incorporation de polymère dans du textile qui, dans le cadre de tension trop importante, risque de se fissurer et de perdre en performance. Ceci n'est évidemment pas souhaitable dans le cadre d'une application commerciale d'un produit non consommable. Pour résoudre ce problème, des recherches sont faites pour créer des polymères ayant des propriétés régénérantes [65,66].

Les électrodes **tattoo** ne présentent pas de performances acceptables dans un cadre applicatif. Notamment, le support est trop fragile et la connexion est trop complexe. Cependant, une approche intéressante vis à vis de la connexion de patch a été étudiée ici, pouvant améliorer la performance de systèmes embarqués dans des textiles. Mon travail sur ces papiers tattoo temporaires a permis de valider l'utilisation du PEDOT:PSS et de l'impression jet d'encre dans le cadre de la fabrication de patch électrophysiologique sur des supports fins et fragiles.

Quoi qu'il en soit, malgré toutes les limites à chacun des types de substrats présentés, le PEDOT : PSS, le gel ionique solide et l'impression jet d'encre se sont révélés être des matériaux et des procédés de fabrications très intéressants dans le cadre de la fabrication de capteurs de signaux électrophysiologiques sur des substrats divers.

Ces cas d'études de fabrication d'électrodes sèches nous ont permis de fabriquer une matrice qui a brièvement été testée dans le cadre de la détection des zones d'innervations (Chapitre II, figure 5b). Cependant, pour des raisons de temps, il n'a pas été possible d'aller au bout des expérimentations nécessaires à la réponse aux questions que nous nous sommes posées. Dans le cadre du test des matrices pour la réalisation d'un contrôle de la prothèse embarquée, comme présenté dans l'introduction, le matériel d'expérimentation doit encore être développé. Cependant, au vu des résultats obtenus, la performance des matrices en substrat Kapton devrait, à mon sens, pouvoir être valide dans le cadre du contrôle d'une prothèse. Dans le cadre de l'exploration des zones d'innervations, de nombreuses questions restent toutefois irrésolues, comme présenté dans la discussion du chapitre VI. De plus, d'autres algorithmes de détection seraient à tester vis-à-vis de la détection de zones d'innervations multiples [57]. Après la validation de la matrice et des algorithmes, il faudra multiplier les enregistrements chez des personnes saines et amputées dans le but de tester l'hypothèse de la poly-innervation des fibres musculaires suite à l'amputation.

Un large domaine de recherche en matériaux s'intéresse aujourd'hui aux applications possibles des polymères. Le PEDOT :PSS est un bon exemple avec de nombreuses possibilités dans les domaines de l'encapsulation antistatique, de l'électronique souple, des OLED, des panneaux solaires et des écrans tactiles transparents. Dans le domaine médical, plusieurs propriétés me paraissent intéressantes et seraient à exploiter en plus de celles présentées par mes travaux. Il est possible de créer des films de PEDOT :PSS transparents se qui pourrait permettre de faire des électrodes transparentes. Celles-ci pourraient permettre à un chirurgien d'enregistrer des grandeurs électrophysiologiques proches du site d'opération tout en gardant la vision sur ce qu'il fait (par exemple en cas d'une chirurgie proche d'un nerf). La souplesse du PEDOT :PSS est recherchée dans le cadre du développement d'une nouvelle génération d'électrodes implantées dans le cerveau. En effet, la souplesse des électrodes permet de créer moins de stress mécanique avec les tissus environnants limitant la réaction du corps [67]. Enfin, les caractéristiques semi-conductrices du PEDOT :PSS pourraient permettre l'élaboration de briques électroniques élémentaires. Ces briques élémentaires pourraient ensuite permettre la création de circuits électroniques souples, sans

métaux et transparents. Le PEDOT :PSS ouvre alors un très large champ des possibles qui restent à exploiter.

Références

[1] INSEE, **2004**.
[2] Advanced Amputee Solutions, **2010**.
[3] A. Touillet, L. Peultier, C. Nicol, N. Jarrassé, I. Loiret, N. Martinet, J. Paysant, J. De Graaf, *Nat. Sci. Rep.* **n.d.**, *Sous révision*.
[4] E. Raffin, P. Giraux, K. T. Reilly, *Cortex* **2012**, *48*, 746.
[5] K. T. Reilly, C. Mercier, M. H. Schieber, A. Sirigu, *Brain* **2006**, *129*, 2211.
[6] E. Biddiss, T. Chau, *Med. Eng. Phys.* **2008**, *30*, 403.
[7] N. Jarrasse, C. Nicol, A. Touillet, F. Richer, N. MARTINET, J. Paysant, J. B. De Graaf, *IEEE Trans. Neural Syst. Rehabil. Eng.* **2017**, *25*, 68.
[8] N. Jarrassé, C. Nicol, F. Richer, A. Touillet, N. Martinet, J. Paysant, J. B. D. Graaf, in *2017 Int. Conf. Rehabil. Robot. ICORR*, **2017**, pp. 1239–1245.
[9] P. Konrad, *Pract. Introd. Kinesiol. Electromyogr.* **2006**, *1*.
[10] P. A. Lynn, N. D. Bettles, A. D. Hughes, S. W. Johnson, *Med. Biol. Eng. Comput.* **1978**, *16*, 651.
[11] M. M. Merzenich, R. J. Nelson, M. P. Stryker, M. S. Cynader, A. Schoppmann, J. M. Zook, *J. Comp. Neurol.* **n.d.**, *224*, 591.
[12] H. Flor, T. Elbert, S. Knecht, C. Wienbruch, C. Pantev, N. Birbaumers, W. Larbig, E. Taub, *Nature* **1995**, *375*, 482.
[13] Y. Vandermeeren, E. Bastings, D. Good, E. Rouiller, E. Olivier, *Rev. Neurol. (Paris)* **2003**, *159*, 259.
[14] C. Xerri, J. Coq, M. Merzenich, W. Jenkins, *J. Physiol.-Paris* **1996**, *90*, 277.
[15] C. Xerri, *Comptes Rendus Académie Sci. - Ser. III - Sci. Vie* **1998**, *321*, 135.
[16] C. Xerri, M. M. Merzenich, W. Jenkins, S. Santucci, *Cereb. Cortex* **1999**, *9*, 264.
[17] M. Gagné, S. Hétu, K. T. Reilly, C. Mercier, *Hum. Brain Mapp.* **n.d.**, *32*, 509.
[18] C. Mercier, K. T. Reilly, C. D. Vargas, A. Aballea, A. Sirigu, *Brain* **2006**, *129*, 2202.
[19] C. W.-H. Wu, J. H. Kaas, *Neuron* **2000**, *28*, 967.
[20] H.-X. Qi, W. S. Phillips, J. H. Kaas, *Somatosens. Mot. Res.* **2004**, *21*, 229.
[21] R. V. KRISHNAN, *Int. J. Neurosci.* **2005**, *115*, 1451.
[22] M. Gazzoni, D. Farina, R. Merletti, *J. Neurosci. Methods* **2004**, *136*, 165.
[23] P. Leleux, C. Johnson, X. Strakosas, J. Rivnay, T. Hervé, R. M. Owens, G. G. Malliaras, *Adv. Healthc. Mater.* **2014**, *3*, 1377.
[24] J.-Y. Baek, J.-H. An, J.-M. Choi, K.-S. Park, S.-H. Lee, *Sens. Actuators Phys.* **2008**, *143*, 423.
[25] K.-P. Hoffmann, R. Ruff, in *29th Annu. Int. Conf. IEEE Eng. Med. Biol. Soc. 2007 EMBS 2007*, **2007**, pp. 5739–5742.
[26] D. Khodagholy, T. Doublet, M. Gurfinkel, P. Quilichini, E. Ismailova, P. Leleux, T. Herve, S. Sanaur, C. Bernard, G. G. Malliaras, *Adv. Mater.* **2011**, *23*, H268.
[27] A. Campana, T. Cramer, D. T. Simon, M. Berggren, F. Biscarini, *Adv. Mater.* **2014**, *26*, 3874.
[28] G. A. Salvatore, N. Münzenrieder, T. Kinkeldei, L. Petti, C. Zysset, I. Strebel, L. Büthe, G. Tröster, *Nat. Commun.* **2014**, *5*, DOI 10.1038/ncomms3982.
[29] J. Viventi, D.-H. Kim, L. Vigeland, E. S. Frechette, J. A. Blanco, Y.-S. Kim, A. E. Avrin, V. R. Tiruvadi, S.-W. Hwang, A. C. Vanleer, D. F. Wulsin, K. Davis, C. E. Gelber, L. Palmer, J. Van der Spiegel, J. Wu, J. Xiao, Y. Huang, D. Contreras, J. A. Rogers, B. Litt, *Nat. Neurosci.* **2011**, *14*, 1599.
[30] G.-T. Hwang, M. Byun, C. K. Jeong, K. J. Lee, *Adv. Healthc. Mater.* **2015**, *4*, 646.
[31] D. A. Koutsouras, E. Bihar, J. A. Fairfield, M. Saadaoui, G. G. Malliaras, in *Green Mater. Electron.*, Wiley-Blackwell, **2017**, pp. 55–89.

[32] S. Takamatsu, T. Lonjaret, D. Crisp, J.-M. Badier, G. G. Malliaras, E. Ismailova, *Sci. Rep.* **2015**, *5*, DOI 10.1038/srep15003.
[33] T. Adrega, S. P. Lacour, *J. Micromechanics Microengineering* **2010**, *20*, 055025.
[34] S. Bidoki, *Ink-Jet Printing of Conductive Patterns on Textile Fabrics*, **2004**.
[35] H.-H. Lee, K.-S. Chou, K.-C. Huang, *Nanotechnology* **2005**, *16*, 2436.
[36] G. D. Martin, S. Hoath, I. Hutchings, *Inkjet Printing - The Physics of Manipulating Liquid Jets and Drops*, **2008**.
[37] A. Haldar, S. D. Yambem, K.-S. Liao, N. J. Alley, E. P. Dillon, A. R. Barron, S. A. Curran, *Thin Solid Films* **2011**, *519*, 6169.
[38] T. Shimoda, K. Morii, S. Seki, H. Kiguchi, *Inkjet Printing of LED Polymer Displays*, **2003**.
[39] S. B. Fuller, E. J. Wilhelm, J. M. Jacobson, *J. Microelectromechanical Syst.* **2002**, *11*, 54.
[40] S. H. Eom, S. Senthilarasu, P. Uthirakumar, S. C. Yoon, J. Lim, C. Lee, H. S. Lim, J. Lee, S.-H. Lee, *Org. Electron.* **2009**, *10*, 536.
[41] E. Macis, M. Tedesco, P. Massobrio, R. Raiteri, S. Martinoia, *J. Neurosci. Methods* **2007**, *161*, 88.
[42] J. Y. Kim, J. H. Jung, D. E. Lee, J. Joo, *Synth. Met.* **2002**, *126*, 311.
[43] N. Kim, S. Kee, S. H. Lee, B. H. Lee, Y. H. Kahng, Y.-R. Jo, B.-J. Kim, K. Lee, *Adv. Mater.* **2014**, *26*, 2268.
[44] M. Berggren, A. Richter-Dahlfors, *Adv. Mater.* **2007**, *19*, 3201.
[45] S.-C. Luo, E. Mohamed Ali, N. C. Tansil, H. Yu, S. Gao, E. A. B. Kantchev, J. Y. Ying, *Langmuir* **2008**, *24*, 8071.
[46] A. Zucca, C. Cipriani, Sudha, S. Tarantino, D. Ricci, V. Mattoli, F. Greco, *Adv. Healthc. Mater.* **2015**, *4*, 983.
[47] L. Bareket, L. Inzelberg, D. Rand, M. David-Pur, D. Rabinovich, B. Brandes, Y. Hanein, *Sci. Rep.* **2016**, *6*, DOI 10.1038/srep25727.
[48] H. Piitulainen, A. Botter, R. Merletti, J. Avela, *J. Electromyogr. Kinesiol.* **2013**, *23*, 302.
[49] N. Östlund, B. Gerdle, J. Stefan Karlsson, *J. Electromyogr. Kinesiol.* **2007**, *17*, 549.
[50] R. G. Scalisi, M. Paleari, A. Favetto, M. Stoppa, P. Ariano, P. Pandolfi, A. Chiolerio, *Org. Electron.* **2015**, *18*, 89.
[51] P. A. Lynn, *IEEE Trans. Biomed. Eng.* **1979**, *BME-26*, 564.
[52] T. Masuda, T. Sadoyama, *IEEE Trans. Biomed. Eng.* **1988**, *35*, 623.
[53] T. W. Beck, J. M. DeFreitas, M. S. Stock, *Comput. Methods Programs Biomed.* **2012**, *105*, 13.
[54] L. Mesin, M. Gazzoni, R. Merletti, *J. Electromyogr. Kinesiol.* **2009**, *19*, e413.
[55] C. Cescon, in *IEEE Int. Workshop Med. Meas. Appl. 2006 MeMea 2006*, **2006**, pp. 87–90.
[56] K. Ullah, C. Cescon, B. Afsharipour, R. Merletti, *J. Electromyogr. Kinesiol.* **2014**, *24*, 860.
[57] H. R. Marateb, M. Farahi, M. Rojas, M. A. Mañanas, D. Farina, *PLOS ONE* **2016**, *11*, e0167954.
[58] B. K. P. Horn, B. G. Schunck, *Artif. Intell.* **1981**, *17*, 185.
[59] L. Mesin, *Comput. Biol. Med.* **2015**, *57*, 8.
[60] T. Lei, M. Guan, J. Liu, H.-C. Lin, R. Pfattner, L. Shaw, A. F. McGuire, T.-C. Huang, L. Shao, K.-T. Cheng, J. B.-H. Tok, Z. Bao, *Proc. Natl. Acad. Sci.* **2017**, *114*, 5107.
[61] V. R. Feig, H. Tran, Z. Bao, *ACS Cent. Sci.* **2018**, *4*, 337.
[62] S. A. Odhiambo, G. De Mey, C. Hertleer, A. Schwarz, L. Van Langenhove, *Text. Res. J.* **2014**, *84*, 347.
[63] Y. Ding, M. A. Invernale, G. A. Sotzing, *ACS Appl. Mater. Interfaces* **2010**, *2*, 1588.
[64] I. del Agua, D. Mantione, U. Ismailov, A. Sanchez-Sanchez, N. Aramburu, G. G. Malliaras, D. Mecerreyes, E. Ismailova, *Adv. Mater. Technol.* **2018**, DOI 10.1002/admt.201700322.
[65] Y. J. Tan, J. Wu, H. Li, B. C. K. Tee, *ACS Appl. Mater. Interfaces* **2018**, *10*, 15331.
[66] S. Terryn, G. Mathijssen, J. Brancart, T. Verstraten, G. V. Assche, B. Vanderborght, *IEEE Trans. Robot.* **2016**, *32*, 736.
[67] R. Green, M. R. Abidian, *Adv. Mater.* **n.d.**, *27*, 7620.

Résumé

Le travail de cette thèse est né suite aux résultats récents que 77% des patients amputés du membre supérieur ont un membre fantôme mobile. Ces patients déclarent pouvoir faire divers mouvements volontaires avec leur main fantôme. De façon intéressante, cette mobilité fantôme est systématiquement associée à des activités musculaires au niveau du membre résiduel (moignon) qui sont spécifiques au type de mouvement exécuté. L'équipe de chercheurs dans laquelle ce présent travail est fait a montré que ces contractions musculaires peuvent être utilisées pour le contrôle de prothèses, qui devient alors naturel. Cependant, (1) ce contrôle « basé fantôme » est pour l'instant validé en contexte de laboratoire, et (2) les phénomènes entourant les membres fantômes sont encore mal compris, notamment leur origine neurophysiologique. Ce travail de thèse CIFRE a visé à élaborer des matrices d'électrodes fines afin de détecter les activités musculaires associées aux mouvements fantômes pour (1) les incorporer dans l'emboiture de la prothèse afin de pouvoir faire des tests avec des prothèses portées, et (2) d'explorer les présumées réorganisations neuromusculaires au niveau du membre résiduel. Ces objectifs ont amené à développer des électrodes fines et sèches sur divers supports : le Kapton en tant que matériau fin, souple et solide, le papier en tant que potentielle électrode jetable et peu onéreuse, le textile pour sa souplesse et son utilisation appréciée dans l'emboiture des prothèses et le tattoo temporaire pour sa capacité à épouser parfaitement les aspérités de la peau. Cette étude exhaustive de supports a été permise par l'utilisation couplée d'un polymère conducteur apprécié dans la littérature actuel, le PEDOT :PSS, pour la fabrication d'électrodes et d'une méthode de fabrication par jet de matière. Les électrodes sèches ont été caractérisées et comparées à un standard sur le marché, des électrodes Ag/AgCl avec un gel conducteur liquide. Une matrice d'électrodes sèches et fines a ainsi été créée donnant enfin la possibilité d'étudier son incorporation dans le manchon de prothèses ainsi que la localisation des zones d'innervations. Ce dernier point a nécessité l'étude de diverses méthodes d'analyses des signaux électromyographiques connues dans la littérature, telles que le calcul du « root mean square », du « mean power frequency », de la « cross-correlation », et enfin, de l'utilisation d'un algorithme proposé par Horn et Schunk (1981). Pour conclure, ces travaux ont permis de diversifier les techniques et matériaux de création d'électrodes sèches et permettront enfin les tests de contrôle basé « mouvement fantôme » de prothèses myoélectriques *portées*, ainsi que l'étude de la réorganisation des jonctions neuromusculaires du membre résiduel après amputation du membre supérieur.

Summary

The present work has its origin in recent results showing that 77% of upper limb amputees declare having phantom limb mobility. These patients are able to make different types of voluntary movements with their phantom hand. Interestingly, this phantom mobility is associated to residual muscle activity in stump of which the pattern is systematically varying with the type of executed movements. The team conducting this project was able to develop a method of controlling myoelectric prostheses based on these muscle contractions, which makes the control much more natural and potentially increases the number of degrees of freedom. However, (1) this phantom-based mode of control is only validated in a laboratory setup without actually wearing the prosthesis on the residual limb, and (2) while it seems possible to use phantom mobility, we are still far from understanding its neurophysiological origin. The present work aimed to develop matrices of thin dry electrodes in order to (1) allow the creation of an embedded prosthesis with phantom-mobility-based control, and (2) explore the possible reorganization of motor endplates in the residual limb. These goals leaded to the fabrication of electrodes on multiple substrates. Kapton was investigated as a substrate for its robustness while staying very flexible and thin, and paper for its potential as cheap disposable electrodes. Textile was explored for its flexibility and its use in the prosthesis sleeve and in embedded healthcare devices in general. Finally, temporary tattoos were tested as a potential substrate for the smooth contact it provides with the skin and its potential to use it in patch creation. The possibility to work on such different substrates was permitted by a biocompatible conducting polymer, PEDOT:PSS, used for the fabrication of the electrodes, and the use of inkjet printing technology. The dry electrodes were characterized and compared to wet Ag/AgCl electrodes (containing conducting gel) commonly used in electrophysiological recordings. So, at the end, a matrix of thin and dry electrodes was created with the substrate Kapton, making it possible to study both its incorporation in the prosthesis sleeve and the localization of innervation zones of the residual muscles of upper limb amputees. For the latter, algorithms for the detection of innervations zones, developed in the literature, have been studied with help of a recording with classical electrodes placed on an intact arm. The signals were analyzed using root mean square, mean power frequency and cross-correlation based algorithms, as well as another promising method proposed by Horn and Schunk (1981). In conclusion, the present thesis contributed to the diversification of technics and materials used for the creation of dry electrodes, and now open the study of reorganization of innervation zones in residual limb muscles after upper limb amputation.